การสังเคราะห์บิสฟีนอลเอฟโดยใช้เอสบีเอ-15 ที่มีหมู่ซัลโฟนิกเป็นตัวเร่งปฏิกิริยา

นางสาวเกศรินทร์ วรกิตติธรรม

วิทยานิพนธ์นี้เป็นส่วนหนึ่งของการศึกษาตามหลักสูตรปริญญาวิทยาศาสตรมหาบัณฑิต
สาขาวิชาปิโตรเคมีและวิทยาศาสตร์พอลิเมอร์
คณะวิทยาศาสตร์ จุฬาลงกรณ์มหาวิทยาลัย
ปีการศึกษา 2552

SYNTHESIS OF BISPHENOL-F USING SULFONIC FUCTIONALIZED SBA-15 AS CATALYST

Miss Kessarin Worakittitham

A Thesis Submitted in Partial Fulfillment of the Requirements
for the Degree of Master of Science Program in Petrochemistry and Polymer Science
Faculty of Science
Chulalongkorn University
Academic Year 2009

Thesis Title	SYNTHESIS OF BISPHENOL-F USING SULFONIC FUNCTIONALIZED SBA-15 AS CATALYST
By	Miss Kessarin Worakittitham
Field of Study	Petrochemistry and Polymer Science
Thesis Advisor	Duangamol Nuntasri, Ph.D.

Accepted by the Faculty of Science, Chulalongkorn University in Partial Fulfillment of the Requirements for the Master's Degree

……..Dean of the Faculty of Science

(Professor Supot Hannongbua, Dr. rer. nat.)

THESIS COMMITTEE

……..Chairman

(Associate Professor Supawan Tantayanon, Ph.D.)

……..Thesis Advisor

(Duangamol Nuntasri, Ph.D.)

……..Examiner

(Assistant Professor Warinthorn Chavasiri, Ph.D.)

……..Examiner

(Aticha Chaisuwan, Ph.D.)

……..External Examiner

(Gamolwan Tumcharern, Ph.D.)

เกศรินทร์ วรกิตติธรรม : การสังเคราะห์บิสฟีนอลเอฟโดยใช้เอสบีเอ-15 ที่มีหมู่ซัลโฟนิกเป็นตัวเร่งปฏิกิริยา (SYNTHESIS OF BISPHENOL-F USING SULFONIC FUNCTIONALIZED SBA-15 AS CATALYST) อ.ที่ปรึกษาวิทยานิพนธ์หลัก: อ. ดร. ดวงกมล นันทศรี, 110 หน้า

ได้สังเคราะห์ตัวเร่งปฏิกิริยาเอสบีเอ-15 ที่มีหมู่โพรพิลซัลโฟนิกและเอริลซัลโฟนิกด้วยวิธีสังเคราะห์แบบขั้นตอนเดียวภายใต้ภาวะที่เป็นกรดโดยใช้ไทรบล็อกโคพอลิเมอร์ชนิด P123 (พอลิเอทิลีนออกไซด์$_{20}$-พอลิโพรพิลีนออกไซด์$_{70}$-พอลิเอทิลีนออกไซด์$_{20}$) เป็นสารชี้นำโครงสร้าง องค์ประกอบของเจลของเอสบีเอ-15 ที่มีหมู่โพรพิลซัลโฟนิกเป็น 0.0369 TEOS: 0.0041 MPTMS: 0.0369 H_2O_2: 0.24 HCl: 6.9046 H_2O: 0.0007 P123 นอกจากนี้องค์ประกอบของเจลของเอสบีเอ-15 ที่มีหมู่เอริลซัลโฟนิกเป็น 0.0369 TEOS: 0.0041 CSPETMS: 0.0369 H_2O_2: 0.24 HCl: 6.9046 H_2O: 0.0007 P123 จากนั้นตรวจสอบลักษณะเฉพาะของวัสดุที่สังเคราะห์ได้ด้วยเทคนิคการเลี้ยวเบนของรังสีเอกซ์ เทคนิคการดูดซับไนโตรเจน การวิเคราะห์ปริมาณซัลเฟอร์ คาร์บอนนิวเคลียร์แมกเนติกเรโซแนนซ์สำหรับสถานะของแข็ง และกล้องจุลทรรศน์อิเล็กตรอนแบบส่องกราด ทดสอบประสิทธิภาพความว่องไวของเอสบีเอ-15 ที่มีหมู่โพรพิลซัลโฟนิกและเอริลซัลโฟนิกด้วยปฏิกิริยาการเตรียมบิสฟีนอลเอฟจากฟีนอลและฟอร์มาลดีไฮด์ภายใต้ภาวะที่แตกต่างกัน ภาวะที่เหมาะสมในการเตรียมบิสฟีนอลเอฟคืออัตราส่วนโมลของฟีนอลต่อฟอร์มาลดีไฮด์เท่ากับ 30 อัตราส่วนระหว่างตัวเร่งปฏิกิริยาต่อฟอร์มาลดีไฮด์เท่ากับ 15% โดยน้ำหนัก ที่อุณหภูมิ 90 องศาเซลเซียส เป็นเวลา 1 ชั่วโมงภายใต้ภาวะที่ไม่มีตัวทำละลาย นอกจากนี้ได้เปรียบเทียบประสิทธิภาพของตัวเร่งปฏิกิริยาที่สังเคราะห์ได้กับตัวเร่งปฏิกิริยาชนิดอื่น ได้แก่ เรซินแลกเปลี่ยนไอออน ซีโอไลต์ และอลูมิเนียม-วัสดุที่มีรูพรุนขนาดกลาง ท่ามกลางตัวเร่งปฏิกิริยาวิวิธพันธุ์พบว่า เอสบีเอ-15 ที่มีหมู่โพรพิลซัลโฟนิกได้แสดงประสิทธิภาพที่ดีเนื่องจากสามารถให้ปริมาณบิสฟีนอลเอฟ 98% และจำเพาะต่อ *4,4'*-ไอโซเมอร์ นอกจากนี้ตัวเร่งปฏิกิริยาที่ปรับสภาพเหมือนใหม่แล้วมีความว่องไวและให้ผลิตภัณฑ์ที่มีสัดส่วนไอโซเมอร์ใกล้เคียงกับที่ได้จากตัวเร่งปฏิกิริยาที่ยังไม่ได้ใช้งาน ด้วยเหตุนี้เอสบีเอ-15 ที่มีหมู่โพรพิลซัลโฟนิกสามารถใช้เป็นตัวเร่งปฏิกิริยาที่มีประสิทธิภาพในการเตรียมบิสฟีนอลเอฟ

สาขาวิชา ปิโตรเคมีและวิทยาศาสตร์พอลิเมอร์ ลายมือชื่อนิสิต .....

ปีการศึกษา 2552 ลายมือชื่ออ.ที่ปรึกษาวิทยานิพนธ์หลัก .....

5072219423: MAJOR PETROCHEMISTRY AND POLYMER SCIENCE
KEYWORDS: SBA-15-Pr-SO_3H / SBA-15-Ar-SO_3H / MPTMS / CSPETMS/ ZEOLITE / BISPHENOL-F

KESSARIN WORAKITTITHAM: SYNTHESIS OF BISPHENOL-F USING SULFONIC FUNCTIONALIZED SBA-15 AS CATALYST. THESIS ADVISOR: DUANGAMOL NUNTASRI, Ph.D., 110 pp.

Sulfonic functionalized SBA-15 catalysts, SBA-15-Pr-SO_3H and SBA-15-Ar-SO_3H, were synthesized by direct synthesis under acidic condition using triblock P123 (poly(ethylene oxide)$_{20}$–poly(propylene oxide)$_{70}$–poly(ethylene oxide)$_{20}$) copolymer as a structure directing agent. The gel composition of SBA-15-Pr-SO_3H was 0.0369 TEOS: 0.0041 MPTMS: 0.0369 H_2O_2: 0.24 HCl: 6.9046 H_2O: 0.0007 P123. In addition, the gel composition of SBA-15-Ar-SO_3H was 0.0369 TEOS: 0.0041 CSPETMS: 0.0369 H_2O_2: 0.24 HCl: 6.9046 H_2O: 0.0007 P123. The synthesized materials were characterized by X-ray powder diffraction, nitrogen sorption analysis, sulfur elemental analysis, solid state ^{13}C-MAS-NMR and scanning electron microscopy. Catalytic performances of SBA-15-Pr-SO_3H and SBA-15-Ar-SO_3H were studied in catalyzing the phenol with formaldehyde to form bisphenol-F under different conditions. The optimum condition on bisphenol-F preparation was phenol to formaldehyde molar ratio of 30 mol mol^{-1}, catalyst to formaldehyde weight ratio of 15 wt% at 90°C for 1 h under the absence of solvent. Furthermore, catalytic activity of the synthesized catalyst was compared with other catalysts such as ion-exchanged resins, zeolites and Al-mesoporous materials. Among various heterogeneous catalysts, SBA-15-Pr-SO_3H exhibited high catalytic activity due to giving high bisphenol-F yield of 98% and selective to *4,4'*-isomer. Moreover, the regenerated catalyst revealed similar activity and performed the product isomer distribution closing to the fresh one. Thus, SBA-15-Pr-SO_3H catalyst was able to be an efficient catalyst for bisphenol-F preparation.

Field of Study: Petrochemistry and Polymer Science Student's Signature .....

Academic Year: 2009 Advisor's Signature .....

ACKNOWLEDGEMENTS

The accomplishment of this thesis can be attributed to the extensive support and assistance from Dr. Duangamol Nuntasri, my thesis advisor. I would like to sincere gratitude to her for valuable advice and guidance in this research as well as extraordinary experiences throughout the work.

I would like to thank sincerely my gratitude to the chairman and the examiners of this thesis committee for all of their comment and useful suggestion about this research.

I would like to gratefully thank Department of Chemistry and Program of Petrochemistry and Polymer Science, Faculty of Science, Chulalongkorn University for the valuable knowledge and experience. I would like to thank Thailand Japan Technology Transfer Project for supporting instruments. Moreover, I deeply appreciate National Center of Excellence for Petroleum, Petrochemicals, and Advanced Materials (NCE-PPAM) for partial lab expense supporting.

Many thanks go in particular to the members of Materials Chemistry and Catalysis Research Unit and my friends for their sincere help and kindness. Finally, I deeply wish to thank my family for their entirely care and understanding during my graduate study.

CONTENTS

CHAPTER **Page**

CHAPTER **Page**

CHAPTER **Page**

CHAPTER **Page**

LIST OF TABLES

Table **Page**

LIST OF FIGURES

Figure **Page**

Figure **Page**

Figure **Page**

LIST OF SCHEMES

Scheme **Page**

LIST OF ABBREVIATIONS

Å	Angstrom
a.u.	Arbitrary unit
BET	Brunauer-Emmett-Teller
BJH	Barret, Joyner, and Halenda
BADGE	bisphenol-A diglycidyl ether
BFDGE	bisphenol-F diglycidyl ether
BPA	Bisphenol-A
BPF	Bisphenol-F
^{o}C	Degree Celsius
CMC	critical micelle concentration
CSPTMS	2-(4-chlorosulfonylphenyl)ethyltrimethoxysilane
DTP	dodocatungstophosphoric acid
GC	Gas chromatography
g	Gram (s)
h	Hour
MAS-NMR	Magic angle spinning-nuclear magnetic resonance
MPTMS	(3-mercaptopropyl)trimethoxysilane
MS	Mass spectroscopy
μm	Micrometer (s)
ml	Milliliter (s)
min	Minute (s)
M	Molarity
nm	Nanometer (s)
%	Percentage
SEM	Scanning electron microscopy
TCD	Thermal Conductivity Detector
TEOS	Tetraethyl orthosilicate
XRD	X-ray diffraction

CHAPTER I

INTRODUCTION

1.1 Background

Bisphenol F, commonly abbreviated as BPF, is an organic compound with two phenolic rings joined together through a methylene bridge. BPF is an industrially important raw material for the preparation of epoxy resins and polycarbonates that are used in the molding, casting, sealing, coating, encapsulating, reinforced plastics and other chemical industries [1-2]. Generally, when the molecular weight of the epoxy resin is increased, physical properties such as flexibility and impact resistance, chemical properties such as solvent resistance and corrosion resistance are improved, but the melt viscosity and solution viscosity of the epoxy resins increases. Hence, epoxy resins need to have lower melt viscosity and solution viscosity to enable reduced volatile content and increased solid resin content when dissolved in a solvent. To decrease using volatile content, incorporating BPF into epoxy resins is an alternative. Bisphenol-F epoxy resin has relatively low viscosity compared with bisphenol-A epoxy resin. Especially, BPF having high content of ortho-ortho isomer and ortho-para isomer will improve melt viscosity and solution viscosity of epoxy resins [3].

BPF is commonly produced by condensation reaction of phenol and formaldehyde in the presence of acid catalyst. It is an isomeric mixture of bis(2-hydroxyphyenyl)methane, bis(4-hydroxyphenyl)methane and 2-hydroxyphenyl-4-hydroxyphenylmethane. In the conventional method, strong inorganic acid solutions such as HCl, H_2SO_4 and H_3PO_4 are used as catalyst for the preparation of BPF. However, using homogeneous acid catalysts will cause several disadvantages such as reactor corrosion and difficulty in catalytic separation. To avoid these problems, heterogeneous catalysts are found to be environmentally friendly. Solid acids offer advantages of easier separation and reusability. From mentioned above,

heterogeneous acid catalysts were suitable for BPF production. Hence, this research will focus on BPF preparation using sulfonic funcationalized SBA-15 mesoporous materials as catalyst.

1.2 Literature reviews

1.2.1 Synthesis of BPF

In the past, General Electric Company studied a method by reacting a methylol urea (e.g. dimethylol urea, monomethylol urea, etc.) with an excess of phenol [4]. Aqueous mixture of the acids, for instance, HCl and 60% water or 50% sulfuric acid and 50% water were preferably employed. However, this invention had many disadvantages, for example: dimethylol urea was unstable, recrystallization from water gave only a limited yield and recovery of the phenol from water was not always easy.

In accordance with *US Patent 4,400,554*, a method by reacting phenol with formaldehyde in a two-phase mixture containing aqueous phosphoric acid was reported by Monsanto Company [5]. This invention reported that using phosphoric acid instead of other mineral acids as the catalyst improved the color, provided high yield with less amount of acid. Moreover, a high ratio of phenol to formaldehyde minimized the by-product formation but greater energy consumption was caused by the greater load of recycled unreacted phenol.

In 1990, Mitsubishi Petrochemical Company reported in *US Patent 4,937,392* that acidic montmorillonite clay was found to be an active catalyst for BPF synthesis [6]. The molar ratio between phenol and formaldehyde was preferably 25:1 in order to get high content of BPF. Moreover, *4,4'*-BPF could be separated from its isomer by recrystallization with solvent. Thus, highly pure *4,4'*-BPF could be prepared on an industrial scale.

In 2002, *US Patent 6,492,566 B1* disclosed an improved process for the preparation of BPF by reacting phenol with formaldehyde over zeolite catalysts and in the present of methyl ethyl ketone as a solvent at a temperature of 80°C for 3 h. This invention reported that Zeolite H-beta was preferable for both with and without solvent and it provided high phenol conversion and the highest selectivity to *4,4'*-BPF. The advantages of this invention are as follows: a corrosion free plant, and a recyclable zeolite catalyst, no disposal of inorganic by product, higher amounts of *4,4'*-BPF, and greater merit for industrial application due to available and easy-to-handle starting materials [7].

In 2003, mesoporous aluminosilicate Al-MCM-41 catalyst was found to be an effective catalyst for BPF synthesis as reported by Namba et al. [8]. Al-MCM-41 catalysts (Si/Al = 50) were prepared by four difference methods: sol-gel, template-cation exchange using hexadecyltrimethylammonium bromide as surfactant template at 90 °C, hydrothermal and grafting method. They investigated that Al-MCM-41 prepared by grafting method exhibited the highest activity in the BPF synthesis process.

In 2004, Namba *et al*. reported that among the different Al-grafted MCM-41 molecular sieves (having Si/Al ratios from 15 to 200), Al-MCM-41 having a Si/Al ratio of 70 performed the best catalytic performance in the BPF synthesis process which gave the highest yield of 93.1% at 90 °C for 4 h with the phenol to formaldehyde molar ratio of 30 and catalyst to formaldehyde weight ratio of 15 % [9].

In 2006, Namba *et al*. synthesized BPF from the liquid-phase phenol and formaldehyde condensation reaction in the presence of water over microporous zeolite beta with different Si/Al ratios. They investigated that the beta zoelite catalyst with the Si/Al mole ratio of 75 showed the best catalytic performance in the BPF synthesis process which gave the highest yield of 91.2% at 90 °C for 1 h with the phenol to formaldehyde molar ratio of 30 and catalyst to formaldehyde weight ratio of 15 % [2].

In 2009, Rode *et al*. investigated the catalytic activities of various solid acids, such as fumed silica (SiO_2), dodocatungstophosphoric acid (DTP), DTP impregnated on SiO_2, Amberlyst-15 and montmorillonite KSF/0 in BPF preparation. Among the various acid catalysts, 20% DTP/SiO_2 was found to be an effective catalyst for BPF, giving the highest products yield of 34.2% and selectivity of 90.1% to BPF, at 80 ºC for 1 h with a phenol to formaldehyde molar ratio of 5 [10].

Recently, they studied catalytic activity of DTP impregnated on montmorillonite K10 in BPF preparation. Among various loadings of DTP (5-60%), they found that 20% DTP/montmorillonite K10 performed the highest catalytic activity (90% selectivity to BPF with 28% conversion of phenol) at 80°C for 40 min with phenol to formaldehyde molar ratio of 5 [11].

1.2.2 Sulfonic functionalized SBA-15

Melero *et al*. invented the new procedure in the preparation of sulfonic functionalized mesostructure materials. In 2000, they improved the direct synthesis method to create propyl sulfonic functionalized SBA-15 (SBA-15-Pr-SO_3H) [12]. This procedure involved an one-step strategy based on the co-condensation of tetraethyl orthosilicate (TEOS) and (3-mercaptopropyl)trimethoxysilane (MPTMS) in the presence of Pluronic P123 and hydrogen peroxide in HCl aqueous solution. This approach allowed in-situ oxidation of the thiol groups to sulfonic acid groups.

In 2002, Melero *et al*. used the same route for the preparation of ordered SBA-15 containing aryl sulfonic acid groups [13]. The synthesis strategy involved the co-condensation of 2-(4-chlorosulfonylphenyl)ethyltrimethoxysilane (CSPETMS) and TEOS using Pluronic P123 as template under acidic conditions. Hydrolysis of the chlorosulfonyl groups (-$SOCl_2$) to the corresponding sulfonic acid groups was achieved under acidic condensation reaction. The resultant material showed large uniform pore sizes (*ca.* 60 Å) with large surface areas (*ca.* 650 m^2/g), good mesoscopic ordering, and thick walls.

Nowadays, the attachment of organic functionalities to the surface of the SBA-15 mesoporous material by direct method has been used as catalyst in a wide range of acid catalyzed reactions such as esterification and etherification except for BPF preparation [14-17]. From this viewpoint, this research will be studied on catalytic activity of synthesized sulfonic functionalized SBA-15 in BPF synthesis.

1.3 Objective

To investigate the optimum condition in synthesis of BPF using sulfonic functionalized SBA-15 catalyst.

1.4 Scopes of work

1. Synthesize SBA-15-Pr-SO_3H and SBA-15-Ar-SO_3H by direct method.
2. Characterize all prepared catalysts.
3. Determine the optimum condition of BPF synthesis by studying the effect of reaction time, phenol to formaldehyde mole ratio, catalyst to formaldehyde weight ratio, reaction temperature and solvent.
4. Compare catalytic activities of synthesized catalysts with other commercial catalysts.

CHAPTER II

THEORY

2.1 Catalysts

A catalyst is a substance that increased the rate of a chemical reaction by reducing the activation energy (E_a) as shown in Figure 2.1. The highest peak position performing the highest energy refers to the transition state. In typically reaction, the energy required to enter the transition state is high, whereas the energy to transition state decreases in catalytic reaction. In addition, the catalyst may participate in multiple chemical transformations and is not consumed by the reaction.

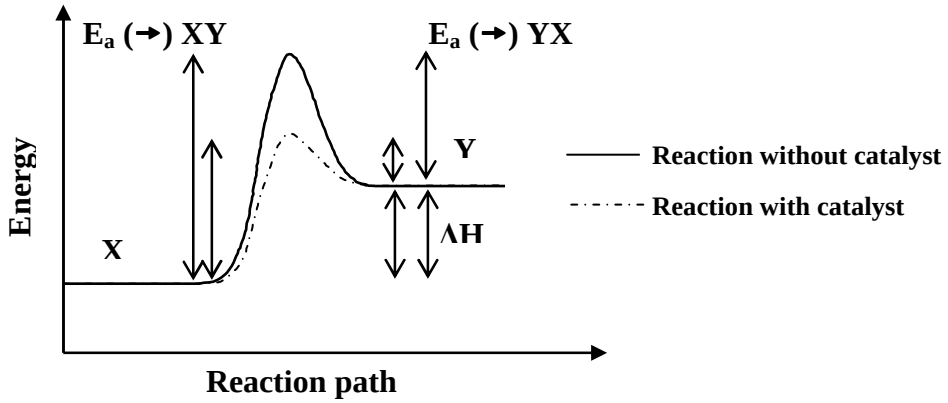

Figure 2.1 The relationship between activation energy (E_a) and enthalpy (ΔH) of the reaction with and without a catalyst [18].

2.2 Properties of industrial catalysts

In general, the suitable catalysts for industrial processes are considered mainly on the three properties [19]:

a) Activity is a measure of how fast one or more reactions proceed which can be defined in terms of kinetics. A high activity catalyst will be given high productivity

when the less amount of the catalyst is utilized or the reaction is performed in mild operating condition, particularly temperature, which enhances selectivity and stability if the thermodynamic is more favorable. It is appropriate to measure reaction rates in the temperature that will be occurred in the reactor.

b) Selectivity of a reaction is the fraction of the starting material that is converted to the expected product. High selectivity catalyst produces high yield of a desired product, whereas undesirable competitive and consecutive reactions are suppressed. This means that the texture of the catalyst (in particular pore size and pore volume) should be improved toward reducing limitation by internal diffusion, which in case of consecutive reactions rapidly reduces selectivity.

c) Stability of a catalyst determines its lifetime in industrial processes. Catalyst stability is influenced by various factors such as decomposition, coking and poisoning. Catalyst deactivation can be followed by measuring activity or selectivity as a function of time. Deactivated catalysts can often be regenerated before they ultimately have to be replaced. The catalyst lifetime is a crucial importance for the economics of process.

Nowadays, the efficient use of raw materials and energy is of major importance, and it is preferable to optimize existing processes than to develop new ones. For various reasons, the target quantities should be given the following order of priority:

Selectivity > Stability > Activity

2.3 Type of the catalysts

Catalysts can be classified into two main types by the boundary of the catalyst and the reactant. Heterogeneous reaction, the catalyst is in a different phase from the reactants, whereas the catalyst in the same phase of reactant is called homogeneous reaction. Thus, the solid catalysts are identified as heterogeneous catalysts, and the liquid catalysts are specified as homogeneous catalysts when assume reactant is liquid. Homogeneous catalysts have a higher degree of dispersion than heterogeneous

catalysts only the surface atoms are active [19]. Summary of the advantage and disadvantage of two-type catalyst is presented in Table 2.1.

Table 2.1 Comparison of homogeneous and heterogeneous catalysts

Consideration	**Homogeneous catalyst**	**Heterogeneous catalyst**
1. Active centers	All metal atoms	Only surface atoms
2. Concentration	Low	High
3. Selectivity	High	Low
4. Diffusion problems	Practically absent	Present (mass-transfer-controlled reaction)
5. Reaction conditions	Mild (50-200°C)	Severe (often >250°C)
6. Applicability	Limited	Wide
7. Activity loss	Irreversible reaction with product (cluster formation), poisoning	Sintering of the metal crystallites, poisoning
8. Structure/ Stoichiometry	Defined	Undefined
9. Modification possibility	High	Low
10. Thermal stability	Low	High
11. Catalyst separation	Sometimes laborious (chemical decomposition, distillation, extraction)	Fixed-bed: unnecessary Suspension: filtration
12. Catalyst recycling	Possible	Unnecessary (fixed-bed) or easy (suspension)
13. Cost of catalyst losses	High	Low

The major disadvantage of homogeneous catalyst is the difficulty of separating the catalyst from the product. Heterogeneous catalysts are either automatically removed in the process (*e.g.* vapor-phase reaction in fixed bed reactor) or separated by simple methods such as filtration or centrifugation. However, in more complicated

processes, distillation, liquid-liquid extraction and ion exchange are necessarily used homogeneous catalysts.

2.4 Porous molecular sieves

Molecular sieves are porous materials that exhibit selective adsorption properties which can be classified on the IUPAC definitions into three main types depending on their pore sizes that are microporous materials, mesoporous materials, and macroporous materials. Properties and examples of these materials are shown in Table 2.2.

Table 2.2 IUPAC classification of porous materials

Type of porous molecular sieve	Pore size (Å)	Examples
Microporous materials	< 20	Zeolites, Activated carbon
Mesoporous materials	20 – 500	M41s, SBA-15, Pillared clays
Macroporous materials	> 500	Glasses

2.4.1 Zeolite structures

Zeolites, a type of molecular sieves, are crystalline aluminosilicates that contain uniform pores and cavities with molecular dimensions. A zeolite has a three dimensional network structure of tetrahedral primary building unit (PBU) which consists of four oxygen anions with either silicon [SiO_4] or aluminum cation [AlO_4]$^-$ in the center as shown in Figure 2.2.

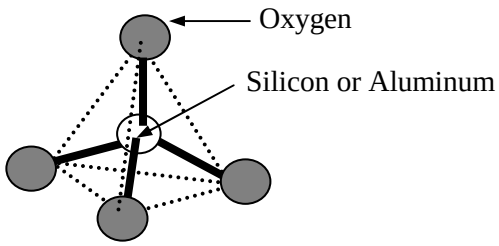

Figure 2.2 A primary building unit of porous materials [20].

A secondary building unit (SBU) consists of selected geometric groupings of those tetrahedral. There are sixteen such building units, which can be used to describe all of the known porous materials structures; for example, 4, 5, 6 and 8-member single rings, 4-4, 6-6, and 8-8-member double rings, and 4-1, 5-1 and 4-4-1 branched rings. The secondary building units (SBU) are illustrated in Figure 2.3.

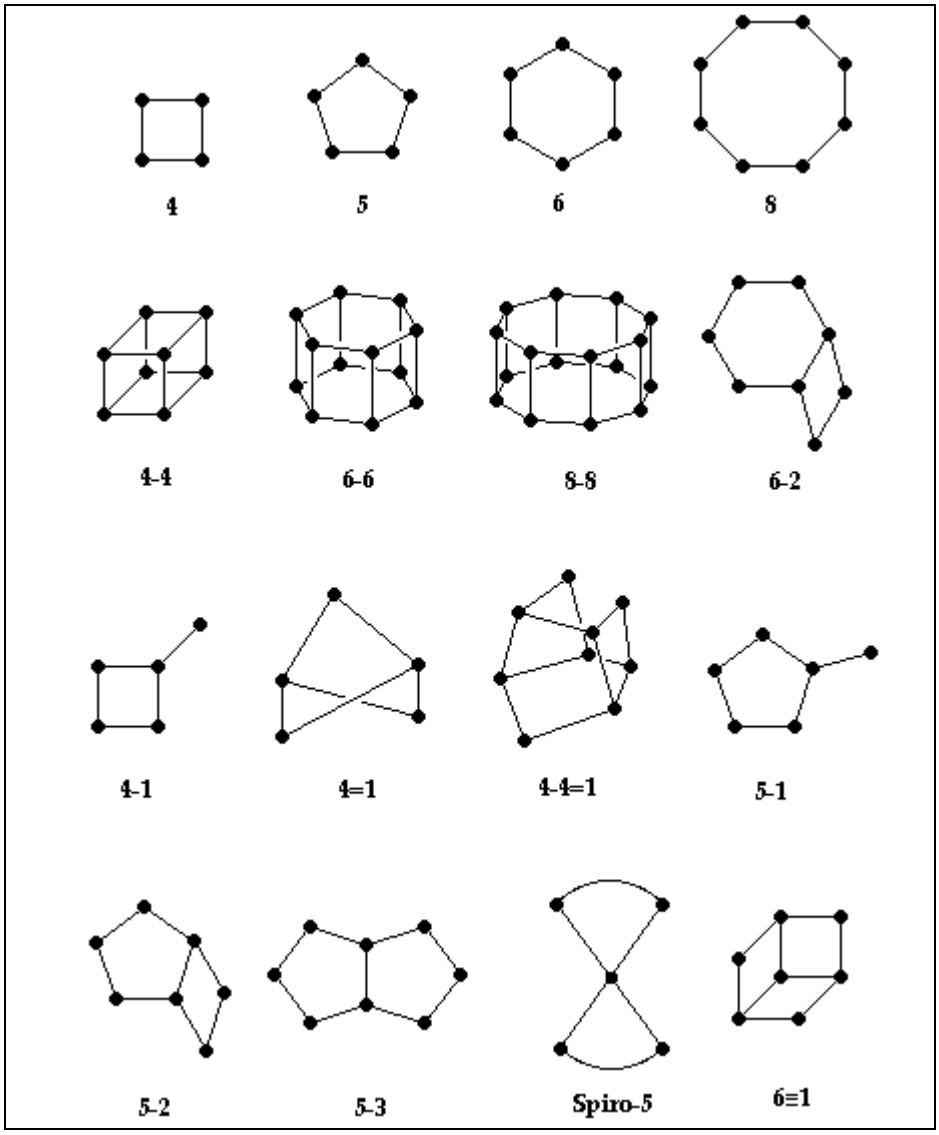

Figure 2.3 Secondary building units (SBUs) in zeolites [21].

The tetrahedrons are mutually connected by sharing oxygen atom as shown in Figure 2.4 which produces the framework of zeolite. The negative charge of the lattice is neutralized by the positive charge of the metal cations. In the basic zeolites these are usually cation of univalent and bivalent metals or their combination. The general formula for the composition of zeolite is

$$M_{x/n}\,[(AlO_2)_x\,(SiO_2)_y].\ w\ H_2O$$

Where M is the cation of valence n, generally from the group I or II ions, although other metals, nonmetals, and organic cations are also possible, w is the number of water molecules. Water molecules are located in the channels and cavities, as the cations that neutralize the negative charge created by the presence of the AlO_2^- tetrahedral unit in the structure.

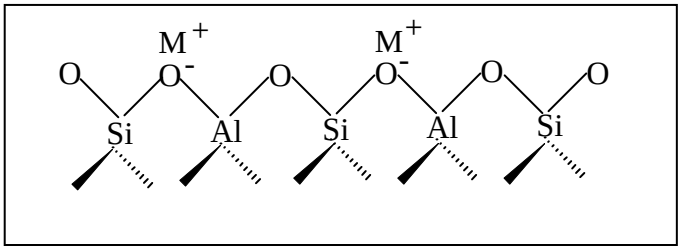

Figure 2.4 The structure of zeolites [20].

The different ring sizes found in zeolites, based on the different number of tetrahedral atoms defining the opening, are shown in Figure 2.5. The ring sizes are often mentioned as the number of oxygen atoms which are equal to the number of tetrahedral atoms.

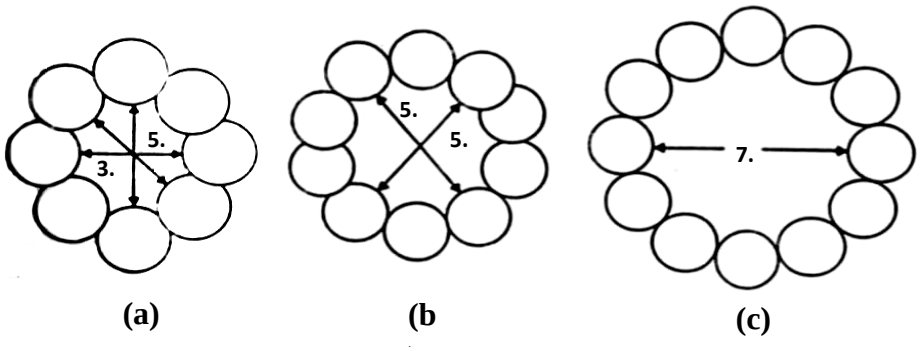

Figure 2.5 Examples of the three types of pore openings in the porous material molecular sieves (a) an 8 ring pore opening (small pore), (b) a 10 ring pore opening (medium pore) and (c) a 12 ring pore opening (large pore) [20].

2.4.2 Properties of zeolites

2.4.2.1 Shape and size selectivity of porous materials

Shape and size selectivity presents a very important role in catalysis. Highly crystalline and regular channel structures are among the principal features that porous material used as catalysts offer over other materials. Shape selectivity is divided into 3 types: reactant shape selectivity, product shape selectivity and transition-state shape selectivity. These types of selectivity are shown in Figure 2.6. Reactant shape selectivity results from the limited diffusivity of some reactants, which cannot effectively enter and diffuse inside the porous materials. Product shape selectivity occurs when diffusing product molecules cannot rapidly escape from the crystal, and undergo secondary reactions. Restricted transition-state shape selectivity is a kinetic effect arising from the local environment around the active site: the rate steady for a certain reaction mechanism is reduced if the necessary transition state is too bulky to form readily.

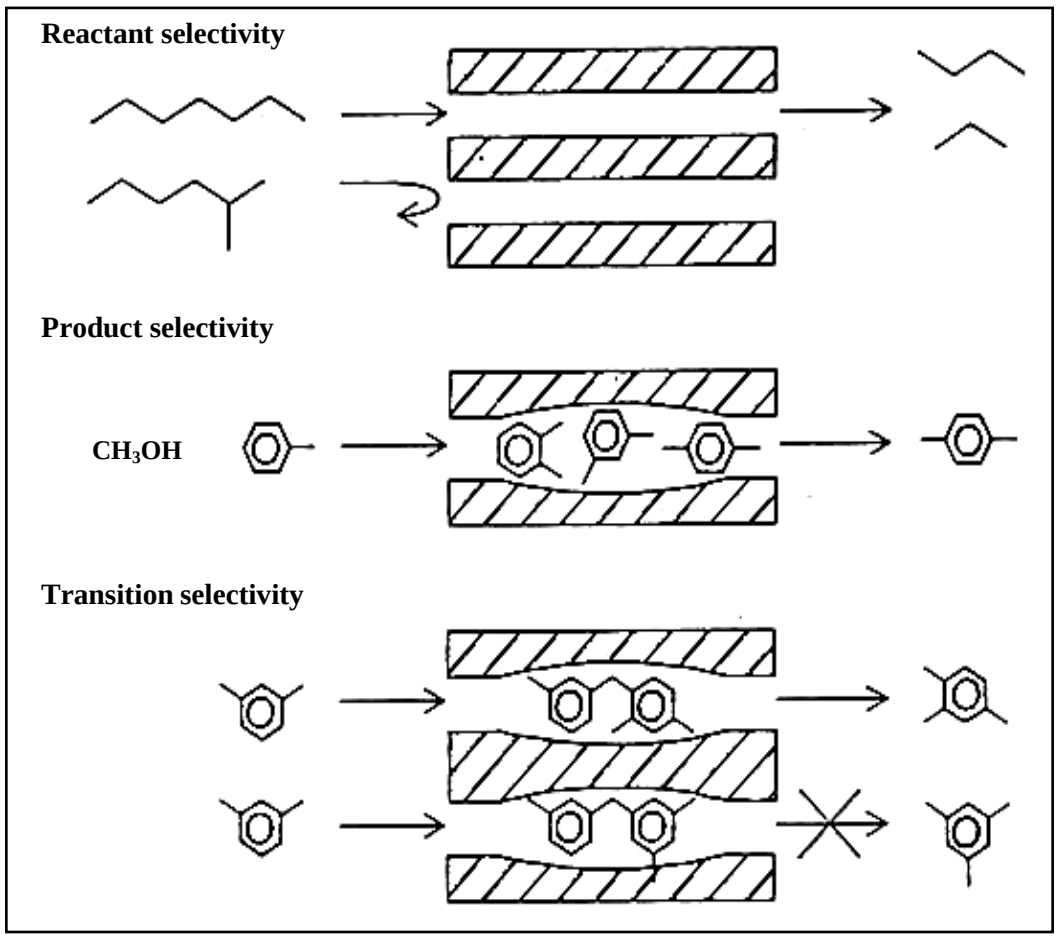

Figure 2.6 Three types of selectivity in porous materials: reactant, product and transition-state shape selectivity [22].

2.4.2.2 Acid sites of zeolites

In addition to the shape and size selective catalysis, the generation of acidic sites in the zeolite pores leads to a highly efficiency in solid-acidic catalysis. The isomorphous replacement of silicon atom with aluminum atom in a tetrahedral site gives rise to a charge imbalance because aluminum atom has lower coordination ability than silicon atom and must be neutralized. This is achieved in two ways in natural zeolites:

- The length of Al-O bond becomes slightly longer.
- A coordination site is made avail for cation to counter the excess negative charge.

In natural zeolites, the excess negative charge is balanced by various cations are present in the neighboring environment *e.g.* K^+, Na^+, Mg^{2+} and Ca^{2+} as exhibited in Figure 2.7 and Figure 2.8. The type of counter ion used to balance the charge plays an important part in the use of the zeolite. For uncomplicated understanding, the cation is replaced with a proton by hydrothermal treatment to form a hydroxyl group at the sharing oxygen atom. The acid site formed behaves as a classic Brønsted, proton donating acidic site as shown in Figure 2.9.

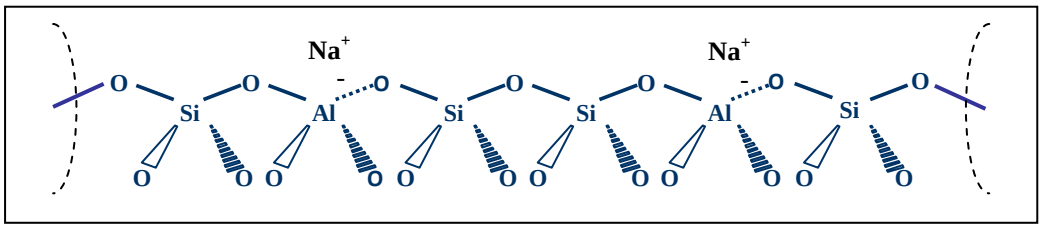

Figure 2.7 Sodium balanced zeolite framework [23].

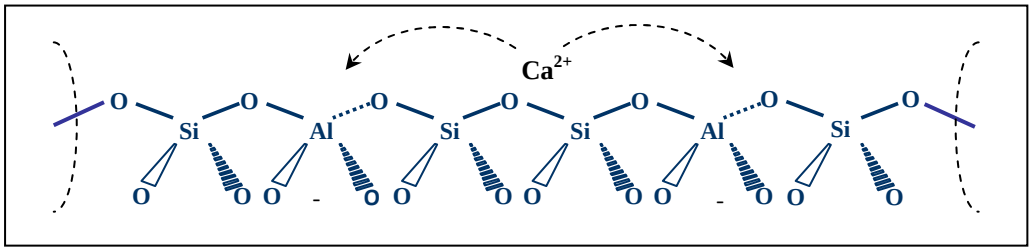

Figure 2.8 Calcium balanced zeolite framework [23].

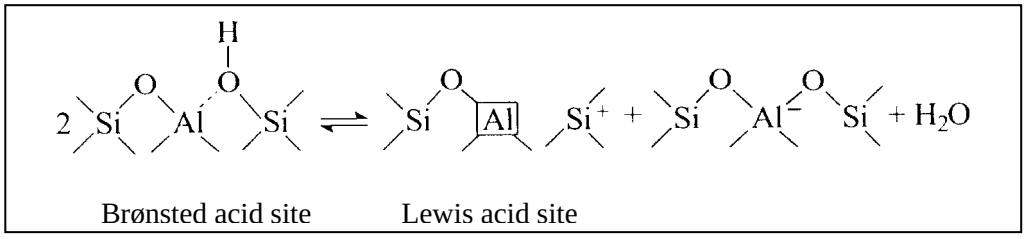

Figure 2.9 Brønsted and Lewis acid sites in zeolites [19].

The highly acidic sites combined with the high selectivity arising from shape selectivity and large internal surface area makes the zeolite as an ideal industrial catalyst. The significance of this acidic proton can be shown easily by comparisons of the experiments in H^+-exchanged zeolites and their equivalent cations from zeolite. For example, the methanol-to-gasoline (MTG) process is highly depended on the presence of the Brønsted proton. If the H-ZSM-5 catalyst is replaced by the purely siliceous analogue of ZSM-5, it has no Brønsted protons, the reaction does not take place at all. Therefore, the modification of zeolite structure can be increased their activity, which are very economically important step for industry.

2.5 Mesoporous materials

Mesoporous materials are a type of molecular sieves, such as silicas or transitional aluminas or modified layered materials such as pillared clays and silicates. Mesoporous silica has uniform pore sizes from 20 to 500 Å and has found great utility as catalysts and sorption media because of the regular arrays of uniform channels. Larger surface area is desired for enhancing of the efficient in the reactions [24].

2.5.1 Classification of mesoporous materials

Mesoporous materials can be classified by different synthetic methods. By varying different types of templates used and pH of gel, synthesizing hexagonal mesoporous materials can be obtained. The interaction of various types of template with inorganic species for assembling these materials are different as summarized in Table 2.3, together with the condition typically employed for a synthesis [24-26].

Table 2.3 Various synthesis conditions of hexagonal mesoporous materials and the types of interaction between templates and inorganic species

Materials	Template	Assembly	Solution
MCM-41	Quaternary ammonium salt	Electrostatic	base or acid
FSM-16	Quaternary ammonium salt	Electrostatic	base
SBA-15	Amphiphilic triblock copolymer	H- bonding	acid (pH<2)
HMS	Primary amine	H- bonding	neutral

MCM-41 and FSM-16 can be synthesized using quaternary ammonium salt as a template. In case of SBA-15, amphiphilic tribock copolymer can be modified as a template and must be synthesized in acidic condition of hydrochloric acid. On the other hand, HMS can be prepared in neutral and environmentally benign condition using primary amine as a template. Although these materials have the same hexagonal structure, some properties are different as shown in Table 2.4.

Table 2.4 Properties of some hexagonal mesoporous materials

Material	Pore size (Å)	Wall thickness (nm)	BET specific surface area (m^2/g)	Framework structure
MCM-41	15-100	1	>1000	Honey comb
FSM-16	15-32	-	680-1000	Folded sheet
SBA-15	46-300	3-6	630-1000	Rope-like
HMS	29-41	1-2	640-1000	Wormhole

2.5.2 Synthesis schemes of mesoporous materials

Crystalline molecular sieves are generally obtained by hydrothermal crystallization. The reaction gel, usually, contains cations (*e.g.* Si^{4+} for silicate materials, Al^{3+} for aluminate materials) to form the framework; anionic species (*e.g.* OH^- and F^-); organic template and solvent (generally water). Typically, the nature of

template can be considered into two parts that are hydrophobic tail on the alkyl chain side and hydrophilic head on the other side. The examples of templates used are primary, secondary tertiary and quaternary amines, alcohols, crown or linear ethers, and as well as polymers. An understanding of how organic molecules interact with each other and with the inorganic frameworks would increase the ability to design rational routes to molecular sieve materials. The organic templates are frequently occluded in the pores of the synthesized material, contributing to the stability of mineral backbone.

2.5.2.1 The behavior of surfactant molecules in an aqueous solution

In a simple binary system of water-surfactant, surfactant molecules can aggregate to form micelles in various types at a particular concentration. The shapes of micelle depend on the concentrations as shown in Figure 2.10.

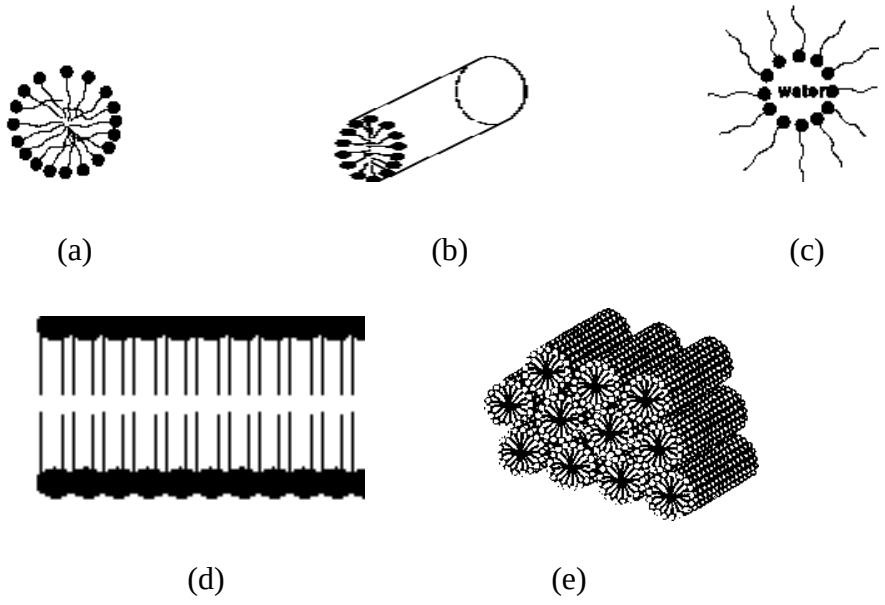

Figure 2.10 Phase sequence of the surfactant-water binary system (a) spherical micelle, (b) rod-shaped micelle, (c) reverse micelle, (d) lamellar phase, and (e) hexagonal phase [27].

At low concentration, they energetically exist as isolated molecules. With increasing concentration, surfactant molecules aggregate together to form isotropic spherical and rod shaped micelles by directing the hydrophobic tails inside and turning the hydrophilic heads outside in order to decrease the system entropy. The initial concentration threshold at which those molecules aggregate to form isotropic micelle is called critical micelle concentration (CMC). The CMC determines thermodynamic stability of the micelles. When the concentration is continuously increased, the micellar shape changes from sphere or rod shapes to hexagonal, lamellar, and inverse micelles. The particular phase present in a surfactant aqueous solution depends not only on the concentrations but also on the natural of surfactant molecules such as its length of the hydrophobic carbon chain, hydrophilic head group, and counter ion. Besides the ionic strength, pH value, and temperature including other additives are the factors determining the shape of micelles.

2.5.2.2 Interaction between inorganic species and surfactant micelles

A number of models have been proposed to explain the formation of mesoporous materials and to provide a rational basis for synthesis routes [27]. On the common level, these models are predicted upon the presence of surfactants in a solution to direct the formation of inorganic mesostructure from stabilized inorganic precursors. The type of interaction between the surfactant and the inorganic species is significantly different depending on the various synthesis routes as shown in Table 2.5.

Table 2.5 Example routes for interactions between the surfactant and the inorganic soluble species

Surfactant type	Inorganic type	Interaction type	Example materials
Cationic (S^+)	I^-	S^+I^-	MCM-41, MCM-48
	I^+X^-	$S^+X^-I^+$	SBA-1, SBA-2, zinc phosphate
	I^0F^-	$S^+F^-I^0$	silica
Anionic (S^-)	I^+	S^-I^+	Al, Mg, Mn, Ga
	I^-M^+	$S^-M^+ I^-$	alumina, zinc oxide
Neutral S^0 or N^0	I^0	S^0I^0 or N^0I^0	HMS, MSU-X, aluminum oxide
	I^+X^-	$S^0X^-I^+$	SBA-15

Where S^x or N^x : surfactant with charge of X

I^x : inorganic species with charge of X

X^- : halogenide anions

F^- : fluoride anion

M^{n+} : with charge of X

Using ionic surfactant (S^+ and S^-), the hydrophilic head mainly binds with inorganic species through electrostatic interactions. There are two possible formation routes. Firstly, direct pathway: surfactant and inorganic species of which charges are opposite interact together directly (S^+I^- and S^-I^+). Another is the indirect pathway, occurring when the charges of surfactant and inorganic species are the same, so the counter ions in solution get involved as charge compensating species for example the $S^+X^-I^+$ path takes place under acidic conditions, in the present of halogenide anions ($X^- = Cl^-$ or Br^-) and the $S^-M^+ I^-$ route is the characteristic of basic media, in the existence of alkaline cation ($M^+ = Na^+$ or K^+). Figure 2.11 shows the possible hybrid inorganic-organic interfaces.

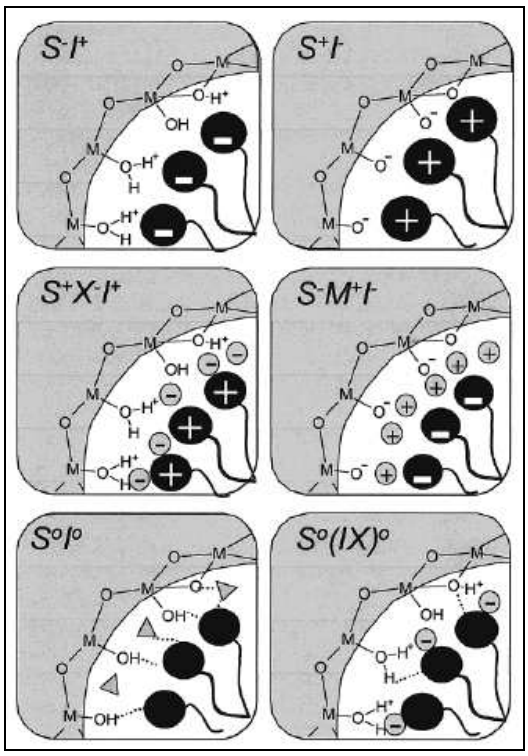

Figure 2.11 Schematic representation of the different types of silica-surfactant interfaces. Dashed line corresponded to H-bonding interactions [27].

In case of non-ionic surfactant (S^0 or N^0), the main interaction between template and inorganic species is hydrogen bonding or dipolar, which is called neutral path i.e. S^0I^0 and $S^0F^-I^+$. Nowadays, non-ionic surfactants give important commercial advantages in comparison to ionic surfactants because they are easily removable, nontoxic, biodegradable and relatively cheap.

2.5.2.3 Formation mechanism of mesoporous materials

Mechanism of mesoporous formation can be classified on the basis of synthetic route into three types exhibited in Figure 2.12:

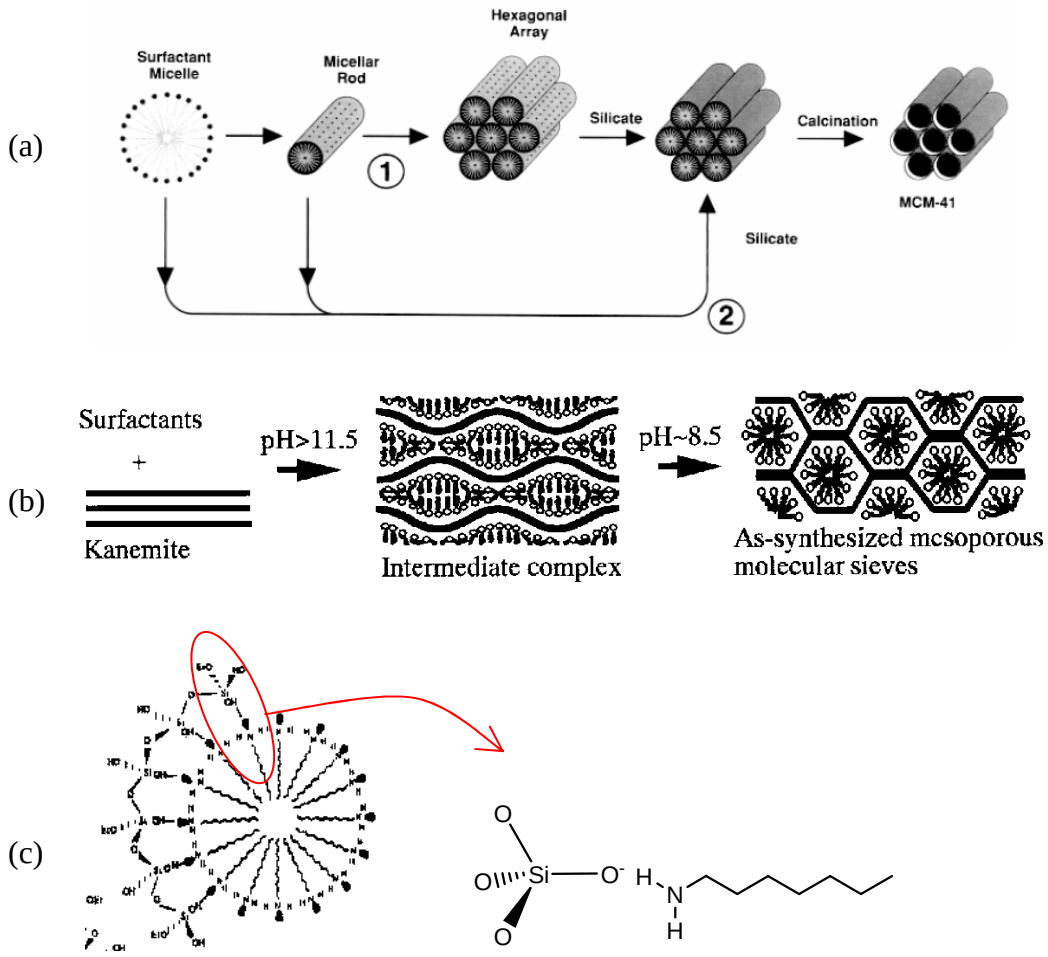

Figure 2.12 Mechanism of mesoporous formation (a) LCT of MCM-41 formation, (b) Folding sheet formation of FSM-16 and (c) H-bonding interaction in HMS formation [28-29]

(a) *Liquid crystal Templating mechanism*: *i.e.* MCM-41. From Figure 2.12(a) there are two main pathways; firstly, liquid crystal phase is intact before silicate species are added or another pathway is the addition of the silicate results in the ordering of the subsequent silicate-encased surfactant micelles.

(b) *Folding sheet formation*: *i.e.* FSM-16. The intercalation of ammonium surfactant into hydrate sodium silicate, which composes of single layered silica sheets called "kanemite" (ideal composition $NaHSi_2O_5.3H_2O$), produces the lamellar-to-hexagonal phase in FSM-16. After the surfactants are ion exchanged into layered structure, the silicate sheets are thought to fold around the surfactants and condense into a hexagonal structure.

(c) *Hydrogen-bonding interaction*: The neutral templating produces mesoporous materials with thicker walls and higher thermal stability as compared to the LCT-derived silicates.

2.5.3 Synthesis strategy of mesoporous material using block-copolymer as structure directing agent

In the synthesis of mesoporous materials such as MCM-41, FSM-16 ionic surfactant *i.e.* the cationic, alkyltrimethyl ammonium (C_nTA^+, $8<n<18$), and anionic surfactant, tertiary amine ($C_nH_{2n+1}N^+(CH_3)_3$) are used as template, respectively. These syntheses are done in extreme (alkaline) pH condition and the obtained materials have pore size in the range of 15 to 100 Å only. However, by this mean, two limitations occur:

(1) The lower stability of the obtained materials: due to the thinner pore wall of materials (8-13 Å).

(2) Difficult to expanding the pore size: the ionic surfactants give a limited pore size. The only way to expand the pore size is in employing swelling agents such as 1,3,5-trimethyl benzene, involving complicate synthesis.

Thus, the block copolymer has been used to solve these problems. Generally, amphiphilic block copolymer has been used in the field of surfactants, detergent manufacturing, emulsifying, coating, etc. The properties of block copolymer can be continuously tuned by adjusting solvent composition, molecular weight, or type of polymers. Figure 2.13 shows typical block copolymer used as templates.

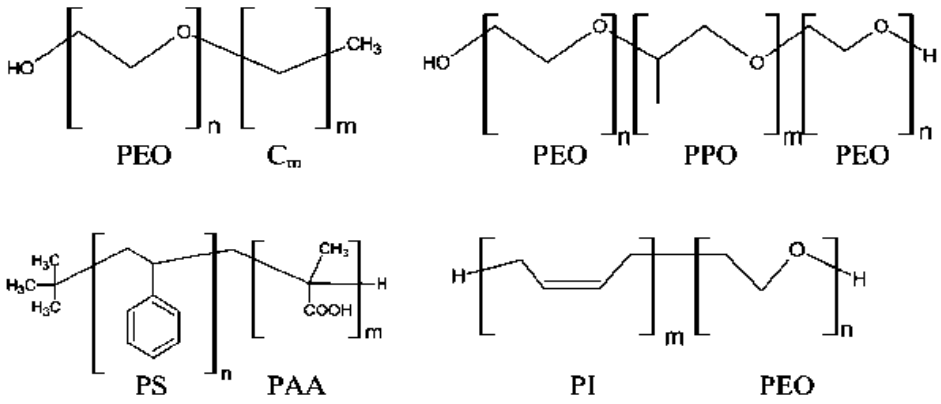

Figure 2.13 Block copolymer used in mesostructured generation [30].

Some advantages of using these block copolymer are:

(1) *The thicker wall thickness* (about 15-40 Å), enhancing hydrothermal and thermal stability of materials.

(2) *Pore diameter can be tuned easier* by varying type or concentration of polymer.

(3) *Easier to remove from mineral framework* by thermal treatment or solvent extraction. Due to the hydrogen bonding interaction between template and inorganic framework, therefore, it should be easier to dissociate as compared to ionic templates (electrostatic interaction).

Interaction between block copolymer template and inorganic species, calls hybrid interphase (HI), is particularly important, especially in PEO-PPO based one. Different possible interactions take place at the HI are schematized in Figure 2.14. Most of the fine HI characterization has been performed on PEO-based (di or triblock) templates. Melosh *et al*. [31] determined that in F127-templated silica monoliths, organization arose for polymer weight fractions higher than 40%. For lower polymericsilica ratios, non-ordered gels were formed. This lack of order was due to a relatively strong interaction (probably of H-bonding type) of the (Si-–O–Si) polymers forming the inorganic skeleton with both PEO and PPO blocks.

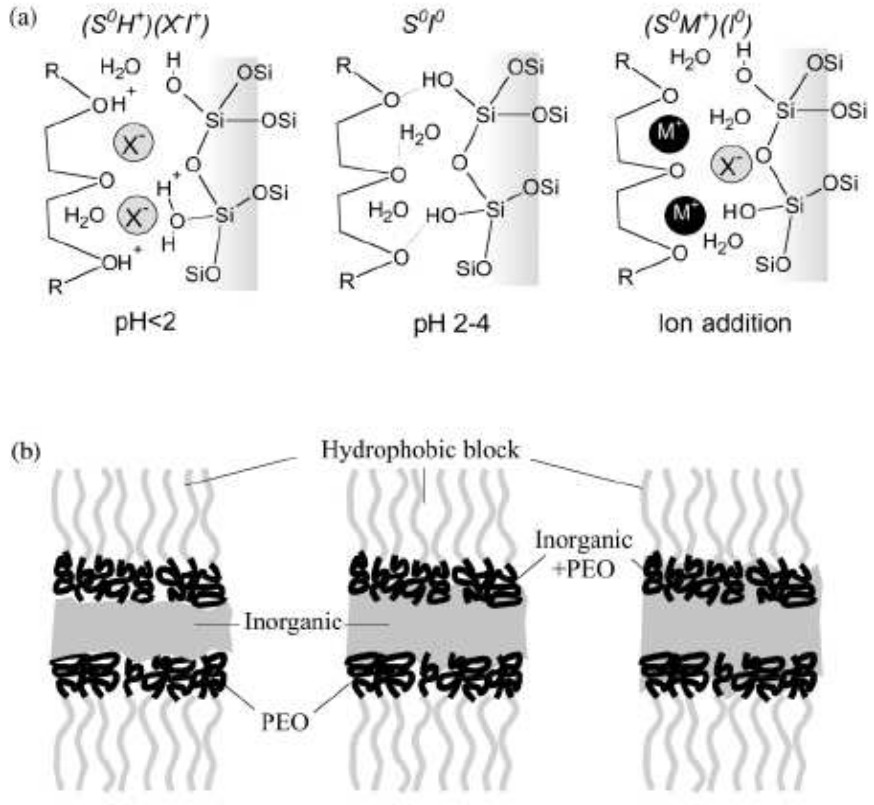

Figure 2.14 (a) Schematic view of the $(S^0H^+)(X^-I^+)$, S^0I^0, and $(S^0M^+)(X^-I^0)$ hybrid interphases (HIs) (b) Three possible structures of a HI composed by a nonionic polymer and an inorganic framework [31].

2.6 SBA-15

2.6.1 Structure and properties of SBA-15

SBA-15 mesoporous material has been synthesized under acidic condition using triblock copolymer as a structure directing agent. This mesoporous material has shown higher hydrothermal stability as compared to MCM-41 due to its thicker pore walls (3.1-6.4 nm). They also posses uniform and hexagonal-structured channel similar to MCM-41 with larger pore size which make them more desirable to deal with bulky molecule. Some properties of MCM-41 and SBA-15 are compared as described in Table 2.6. According to the properties listed in Table 2.6, SBA-15 shows a better performance than MCM-41 in almost of properties.

Table 2.6 Comparison of two well-known mesoporous materials, MCM-41 and SBA-15 in their characteristic properties [28,32]

Properties	**MCM-41**	**SBA-15**
Pore size (Å)	20-100	46-300
Pore volume (mL/g)	>0.7	0.8-1.23
Surface area (m^2/g)	>1000	690-1040
Wall thickness (Å)	10-15	31-64

2.6.2 Synthesis of SBA-15 and formation mechanism

For SBA-15 materials, aging time and temperature are particularly important. Some research found that mesoporous SBA-15 prepared from calcination of an ‘as-prepared’ hybrid precursor contained a significant fraction of microporosity; further aging of the precursor in the mother liquors leads to an improvement on the pore size distribution (Figure 2.15), in agreement with the first work by Stucky *et al*. [32].

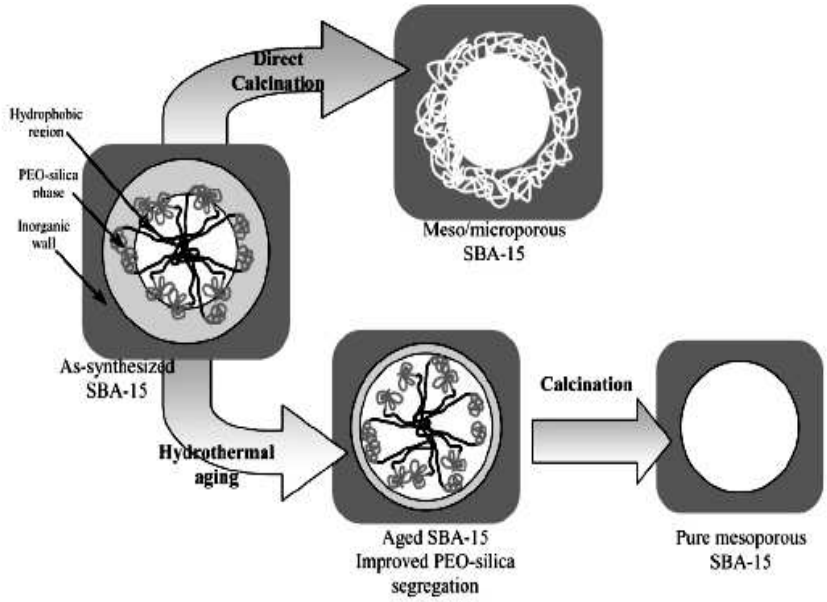

Figure 2.15 Pore evolution upon thermal treatment, depending on pre-treatment and aging [30].

Aging of an as-prepared precipitate at 80–100°C seems to help segregation of the PEO blocks and the inorganic framework, by promoting condensation of the latter. High temperatures also change the polymer behavior. It is known that for T >60°C, PEO blocks become less hydrophilic and expel water similar to PPO blocks when the temperature is higher than 40°C [30]. For a mechanism, firstly alkoxysilane species (TMOS or TEOS) are hydrolyzed as:

$$Si(OEt)_4 + nH_3O^+ \xrightarrow[pH<2]{\text{hydrolysis}} Si(OEt)_{4-n}(H_2O^+)_n + n\ EtOH$$

This is followed by partial oligomerization at the silica. Furthermore, at this condition, the PEO parts of surfactant associate with hydronium ions as followed:

$$-PEO_m- + yHX \xrightarrow{H_2O} -PEO_{m-y}[(EO)\cdot 3H_2O^+]_y \text{---} X_y^-$$

Next, coordination sphere expansion around the silicon atom by anion coordination of the form $X^-SiO_2^+$ may play an important role. The hydrophilic PEO blocks are expected to interact with the protonated silica and thus be closely associated with the

inorganic wall. During the hydrolysis and condensation of the silica species, intermediate mesophase is sometimes observed and further condensation of silica species and organization of the surfactant and inorganic species result in the formation of the lowest energy silica-surfactant mesophase structure allowed by solidifying network.

2.7 Modification of catalysts

Nowadays, the attachment of organic functionalities such as sulfonic acid groups to the surface of siliceous SBA-15 mesoporous material is an interesting research area in heterogeneous catalysis and green chemistry. Basically, two strategies have been generally used to anchor organic groups onto a mesostructured silica surface.

2.7.1 Direct synthesis

Direct synthesis consists of the co-condensation of siloxane and organosiloxane precursors in the presence of the corresponding structure-directing agent.

The preparation of sulfonic-acid modified mesostructured materials is illustrated in Figure 2.16. This method is simplicity, because the incorporation of the organic precursor and the formation of the mesoporous material occur in a single synthetic step. To have a useful catalyst after synthesis, one must be able to extract the template from within the pores to create porosity. Calcination the synthetic material will destroy the incorporated organic functional groups. Extraction technique can be most effectively accomplished by ethanol solution [33-35].

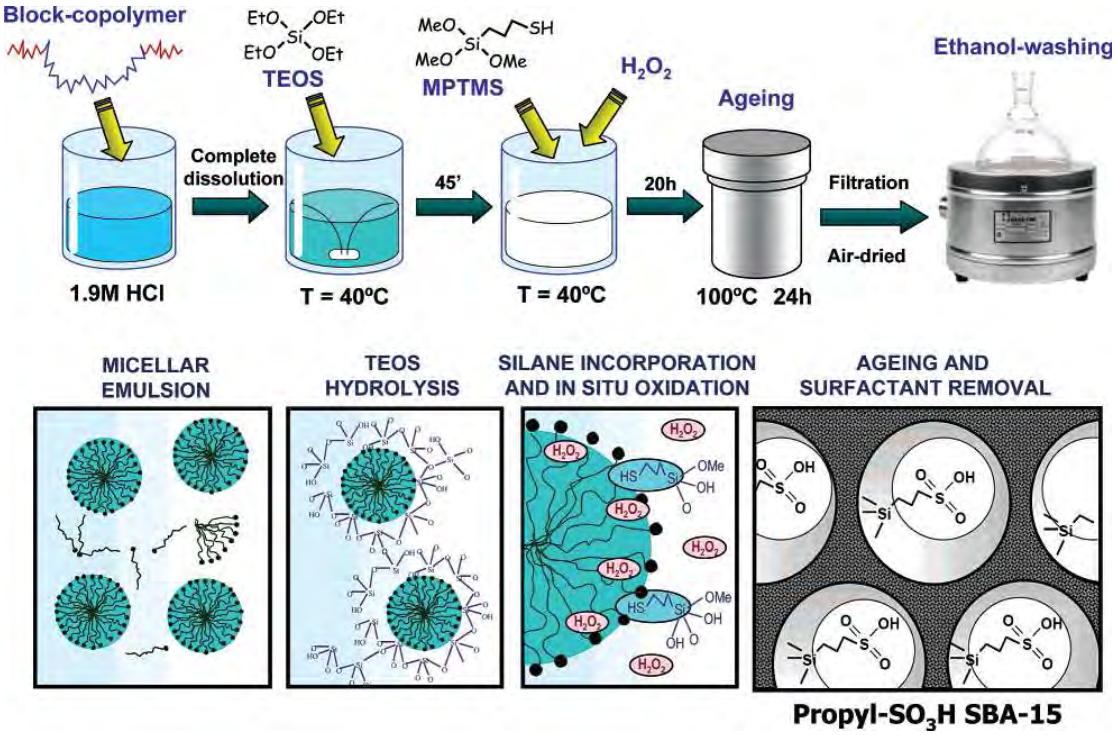

Figure 2.16 In-situ oxidation synthesis strategy for the preparation of sulfonic-acid-modified mesostructured material [34].

2.7.2 Post synthesis (Grafting method)

Grafting procedure based on modification of the silica surface with organic groups through silylation reaction occurring on isolated (≡Si-OH) and germinal (=$Si(OH)_2$) silanol groups using trichloro- or trialkoxyorganosilane and silylamines as organic precursors [34]**.**

Synthesis of sulfonic functionalized SBA-15 by post synthesis is shown in Figure 2.17. In typical procedure, calcined SBA-15 is treated with a silating agent like 3-mercaptopropyltrimethoxysilane (MPTMS) in nonpolar solvent (commonly toluene) to immobilize thiol groups on the surface. These thiol functionalities are then oxidized, normally using hydrogen peroxide. The most apparent advantage of this procedure is good preservation of the mesostructure after post-modification.

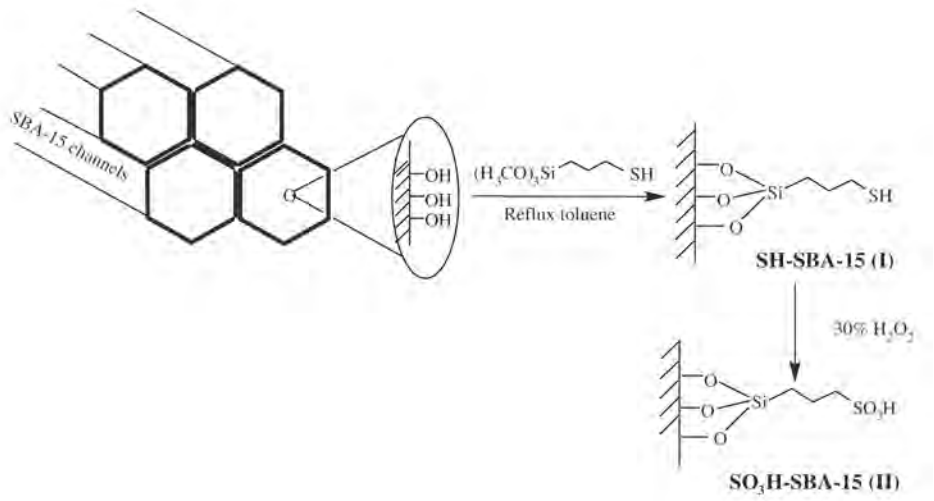

Figure 2.17 Post synthesis procedure for the preparation of sulfonic-acid-modified mesostructured materials [36].

2.8 Commercial catalysts

2.8.1 Nafion

Nafion is a fluorinated polymer-support sulfonic acid discovered in the early 1960s by Walther Grot of DuPont. The molecular weight of Nafion is uncertain due to differences in processing and solution morphology. The structure of Nafion unit is illustrated in Figure 2.18.

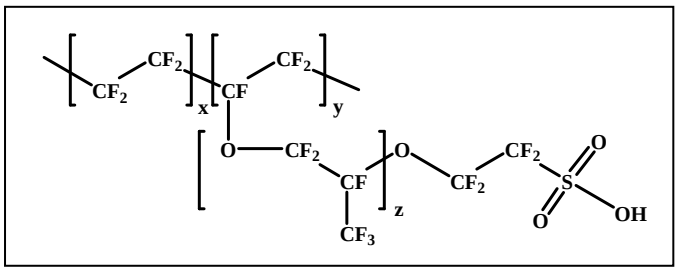

Figure 2.18 The structure of Nafion unit [37].

One major drawback of Nafion is the low surface area (0.02 m^2 g^{-1}). This property results in low activity. To increase this activity, new kind of solid Nafion catalysts have been developed. New generation of Nafion contains nanosized Nafion resin particles entrapped in a highly porous silica matrix. These materials are called SAC (solid acid catalysts) followed by the Nafion loading, *e.g.* Nafion SAC-13 for 13% Nafion in the silica matrix [38].

2.8.2 Amberlyst-15

Amberlyst-15, a registered trademark of Rohm and Hass Company, is an ion-exchange resin which is composed of styrene divinylbenzene copolymer crosslinked with sulfonic acid group. It has been used in a wide range of acid-catalyzed reaction due to having strong acidity. However, surface area of Amberlyst-15 is negligible and thermal stability is very limited. The structure of Amberlyst-15 unit is shown in Figure 2.19

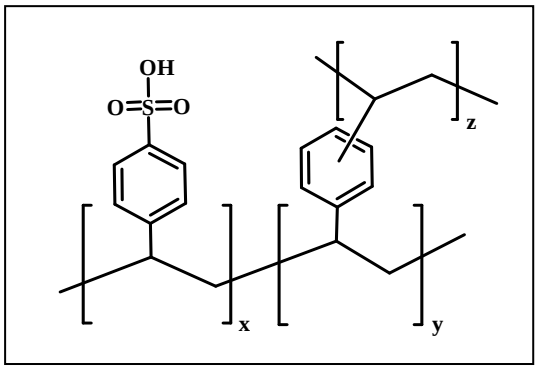

Figure 2.19 The structure of Amberlyst-15 unit [39].

2.9 Characterization of materials

2.9.1 X-ray powder diffraction (XRD)

X-ray powder diffraction (XRD) is an instrumental technique used for identification of minerals, as well as other crystalline materials. XRD is a technique in which a collimated beams of nearly monochromatic. X-rays is directed onto the flat surface of a relatively thin layer of finely ground material. XRD can provide additional information beyond basic identification. If the sample is a mixture, XRD data can be analyzed to determine the proportion of the different minerals present. Other obtained information can include the degree of crystallinity of the minerals present, possible deviations of the minerals from their ideal compositions, the structural state of the minerals and the degree of hydration for minerals that contain water in their structure.

XRD is a reliable technique that can be used to identify mesoporous structure. Typically, the XRD pattern of hexagonal symmetry shows five well-resolved peaks corresponding to lattice planes of Miller indices (100), (110), (200), (210), and (300) [40]. These XRD peaks appear at low angle (2θ angle between 0.5 and 3 degree) because the materials are not crystalline at atomic level, diffraction at higher angles are not observed.

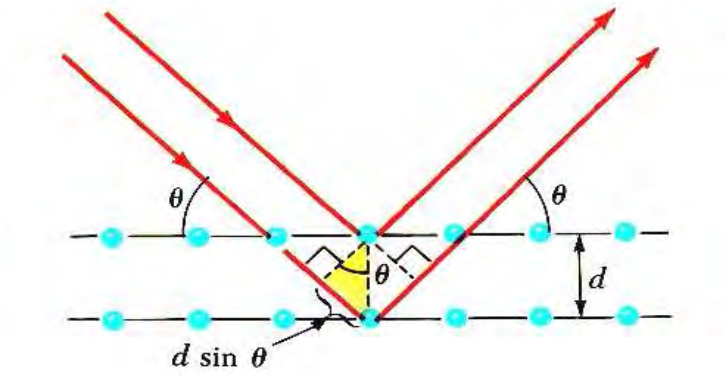

Figure 2.20 Diffraction of X-ray by regular planes of atoms [41].

Figure 2.20 shows a monochromatic beam of X-ray incident on the surface of crystal at an angle θ. The scattered intensity can be measured as a function of scattering angle 2θ. The resulting XRD pattern efficiently determines the different phases present in the sample. Using this method, Braggs' law is able to determine the interplanar spacing of the samples, from diffraction peak according to Bragg's angle.

$$n\lambda = 2\,d\sin\theta$$

Where the integer *n* is the order of the diffracted beam, λ is the wavelength; *d* is the distance between adjacent planes of the crystal (the *d*-spacings) and θ is the angle between the incident beam and these planes.

2.9.2 Nitrogen adsorption-desorption technique

The N_2 adsorption-desorption technique is used to classify the porous materials and its physical properties such as surface area, pore volume, pore diameter and pore-size distribution of solid catalysts. Adsorption of gas by a porous material is described by an adsorption isotherm, the amount of adsorbed gas by the material at a fixed temperature as a function of pressure. Porous materials are frequently characterized in terms of pore sizes derived from gas sorption data [42-43]. The IUPAC classification of adsorption isotherms is illustrated in Figure 2.21.

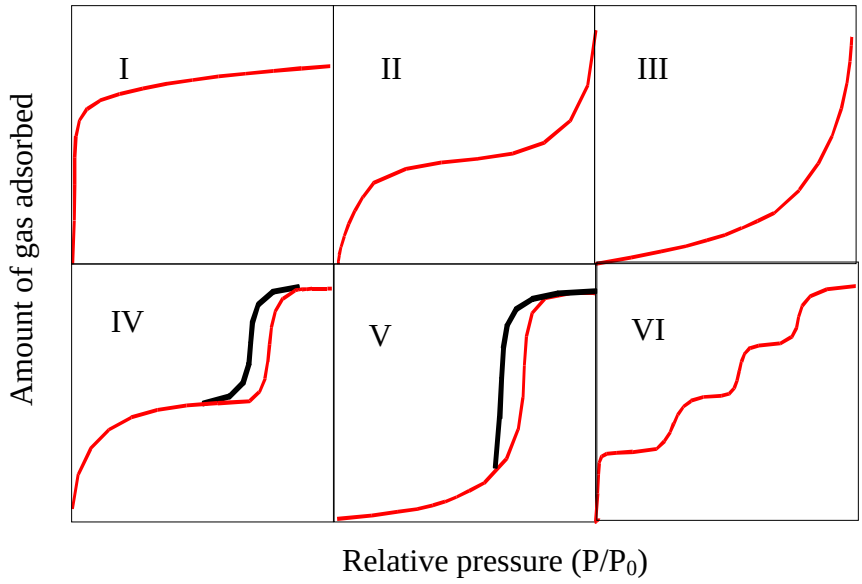

Figure 2.21 The IUPAC classification of adsorption isotherm [42].

As shown in Table 2.7, adsorption isotherms base on the strength of the interaction between the sample surface and adsorptive. Pore size distribution is measured by the use of nitrogen adsorption/desorption isotherm at liquid nitrogen temperature and relative pressures (P/P_o) ranging from 0.05-0.1. The large uptake of nitrogen at low P/P_o indicates filling of the micropores (<20 Å) in the adsorbent. The linear portion of the curve represents multilayer adsorption of nitrogen on the surface of the sample, and the concave upward portion of the curve represents filling of mesoporous and macropores. The multipoint Brunauer, Emmett and Teller (BET) method is commonly used to measure total surface area.

$$\frac{1}{W[(P_o/P)-1]} = \frac{1}{W_m C} + \frac{C-1}{W_m C}(P/P_o)$$

Where W is the weight of nitrogen adsorbed at a given P/P_o, W_m is the weight of gas to give monolayer coverage, and C is a constant that is related to the heat of adsorption. A slope and intercept are used to determine the quantity of nitrogen adsorbed in the monolayer and calculate the surface area. For a single point method, the intercept is taken as zero or a small positive value, and the slope from the

BET plot is used to calculate the surface area. The surface area depends upon the method used, as well as the partial pressures at which the data are collected.

Table 2.7 Features of adsorption isotherms

Type	Interaction between sample surface and gas adsorbate	Porosity	Example of sample-adsorbate
I	relatively strong	Micropores	activated carbon-N_2
II	relatively strong	Nonporous	oxide-N_2
III	weak	Nonporous	carbon-water vapor
IV	relatively strong	Mesopore	silica-N_2
V	weak	Micropores	
		Mesopore	activated carbon-water vapor
VI	relatively strong sample surface has an even distribution of energy	Nonporous	graphite-Kr

2.9.3 Scanning electron microscope (SEM)

The scanning electron microscope (SEM) has unique capabilities for analyzing surfaces and morphology of materials. It is analogous to the reflected light microscope, although different radiation sources serve to produce the required illumination. Whereas the reflected light microscope forms an image from light reflected from a sample surface, the SEM uses electrons for image formation. The different wavelength of these radiation sources result in different resolution levels: electron have much shorter wavelength than light photons, and shorter wavelength are capable of generating the higher resolution information. Enhanced resolution in turn permits higher magnification without loss of detail. The maximum magnification of the light microscope is about 2,000 times; beyond this level is “empty magnification”,

or the point where increased magnification does not provide additional information. This upper magnification limit is a function of the wavelength of visible light, 2000 Å, which equal the theoretical maximum resolution of conventional light microscope. In comparison, the wavelength of electron is less than 0.5 Å, and theoretically the maximum magnification of electron beam instrument is beyond 800,000 times. Because of instrumental parameters, practical magnification and resolution limits are about 75,000 times and 40 Å in a conventional SEM [44]. The SEM consists basically of four systems:

1. The *illuminating/imaging system* produces the electron beam and directs it onto the sample.

2. The *information system* includes the data released by the sample during electron bombardment and detectors which discriminate among analyze these information signals.

3. The *display system* consists of one or two cathode-ray tubes for observing and photographing the surface of interest.

4. The *vacuum system* removes gases from the microscope column which increase the mean free path of electron, hence the better image quality.

2.9.4 CHNS/O Elemental analysis

CHNS/O elemental analysis is a technique dedicated to the simultaneous determination of the amount of (%) of carbon, hydrogen, nitrogen, sulfur and oxygen contained in organic, inorganic and polymeric materials.

The basic principle of CHNS/O analysis is high temperature combustion. The sample weighed in milligrams housed in a tin capsule is dropped into a quartz tube at 1020°C with constant helium flow (carrier gas). A few seconds before the sample drops into the combustion tube, the stream is enriched with a measured amount of high purity oxygen to achieve a strong oxidizing environment which guarantees almost complete combustion/oxidation even of thermally resistant

substances. Then, the combustion gas mixture is driven through an oxidation catalyst zone which reduces nitrogen oxides and sulfur trioxide eventually formed during combustion on catalyst reduction to elemental nitrogen and sulfur dioxide and retains the oxygen excess. The resulting four components of the combustion mixture are detected by a Thermal Conductivity Detector (TCD) in the sequence N_2, CO_2, H_2O and SO_2. Finally, total amounts of C, H and S are calculated. In case of oxygen which is analyzed separately, the sample undergoes immediate pyrolysis in a Helium stream which ensures quantitative conversion of organic oxygen into carbon monoxide separated on a GC column packed with molecular sieves [45].

2.9.5 Solid-state NMR

NMR has established itself as a major and unique analytical tool in the characterization on the structural features of solid materials. In case of sulfonic functionalized mesoporous materials, the presence of alkyl or aryl sulfonic acid groups on the surface of materials is confirmed using ^{13}C solid-state NMR technique.

In solid-state NMR, it can generally deal with powder samples; that are samples consisting of many crystallites with random orientations. The nuclear spin interactions which affect solid-state NMR spectra, chemical shielding, dipole-dipole coupling and quadrupole coupling, are all dependent on the crystallite orientation. As a consequence, the NMR spectrum of a powder sample contains broad lines. Moreover, when the sample has several in equivalent nuclear sites, the powder patterns from each may overlap. The consequent lack of resolution in the NMR spectrum obscures any information that the spectrum may contain [46]. From mentioned above, magic angle spinning (MAS) is a technique often used to perform experiments in solid-state NMR spectroscopy. MAS has been used extensively in the vast majority of solid-state NMR experiments, where its primary task is to remove the effects of chemical shift anisotropy and to assist in the removal of heteronuclear dipolar coupling effects [47].

2.10 Bisphenol-F

Bisphenol-F, commonly abbreviated as BPF, is an organic compound with two phenolic rings joined together through a methylene bridge. BPF is composed of three isomers as shown in Figure 2.22.

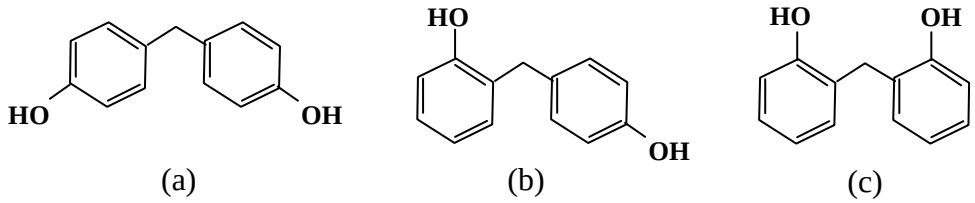

(a) (b) (c)

Figure 2.22 Isomers of BPF (a) Bis(2-hydroxyphenyl)methane (*2,2'*-BPF), (b) 2-hydroxyphenyl-4-hydroxyphenylmethane (*2,4'*-BPF) and (c) Bis(4-hydroxyphenyl)methane (*4,4'*-BPF) [48].

2.10.1 Preparation of BPF

BPF can be produced by condensation reaction of phenol and formaldehyde in the presence of acid catalyst as described in Figure 2.23.

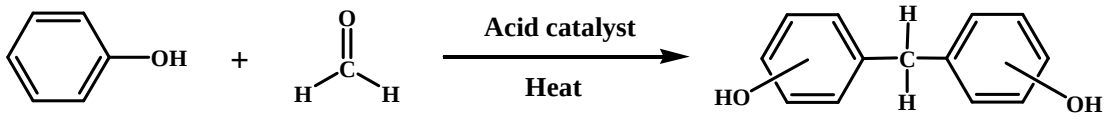

Phenol **Formaldehyde** **Bisphenol-F**

Figure 2.23 Preparation of BPF [49].

The acid catalysts used in the preparation of BPF can be strong inorganic acid solutions (sulfuric acid and hydrochloric acid), super acid (phosphotungstic acid), and solid acids (zeolites, ion-exchange resins, clays and mesoporous materials).

2.10.2 Comparison of bisphenol-F and bisphenol-A

General informations and applications of BPF are compared with bisphenol-A (BPA) as described in Table 2.8.

Table 2.8 Comparison of bisphenol-F and bisphenol-A

	Bisphenol-F	**Bisphenol-A**
Starting materials	Phenol+Formaldehyde	Phenol+Acetone
Used products	Isomeric mixture (*2,2'*-BPF+*2,4'*-BPF+*4,4'*-BPF)	*4,4'*-BPA
Applications	Preparation of epoxy resins and polycarbonates (Mainly used in epoxy resin production)	Preparation of epoxy resins and polycarbonates

2.11 Applications of BPF

BPF is an industrially important raw material for the preparation of epoxy resins and polycarbonates.

2.11.1 BPF type epoxy resin

BPF type epoxy resin is generally produced from a reaction between bisphenol-F, epichlorohydrin and sodium hydroxide (Figure 2.24). The ends of BPF are attached by two glycidyl groups, creating bisphenol-F diglycidyl ether (BFDGE). The glycidyl groups on both ends of the BPF are also referred to as oxirane or epoxy group. By changing the ratio of epichlorohydrin to BPF, Liquid epoxy resins can be further reacted with BPF by chain extension to form solid epoxy resins with varying *n* values.

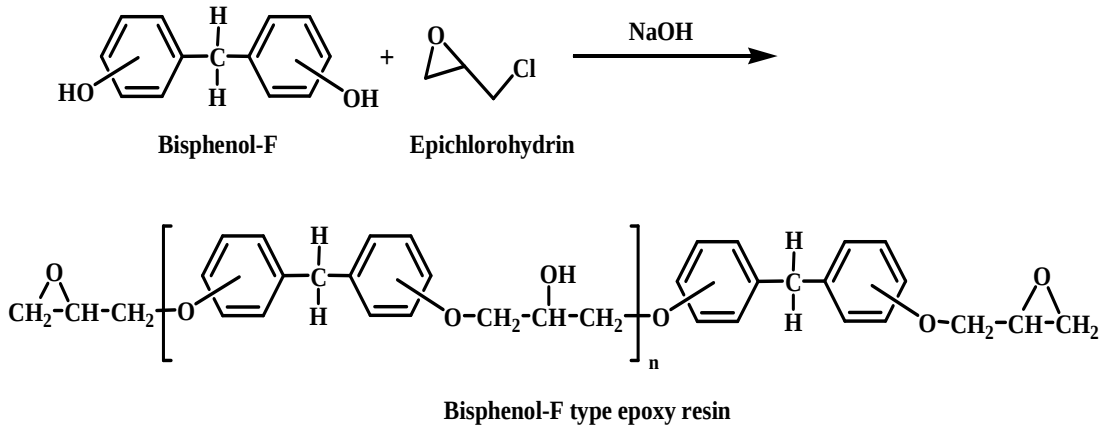

Figure 2.24 Preparation of bisphenol-F diglycidyl ether (BFDGE) [50].

In general, BFDGE in common use is a mixture of *2,2'*-BPF, *2,4'*-BPF and *4,4'*-BPF. It is a viscous liquid at ambient temperature because the formers of *2,2'*-BPF and *2,4'*-BPF prevent solidification. In contrast, *4,4'*-BPF type epoxy resin is crystalline at ambient temperature (Figure 2.25). In comparison with bisphenol-A diglycidyl ether (BADGE), epoxy resin with high ortho BPF (*2,2'*-BPF and *2,4'*-BPF) has lower viscosity (e.g. melt viscosity, solution viscosity) and good physical properties such as flexibility [3]. In addition, BPFDGE can use in blends with other resins such as BADGE in order to allow high solids formulations with good chemical resistance.

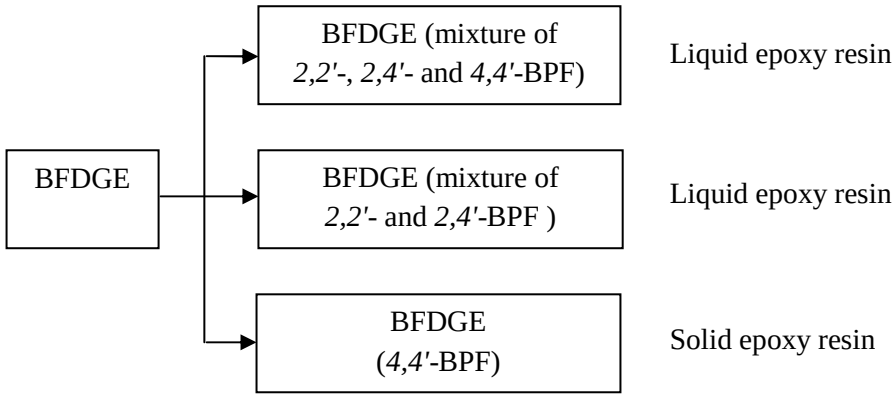

Figure 2.25 Types of bisphenol-F diglycidyl ether (BFDGE) [51].

BFDGE is used in wide range of industry including digital metal products (e.g. CDs, DVDs), electrical and electronic equipment, lacquer coatings in cans and dental composites and sealants [52].

2.11.2 BPF type polycarbonate

Polycarbonate, a particular group of thermoplastic polymers, has functional groups linked together by carbonate groups (-O-(C=O)-O) in a long molecular chain. BPF type polycarbonate can be synthesized from BPF and phosgene (carbonyl dichloride, $COCl_2$) as described in Figure 2.26.

Step I

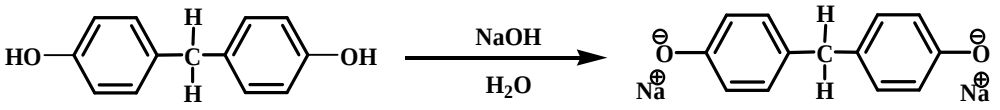

Step II

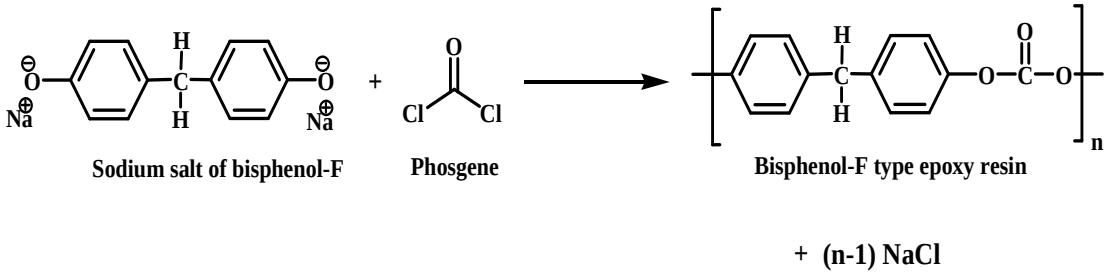

Figure 2.26 Process for synthesis of BPF type polycarbonate [50].

BPF type polycarbonate has uniquely high impact strength and exceptional clarity. These unique properties have resulted in applications such as bulletproof window, break resistant lense, compact disc, etc. [53].

2.12 Purification of BPF

At present, fractional distillation is a suitable method for preparing highly pure BPF from reaction mixture [5, 53]. The distillation step is preferably performed by providing a distillation apparatus equipped with a still, a partial condenser and a complete condenser. Crude BPF is continuously supplying to the still maintained at a temperature ranging from 220 to 250 °C and a pressure ranging from 1 to 5 mmHg. Then, BPF is condensed to form liquid distillate while by-products are appeared in still-bottom. The obtained BPF has high purity (not less than 95 wt%).

On the other hand, it is well known that *4,4'*-BPF can be advantageously prepared on an industrial scale. Thus, separation of *4,4'*-BPF from the other components of BPF is carried out by recystallization [6]. This procedure may be achieved at any temperature without limitation. However, crude BPF may be generally heated to the boiling point of the solvent and thus dissolved therein. The solution is allowed to cool down to room temperature. Thus *4,4´*-BPF will crystallize out at a high purity. The suitable solvent is ethylbenzene to give highest purity of 97.2%. Although a single recrystallization can give a sufficiently high purity of the *4,4´*-BPF, the purity can be further elevated by repeating the recrystallization. The residue is rich in *2,4´*-BPF and *2,2´*-BPF. When it is used as a starting material for preparing epoxy resins, it gives a characteristic suitable for civil uses, which will hardly crystallizes and have a high workability. The purification procedure of BPF production is summarized in Scheme 2.1.

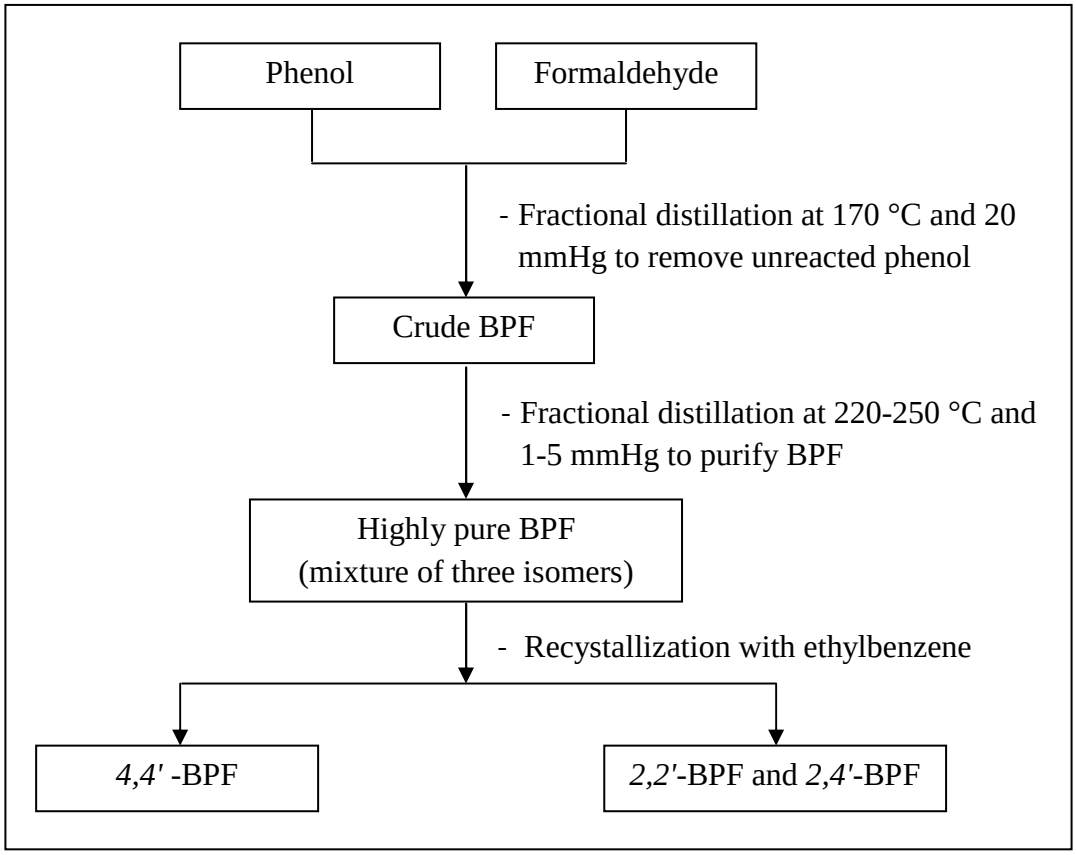

Scheme 2.1 Purification procedure of BPF production [5-6].

CHAPTER III

EXPERIMENTS

3.1 Instruments and apparatus

3.1.1 Oven

Crystallization of sulfonic functionalized SBA-15 during the synthesis was carried out at a temperature of 100^{o}C in static condition using UM-500 oven as heater.

3.1.2 X-ray powder diffractometer (XRD)

The XRD patterns of synthesized mesoporous materials were identified using a Rigaku D/MAX-2200 Ultima^{+} X-ray diffractometer equipped with Cu target X-ray tube (40 kV, 30mA) at 2-theta angle between 0.5 to 3.00 degree with a scan speed of 1.00 degree/min and sampling width of 0.02 degree. The scattering slit, divergent slit and receiving slit were fixed at 0.5 degree, 0.5 degree, and 0.15 mm, respectively. The measured diffractograms were analyzed using MDI software (Jade 6.5).

3.1.3 Surface area analyzer

N_2 adsorption-desorption isotherms, BET specific surface area, and pore size distribution of the catalysts were carried out using a BEL Japan, BELSORP-mini instrument. The sample weights were nearly 40 mg and weighted exactly after pretreatment at 150 $^{\circ}$C for 3 h before each measurement.

3.1.4 Scanning electron microscope (SEM)

The morphology and particle sizes of the catalysts were observed using a JEOL JSM-6480 LV scanning electron microscope. All samples were coated with spluttering gold under vacuum.

3.1.5 ^{13}C-NMR spectrometer

Solid state ^{13}C-NMR spectra were performed using the Bruker Advance DPX 300 MHz NMR spectrometer.

3.1.6 Elemental analyzer

Sulfur content in the catalysts were determined using the Perkin Elmer (PE2400 Series II) CHNS/O analyzer.

3.1.7 Gas chromatograph (GC)

Reaction mixtures from BPF synthesis were analyzed using a Varian CP 3800 gas chromatograph equipped with a 50 m length × 0.25 mm inner diameter CP-Sil 5 capillary column (equivalent to DB-1 column). The detector was a flame ionization detector (FID). The sample volumes were 1 μL. The column oven heating program was illustrated in Figure 3.1.

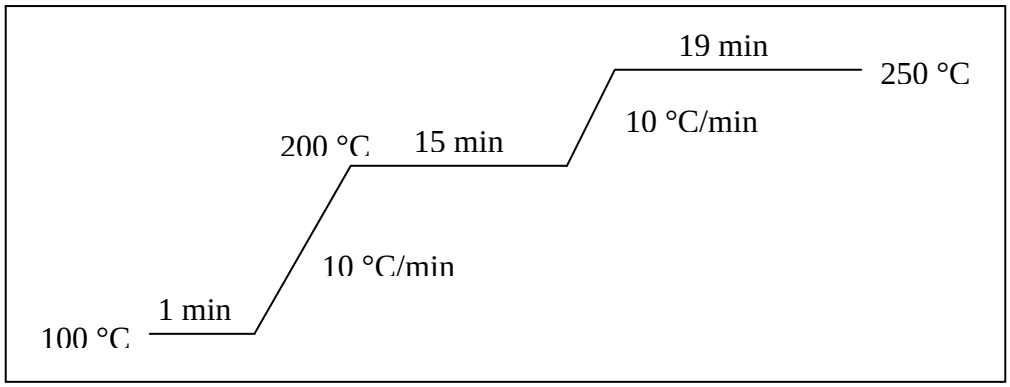

Figure 3.1 The GC heating condition for BPF analysis.

3.1.8 Gas chromatograph-mass spectrometer (GC-MS)

Qualitative analysis of liquid sample was confirmed with GC-MS technique. GC system network of Varian CP-3800 gas chromatograph equipped with a 50 m length × 0.25 mm inner diameter VF-1ms capillary column, mass selective detector network of Varian Saturn 2200 GC/MS/MS were used.

3.2 Chemicals

1. Triblock copolymer pluronic P123 (PEO_{20}-PPO_{70}-PEO_{20}, average molecular weight = 5800) (Aldrich)
2. Tetraethyl orthosilicate, TEOS (Fluka, 98 %)
3. Hydrochloric acid, HCl (Fluka, 37 %)
4. (3-Mercaptopropyl)trimethoxysilane, MPTMS (Aldrich, 95 %)
5. Hydrogen peroxide (Merck, 30 %)
6. 2-(4-Chlorosulfonylphenyl)ethyltrimethoxysilane, CSPETMS (Gelest, 50 % in methylene chloride)
7. Phenol (Merck, 99.6 %)
8. Formaldehyde (Merck, 37.9 %)
9. Bis(2-hydroxyphenyl)methane (Aldrich, 98%)
10. *4,4´*-Methylenediphenol (Fluka, 98 %)
11. *2,4´*-Dihydroxydiphenylmethane (TCI, 98 %)
12. Bisphenol-A (Aldrich, 97 %)
13. Acetonitrile (Fisher Scientific, 99%)
14. 2,4-Dinitrophenylhydrazine, 2,4-DNPH (RANKEM, 98%)
15. Ethanol (Merck, 99%)
16. Sodium chloride (CARLO ERBA, 99.5%)
17. Sodium hydroxide (Merck, 99%)
18. Toluene (CARLO ERBA, 99.5%)
19. Methyl isobutyl ketone (CARLO ERBA, 99.5%)

3.3 Synthesis of catalysts

3.3.1 Synthesis of propyl sulfonic functionalized SBA-15 mesoporous material (SBA-15-Pr-SO_3H)

SBA-15-Pr-SO_3H was synthesized using the gel mole composition of 0.0369 TEOS: 0.0041 MPTMS: 0.0369 H_2O_2: 0.24 HCl: 6.9046 H_2O: 0.0007 P123 reported by Melero *et al*. [12]. In a typical procedure, triblock copolymer Pluronic P123 as template was dissolved in 1.9 M HCl solution at room temperature under stirring. The solution was heated at 40°C. Subsequently, TEOS was added dropwise and stirred at 40°C for 45 min. Then, 30 wt% H_2O_2 and MPTMS were added and stirred for 1 h and then aged at 40^{o}C for 20 h with stirring. The resulting gel was transferred to a Teflon-lined autoclave for hydrothermal crystallization at 100^{o}C for 24 h. As-synthesized SBA-15-Pr-SO_3H was separated by filtration, washed with deionized water for several times, and dried overnight. The template was removed by refluxing with ethanol for 24 h (1 g of as-synthesized SBA-15-Pr-SO_3H per 400 mL of ethanol). The procedure for synthesizing the SBA-15-Pr-SO_3H was illustrated in Scheme 3.1.

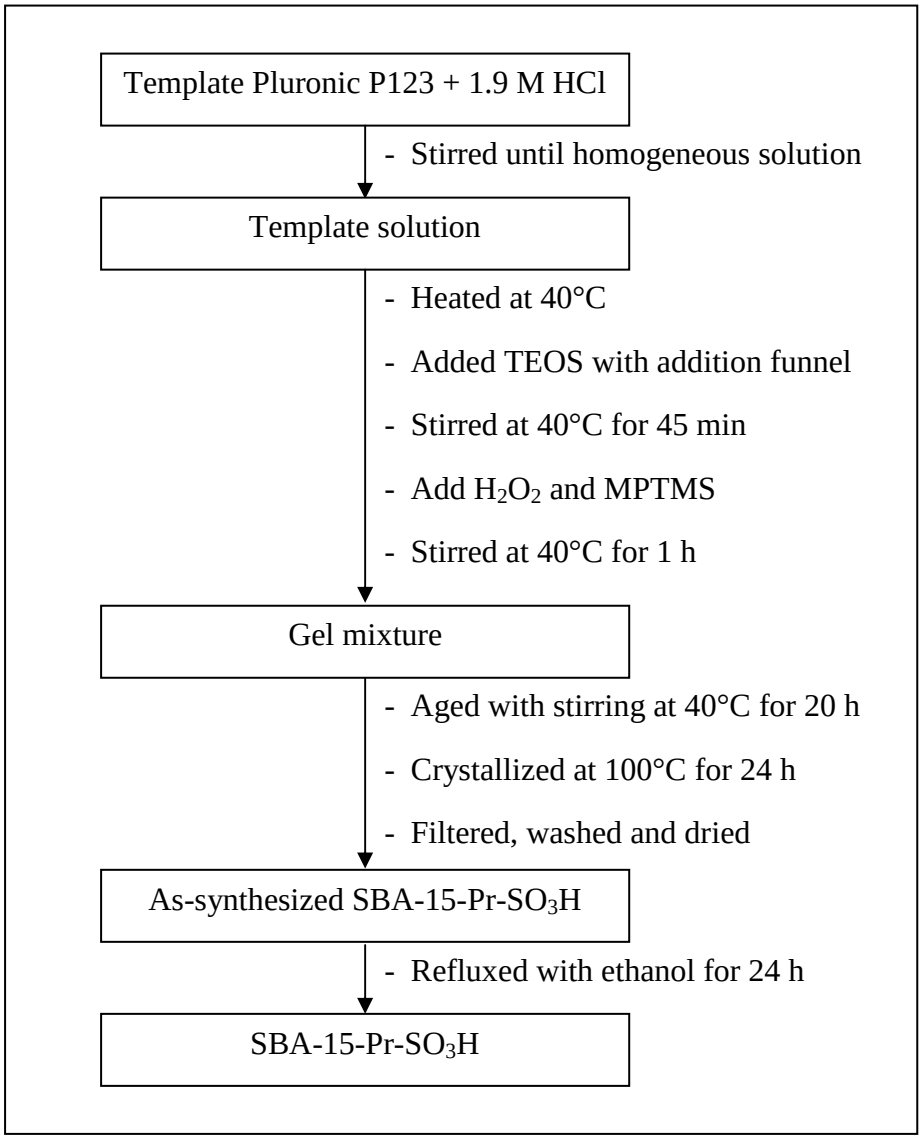

Scheme 3.1 Preparation diagram for SBA-15-Pr-SO_3H.

3.3.2 Synthesis of aryl sulfonic functionalized SBA-15 mesoporous material (SBA-15-Ar-SO_3H)

SBA-15-Ar-SO_3H synthesis was followed by the reported method of Melero *et* al. [13]. SBA-15-Ar-SO_3H was synthesized from the gel mole composition of 0.0369 TEOS: 0.0041 CSPETMS: 0.0369 H_2O_2: 0.24 HCl: 6.9046 H_2O: 0.0007 P123. A typical synthesis was same as SBA-15-Pr-SO_3H synthesis except for changing MPTMS to CSPETMS.

3.4 Acid-base titration

The acid capacities of sulfonic acid groups in the functionalized mesoporous materials were quantified using 2M NaCl solution as the ion-exchange agent (Scheme 3.2). Approximately 0.05 g of the catalyst was added to 15 mL of the salt solution and allowed to equilibrate for 30 min. Thereafter, it was titrated using phenolphthalein as indicator by dropwise addition of 0.01M NaOH solution [14].

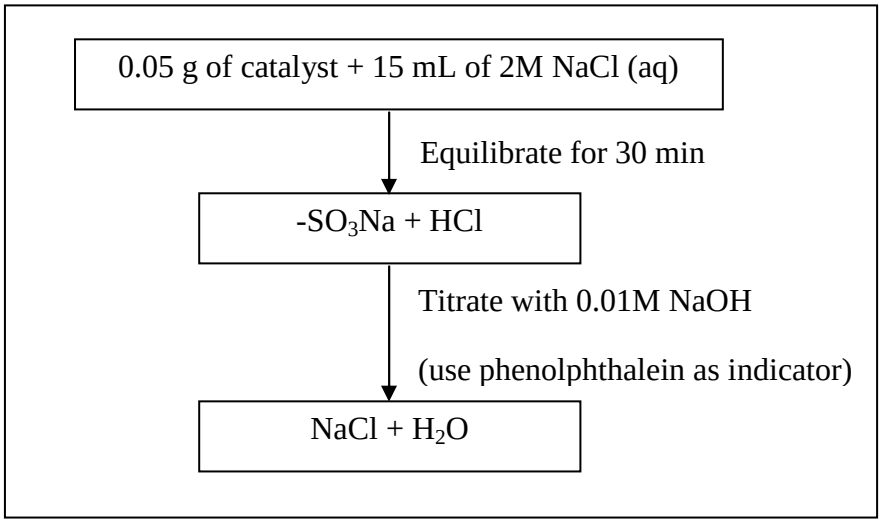

Scheme 3.2 Diagram for acid-base titration [14].

3.5 Procedure in BPF synthesis

The synthesis of BPF was carried out in a round-bottomed flask fitted with a reflux condenser. In each experiment, 5 g of phenol, catalyst and 37.9 wt% aqueous formaldehyde solution were added to a round-bottomed flask. Then, the reaction mixture was heated to the desired reaction temperature and kept constant for a period of time. After completion of the reaction, the reaction mixture was cooled down and then catalyst was filtered. The obtained products were confirmed using GC-MS technique and compared to the authentic samples. Likewise, the reaction mixture was quantitatively analyzed by gas chromatography.

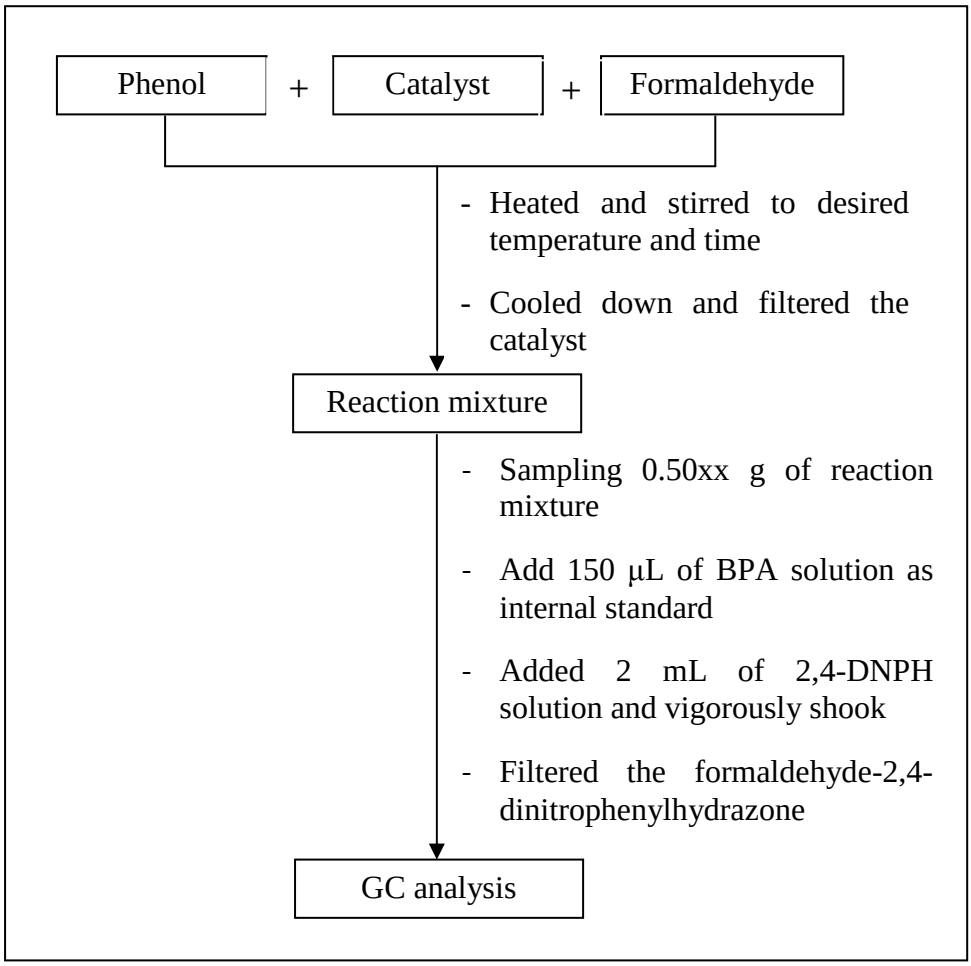

Scheme 3.3 Diagram for BPF preparation and analysis.

3.6 Parameters affecting BPF preparation

3.6.1 Effect of reaction time

The reaction was studied at different reaction time of 0.25, 0.5, 0.75, 1 and 4 h.

3.6.2 Effect of phenol to formaldehyde molar ratio

In this topic, experiments were conducted with phenol to formaldehyde molar ratio of 7.5, 15 and 30.

3.6.3 Effect of catalyst to formaldehyde weight ratio

In this work, effect of catalyst amount was performed in terms of catalyst to formaldehyde weight ratio. The experiments were carried out using catalyst to formaldehyde weight ratio in the range of 0 to 30.

3.6.4 Effect of temperature

The reaction temperature was varied to 50, 70, 90 and 110°C.

3.6.5 Effect of solvent types

To investigate the effect of solvent types on the catalytic activity, the reaction was carried out similar to the procedure in Section 3.5 using 2 mL of different solvents: toluene, methyl isobutyl ketone (MIBK), acetonitrile and H_2O.

3.6.6 Effect of various catalysts

Catalytic activities of sulfonic functionalized SBA-15 mesoporous materials were compared with Al-SBA-15 and commercial catalysts such as H-beta, ZSM-5, Nafion SAC- 13 and Amberlyst-15.

3.7 Standard solution and calibration solution

3.7.1 *2,2'*-BPF standard solution

3.7.1.1 Stock standard solution (0.2 M)

A 0.4 g of *2,2'*-BPF was accurately weighed in a 10 mL volumetric flask and made up to the mark with acetonitrile.

3.7.1.2 Working standard solution (0.1, 0.05, 0.025 and 0.0125 M)

The working standard solutions were prepared by dilution of the standard solution using a pipette and then made up to the mark with acetonitrile.

3.7.2 *2,4'*-BPF standard solution

3.7.2.1 Stock standard solution (0.4 M)

A 0.8 g of *2,4'*-BPF was accurately weighed in a 10 mL volumetric flask and made up to the mark with acetonitrile.

3.7.2.2 Working standard solution (0.2, 0.1, 0.05 and 0.025 M)

The working standard solutions were prepared by dilution of the standard solution using a pipette and then made up to the mark with acetonitrile.

3.7.3 *4,4'*-BPF standard solution

3.7.3.1 Stock standard solution (0.4 M)

A 0.8 g of *4,4'*-BPF was accurately weighed in a 10 mL volumetric flask and made up to the mark with acetonitrile.

3.7.3.2 Working standard solution (0.2, 0.1, 0.05 and 0.025 M)

The working standard solutions were prepared by dilution of the standard solution using a pipette and then made up to the mark with acetonitrile.

3.7.4 Internal standard

For determination of BPF contents, BPA stock solution was used as internal standard. A 0.4 g of BPA was accurately weighed approximately in a 10 mL volumetric flask and made up to the mark with acetonitrile.

3.7.5 Preparation and analysis of the calibration solutions

Each of the five calibration solutions, 500 μL of BPF stock solutions and 150 μL of BPA stock solution were added into the vials using a micropipette. Then, a 1 μL of each reaction mixture was analyzed by GC technique under the condition described in Section 3.1.7.

3.8 Recycle of catalysts

After the first reaction, the used catalyst was filtered and washed several times with ethanol. The catalyst was dried at 80°C overnight, and then this catalyst was denoted as reused catalyst. The regenerated catalyst was treated the reused catalyst with MPMTS in toluene, H_2O_2 and 0.2M H_2SO_4, respectively (Scheme 3.4). Then, catalyst was characterized by XRD, surface area analysis and SEM before testing in subsequent experiment. The reaction was performed in the similar way to what described in Section 3.5.

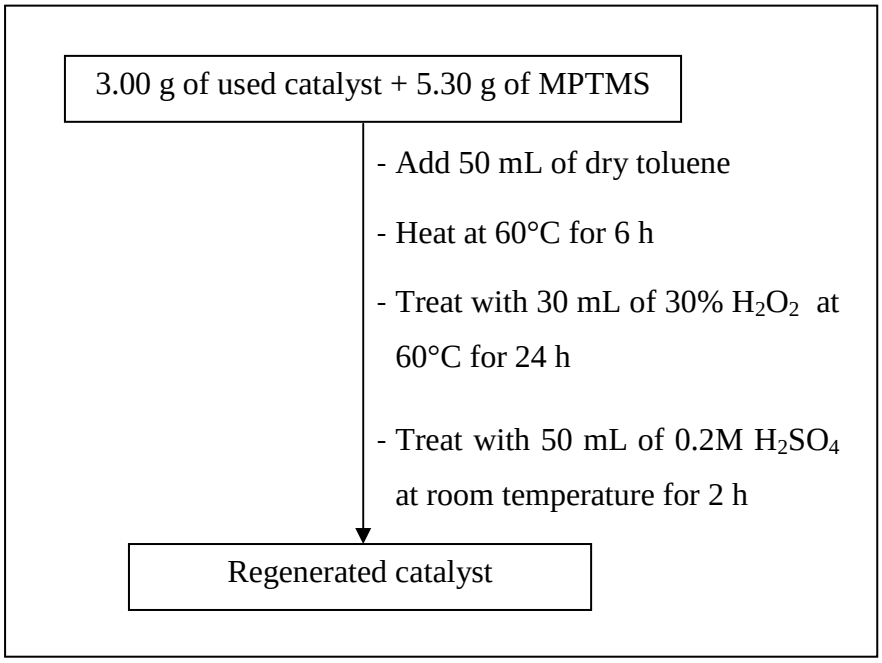

Scheme 3.4 Preparation diagram for regenerated catalyst [54].

CHAPTER IV

RESULTS AND DISCUSSION

4.1 The physico-chemical properties of sulfonic functionalized SBA-15

4.1.1 XRD results

Low angle X-ray powder diffraction patterns of sulfonic functionalized mesoporous materials were shown in Figure 4.1. After removal of triblock copolymer template from the pore of materials, SBA-15-Pr-SO_3H and SBA-15-Ar-SO_3H had one very intense peak and two weak peaks indexed to (100), (110) and (200) diffractions, respectively, indicating the prepared materials contained well-ordered hexagonal structure corresponding to pure SBA-15 [32]. In comparison with SBA-15, the diffraction peaks of sulfonic functionalized SBA-15 materials were slightly shifted to lower 2 theta values, indicating the presence of bulky functional group on the surface of SBA-15 would decrease void volume, then *d*-spacing was increased.

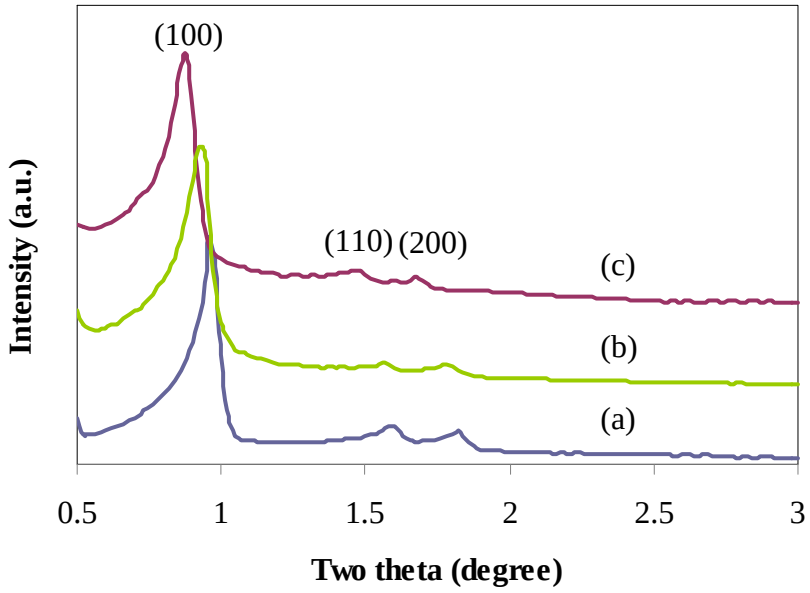

Figure 4.1 X-ray powder diffraction patterns of (a) SBA-15, (b) SBA-15-Pr-SO_3H and (c) SBA-15-Ar-SO_3H.

4.1.2 Sorption properties of sulfonic functionalized SBA-15

4.1.2.1 Sorption properties of SBA-15-Pr-SO_3H

The N_2 adsorption-desorption isotherm and pore size distribution of SBA-15-Pr-SO_3H were shown in Figure 4.2. It performed a type IV adsorption isotherm of IUPAC classification and exhibited a hysteresis loop H1-type which was a characteristic pattern of mesoporous materials [55]. The total specific surface area of SBA-15-Pr-SO_3H was calculated using Brunauer, Emmett and Teller (BET) equation, which was found at 728.14 m^2/g. Likewise, pore size distribution of the synthetic material was evaluated using Barrett-Joiner-Halenda (BJH) method. The narrow pore size distribution was found in SBA-15-Pr-SO_3H at the pore diameter of 7.05 nm which was different from pure SBA-15 (9.23 nm).

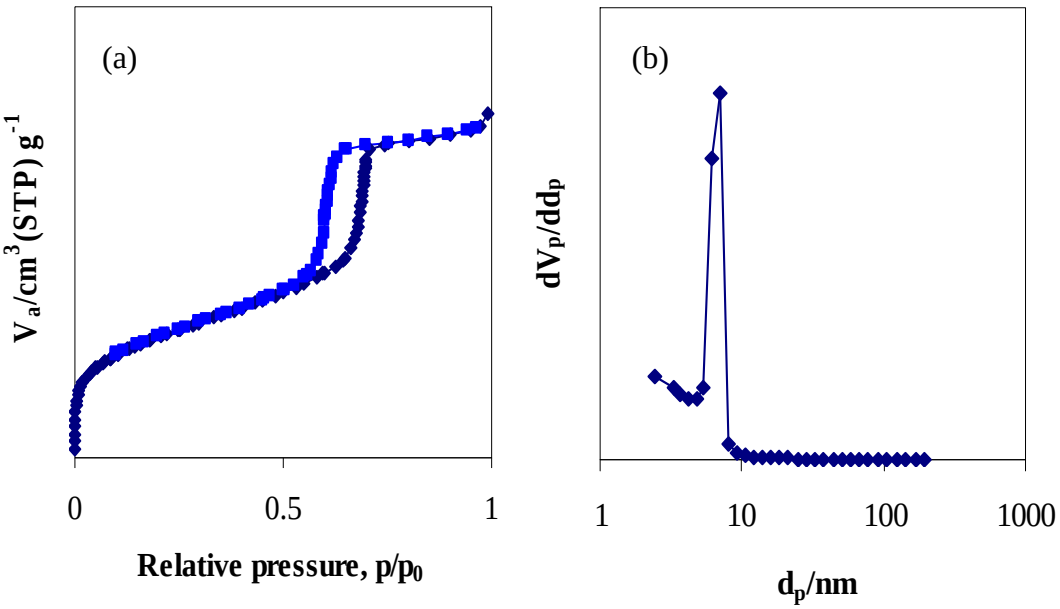

Figure 4.2 (a) N_2 adsorption-desorption isotherm and (b) BJH-pore size distribution of SBA-15-Pr-SO_3H.

4.1.2.2 Sorption properties of SBA-15-Ar-SO_3H

In case of SBA-15-Ar-SO_3H, nitrogen adsorption-desorption isotherm performed hysteresis loop of type IV adsorption isotherm, typical for a mesoporous material with narrow pore size distribution (Figure 4.3(a)). The total specific surface area of SBA-15-Ar-SO_3H was 733.86 m^2/g. Moreover, BJH plot in Figure 4.3(b) showed narrow pore size distribution at the pore diameter 7.05 nm same as SBA-15-Pr-SO_3H.

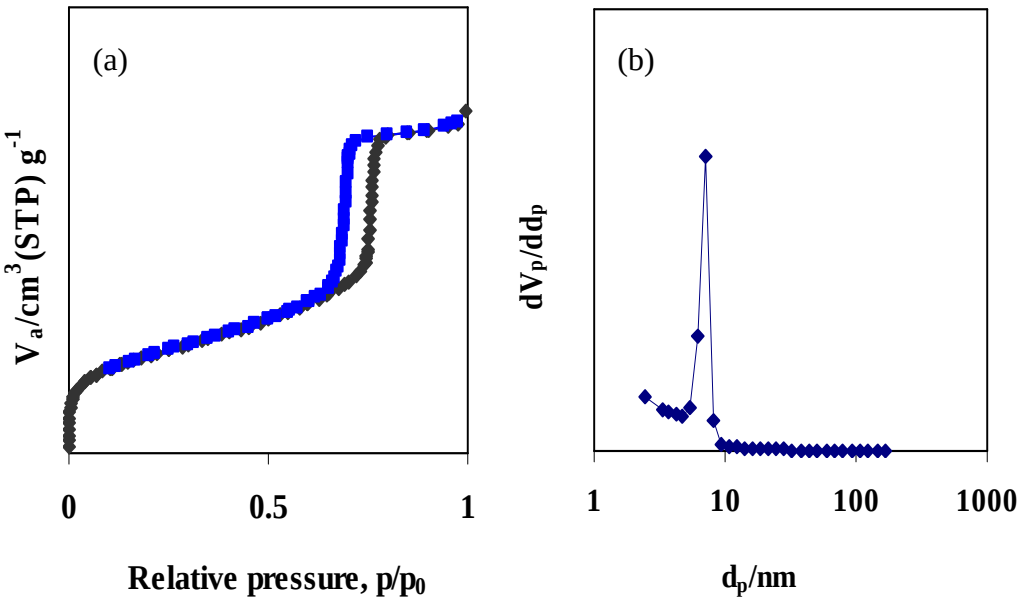

Figure 4.3 (a) N_2 adsorption-desorption isotherm and (b) BJH-pore size distribution of SBA-15-Ar-SO_3H.

From the *d*-spacing of the (100) reflection plane and the pore size distribution determined by N_2 adsorption, the estimated mean thickness of the pore walls of the sulfonic functionalized mesoporous silicas could be calculated based on the equation as follows:

Wall thickness = a_0-pore size

Where; $a_0 = 2 \times d_{(100)} / \sqrt{3}$

$d_{(100)}$ = *d*-spacing of the (100) reflection plane from XRD method

From mentioned equation, it was obvious that wall thickness and *d*-spacing of material were related. Considering to wall thickness (Table 4.1), both SBA-15-Pr-SO_3H and SBA-15-Ar-SO_3H exhibited thicker wall than purely siliceous SBA-15 ought to the appearance of functional groups in the materials. Larger functional group of aryl sulfonic acid would enhance wall thickness. Hence, pore volume of SBA-15-Ar-SO_3H was lower than SBA-15-Pr-SO_3H.

Table 4.1 Textural properties of SBA-15 and sulfonic functionalized SBA-15

Catalyst	**Total specific surface area[a] ($m^2 \cdot g^{-1}$)**	**Pore size distribution[b] (nm)**	**Mesopore volume[b] ($cm^3 \cdot g^{-1}$)**	**$d_{(100)}$[c] (nm)**	**Wall thickness[d] (nm)**
SBA-15	862.13	9.23	1.15	9.56	1.81
SBA-15-Pr-SO_3H	728.14	7.05	0.79	9.59	4.02
SBA-15-Ar-SO_3H	733.86	7.05	0.72	10.08	4.59

[a]Calculated using the BET plot method,
[b]Calculated using the BJH method,
[c]Calculated using XRD, Jade5.6,
[d]Calculated as: a_0-pore size ($a_0 = 2 \times d_{(100)} / \sqrt{3}$)

4.1.3 SEM images

4.1.3.1 SEM images of SBA-15

The SEM images of pure SBA-15 at different magnifications were illustrated in Figure 4.4. Morphology of SBA-15 was uniform pod shape aggregated particles. Furthermore, the average size of particle was 0.8 × 1.1 μm.

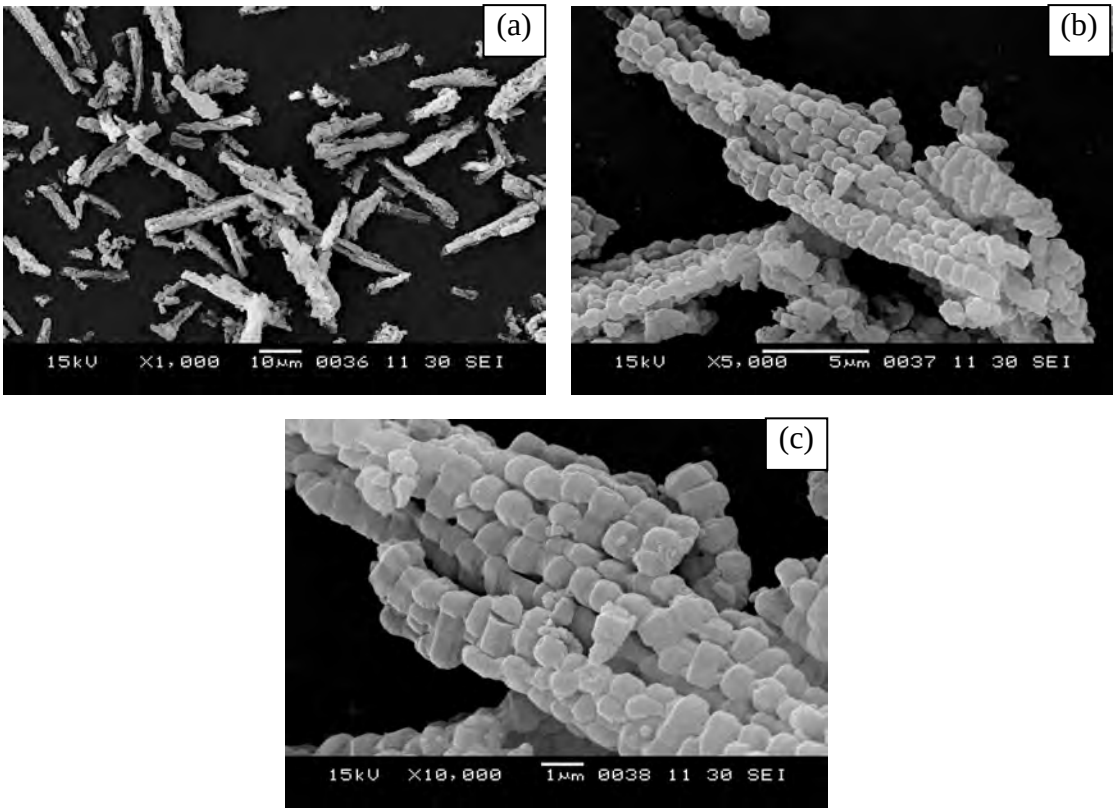

Figure 4.4 SEM images of SBA-15 at different magnifications (a) ×1000, (b) ×5,000, and (c) ×10,000.

4.1.3.2 SEM images of SBA-15-Pr-SO_3H

The SEM images of SBA-15-Pr-SO_3H at different magnifications were shown in Figure 4.5. The sample was aggregated particles with rope-like structure similar to pure SBA-15 with the average particle size was 0.8 × 1.0 μm.

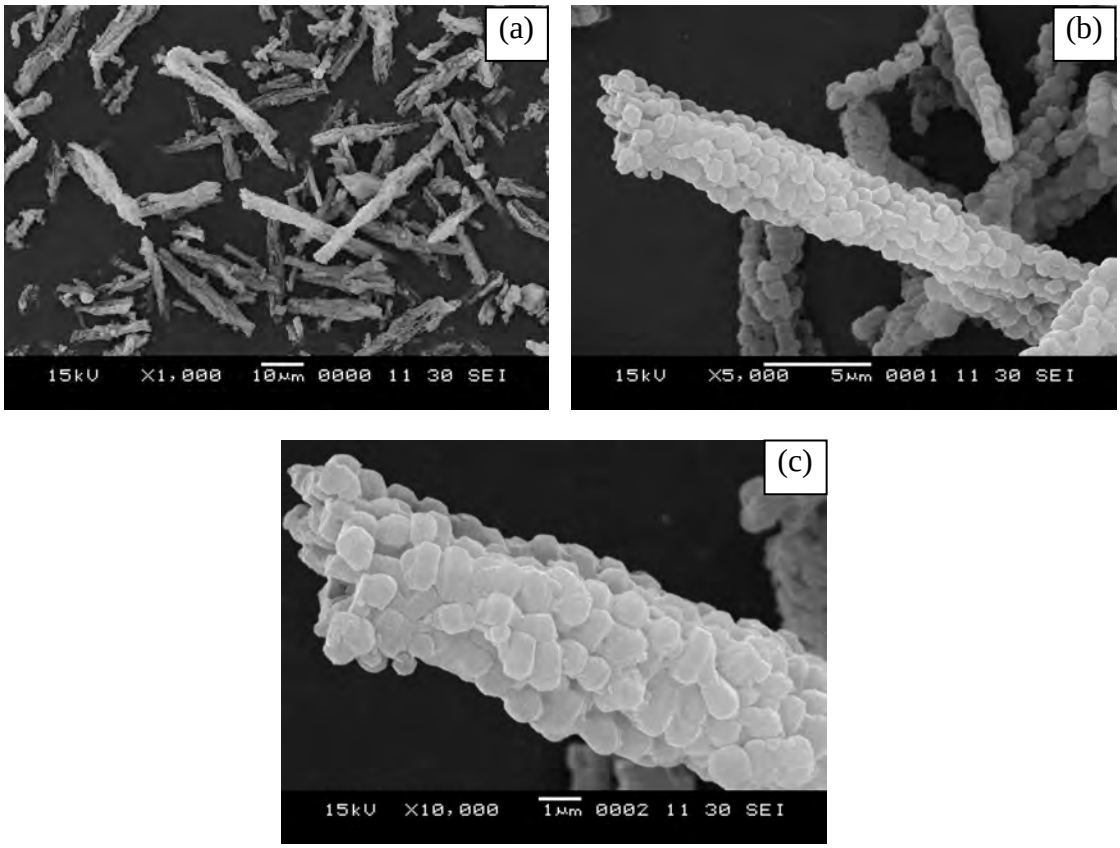

Figure 4.5 SEM images of SBA-15-Pr-SO_3H at different magnifications (a) ×1000, (b) ×5,000, and (c) ×10,000.

4.1.3.3 SEM images of SBA-15-Ar-SO_3H

The SEM images of SBA-15-Ar-SO_3H sample showed small rod particles (Figure 4.6). In addition, the average particle size was 0.5 × 0.8 μm, which showed a bit smaller than SBA-15-Pr-SO_3H. This observation was assumed that lower pore volume of SBA-15-Ar-SO_3H might affect on particle shapes.

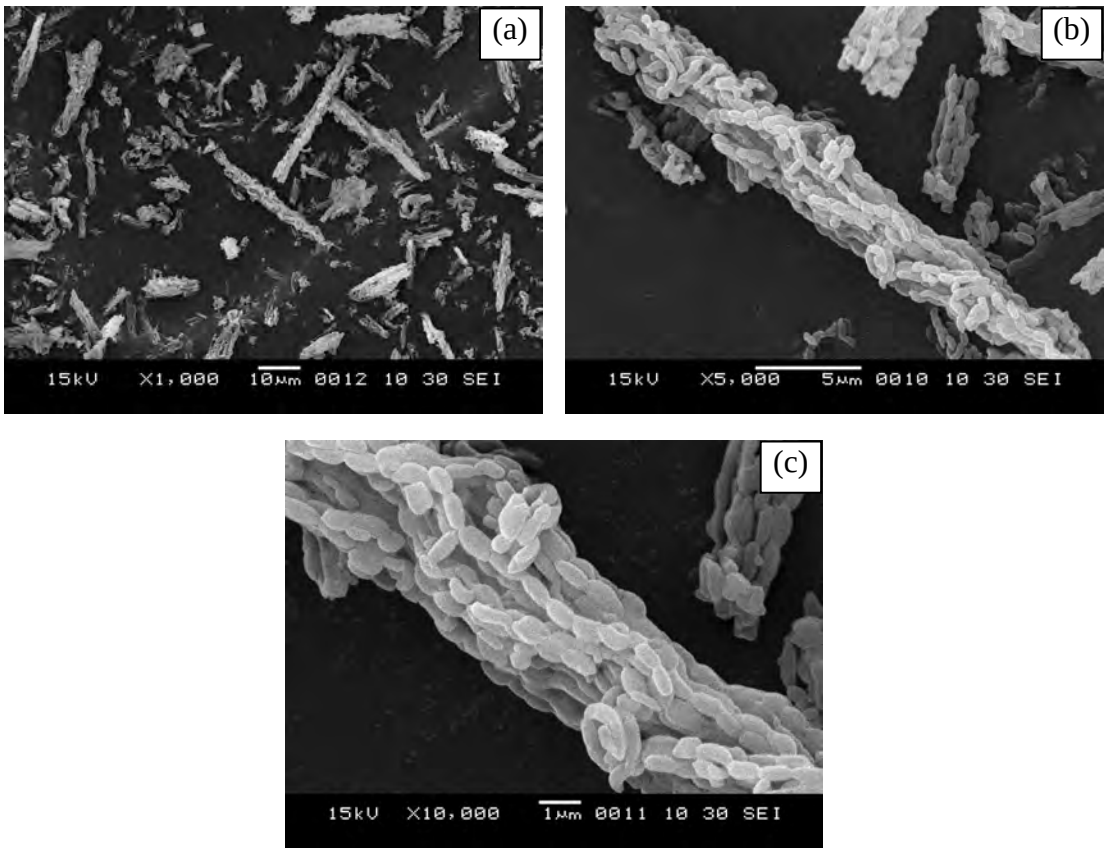

Figure 4.6 SEM images of SBA-15-Ar-SO_3H at different magnifications (a) ×1000, (b) ×5,000, and (c) ×10,000.

4.1.4 ^{13}C-MAS- NMR spectra

The organic nature of the sulfonic functionalized SBA-15 has been investigated by solid state ^{13}C-MAS-NMR (Figure 4.7). The ^{13}C-MAS-NMR spectra of propylsulfonic functionalized SBA-15 performed distinct peaks at 54.0, 18.2 and 11.4 ppm. This evidence confirmed that direct method avoided residual unreacted thiol groups due to absence of the thiol resonance at 27.9 ppm. Thus, it could be concluded that the thiol groups were not present in the material and were completely converted into propylsulfonic groups [12,17]. For the arylsulfonic functionalized SBA-15, the spectra performed two peaks at 15.6 and 28.8 ppm corresponding to the methylene carbon atoms which were adjacent to Si atom and phenyl ring, respectively. In addition, four signals in the down field region at 148.8, 138.5, 128.1 and 126.5 ppm were assigned to carbons on the aromatic ring from the aromatic carbons. These results further confirmed that CSPTMS precursors were co-condensed into the silica material [13,17].

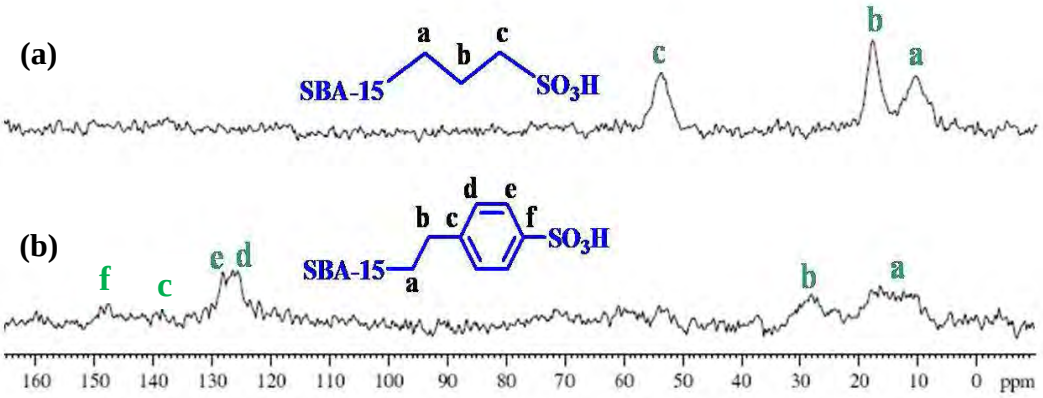

Figure 4.7 The ^{13}C-MAS-NMR spectra of (a) SBA-15-Pr-SO_3H and (b) SBA-15-Ar-SO_3H.

4.1.5 Elemental analysis and acid-base titration

The number of sulfonic acid groups in the mesoporous silica was measured quantitatively by acid-base titration using sodium chloride as ion-exchange agent. The sulfur content of the modified mesoporous silica was determined by elemental analysis. In this work, both SBA-15-Pr-SO_3H and SBA-15-Ar-SO_3H were synthesized using the same mole composition. As a result, the acid values and sulfur contents of two catalysts were nearly equal. In the case of carbon to sulfur, this value was higher than expected, possibly due to the presence of residual surfactant from removing the template.

Table 4.2 Elemental analysis and acid value of sulfonic functionalized SBA-15

Catalyst	Elemental analysis[a] (wt%)			C/S_{Actual}	$C/S_{Theoritical}$	H^+ content[b] (mmol/g)
	C	H	S			
SBA-15-Pr-SO_3H	3.18	2.38	0.56	5.68	5.30	1.01
SBA-15-Ar-SO_3H	10.54	2.72	0.57	18.49	16.30	0.97

[a]Elemental analysis, measured from CHNS/O analyzer,

[b]Acid capacity defined as millimole of acid centers per gram of catalyst, obtained directly by titration (mmol H^+/g)

4.2 Reaction mixture analysis

A gas chromatogram of reaction mixture was shown in Figure A-4. Peak identification was achieved by comparison with authentic samples. Moreover, products and by-products were confirmed by using GC-MS. Mass spectra of products and by-products were presented in Appendix. In condensation reaction between phenol and formaldehyde, desired product was BPF which consisted of three isomeric structures *i.e. 2,2'*-isomer, *2,4'*-isomer and *4,4'*-isomer. Besides, by-products were 2-hydroxybenzyl alcohol and 4-hydroxybenzyl alcohol which were intermediates from this reaction. In this research, BPF was synthesized over acidic porous materials. Higher molecular weight condensation products such as trisphenol isomers might take place in the small quantity. Due to the limited diffusivity of higher molecules outside the porous materials, trisphenol product was not appeared in this reaction mixture. This result was confirmed using the analytic results from GC technique. Structures of obtained products from BPF synthesis were illustrated in Figure 4.8.

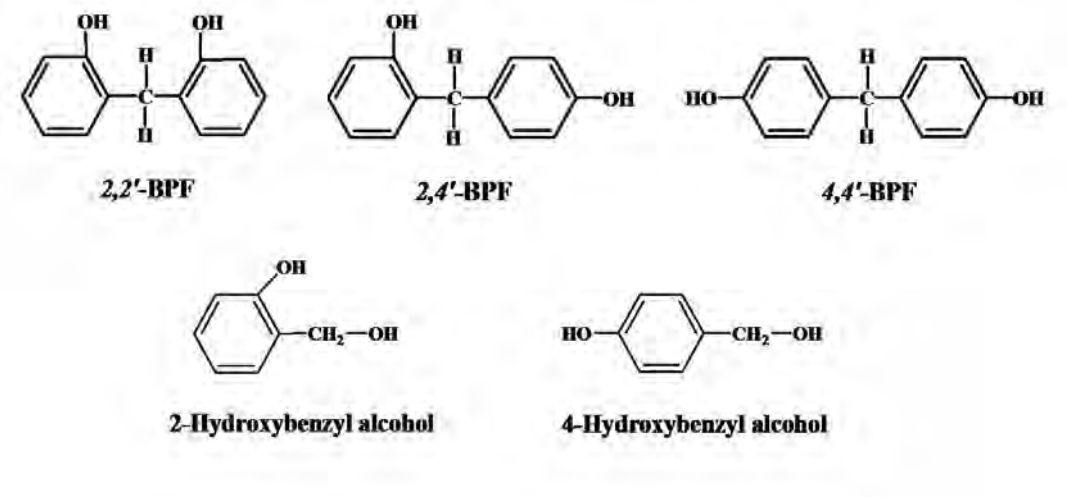

Figure 4.8 Structures of obtained products from BPF synthesis.

For the quantitative analysis, calibration curves of *2,2'*-BPF, *2,4'*-BPF and *4,4'*-BPF were carried out as shown in Appendix. BPF contents were evaluated in terms of (%) BPF yield, (%) BPF selectivity and (%) BPF isomer distribution. In case of formaldehyde, it is well known that formaldehyde cannot be detected by GC-FID directly. Nevertheless, derivatization of formaldehyde with 2,4-dinitrophenylhydrazine (2,4-DNPH) was chosen. 2,4-DNPH could be reacted with carbonyl group of formaldehyde as shown in Figure 4.9. A positive test was signaled by yellow precipitates of dinitrophenylhydrazone [56]. In case of environmental analysis, formaldehyde would be trapped on a silica gel adsorbent coated with 2,4-DNPH. Then, formaldehyde-dinitrophenylhydrazone was eluted with acetonitrile and followed by GC or HPLC analysis. However, the precipitates of dinitrophenylhydrazone were partially dissolved in acetonitrile. Hence, derivatization technique for formaldehyde determination should permit its determination at concentration below the maximum allowed concentration [57-58]. In this work, 2,4-DNPH was added into reaction mixture in order to quench the reaction prior to analysis.

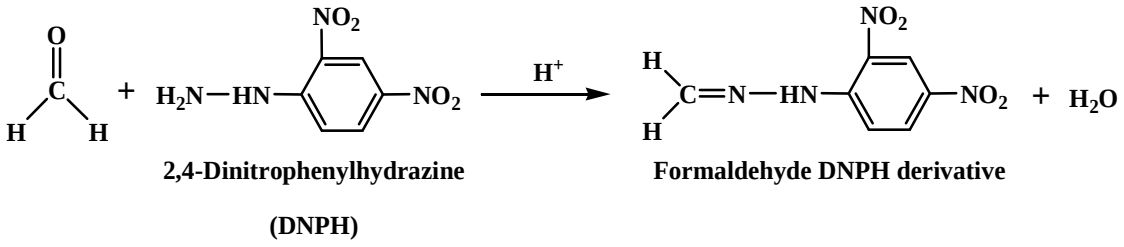

Figure 4.9 Reaction of formaldehyde with 2,4-DNPH [56].

4.3 Catalytic activities of sulfonic functionalized SBA-15 in BPF preparation

In this research, the catalytic performances of synthetic SBA-15 derivatives were evaluated in BPF preparation.

4.3.1 Effect of reaction time

The effect of reaction time was investigated. The catalytic activities of SBA-15-Pr-SO_3H and SBA-15-Ar-SO_3H were performed in Table 4.3 and Table 4.4, respectively. The reaction time was varied in the range of 0.25-4 h. As a result, the BPF yield was increased when the reaction time was risen. At the reaction time of 1 h, SBA-15-Pr-SO_3H could reach high BPF yield closing to 100% indicating the reaction was complete within 1 h. Therefore, the optimum reaction time was 1 h. On the other hand, SBA-15-Ar-SO_3H gave high BPF yield of 93.83% at the same reaction time. However, it was observed that there was almost no change in BPF selectivity and isomer distribution. Both of two catalysts offered BPF selectivity above 95%. In case of BPF isomer distribution, SBA-15-Pr-SO_3H gave *4,4'*-isomer as highest selectivity, whereas SBA-15-Ar-SO_3H preferred *2,4'*-isomer. They performed low selectivity for *2,2'*-isomer owing to high energy of intermediate formation.

Table 4.3 Catalytic activities and BPF isomer distribution in BPF preparation over SBA-15-Pr-SO_3H for different reaction times

Reaction time (h)	% BPF selectivity	% Yield	BPF isomer distribution (%)		
			***2,2'*-BPF**	***2,4'*-BPF**	***4,4'*-BPF**
0.25	97.91	63.42	16.04	39.87	44.09
0.50	98.23	73.64	16.64	39.68	43.68
0.75	98.68	84.63	16.98	39.48	42.53
1	98.13	98.13	16.74	40.96	42.30
4	97.45	97.45	17.16	40.22	42.62

Reaction condition: phenol/formaldehyde = 30 mol mol^{-1}, catalyst/formaldehyde = 15 wt% and temperature = 90°C.

Table 4.4 Catalytic activities and BPF isomer distribution in BPF preparation over SBA-15-Ar-SO_3H for different reaction times

Reaction time (h)	% BPF selectivity	% Yield	BPF isomer distribution (%)		
			***2,2'*-BPF**	***2,4'*-BPF**	***4,4'*-BPF**
0.25	98.42	75.05	17.87	44.89	37.24
0.50	98.47	81.95	16.99	43.27	39.74
0.75	98.85	89.54	16.75	43.45	40.80
1	97.77	93.83	16.54	43.43	40.04
4	97.96	97.96	17.67	44.47	37.86

Reaction condition: phenol/formaldehyde = 30 mol mol^{-1}, catalyst/formaldehyde = 15 wt% and temperature = 90°C.

The corresponding plot of BPF yield over SBA-15-Pr-SO_3H and SBA-15-Ar-SO_3H *versus* reaction time was shown in Figure 4.10. Each result revealed an exponential rise in product yield with initial reaction and then a slow increase in the yield up to the end of the reaction. At first 45 min, kinetic rate of SBA-15-Ar-SO_3H was faster rate than SBA-15-Pr-SO_3H. In contrast, after 45 min, SBA-15-Pr-SO_3H exhibited better performance in BPF production. This result demonstrated that the aryl sulfonic acid sites which has higher polarity than propyl sulfonic acids could be induced with water generated during the reaction. This interaction would lead to the partial deactivation of active sites hindering the access of reactant molecules to the sulfonic sites. The above observation was in agreement with previous literature that the hydrophilicity of the catalyst was paramount importance in determining the activity in water-mediated reactions [16].

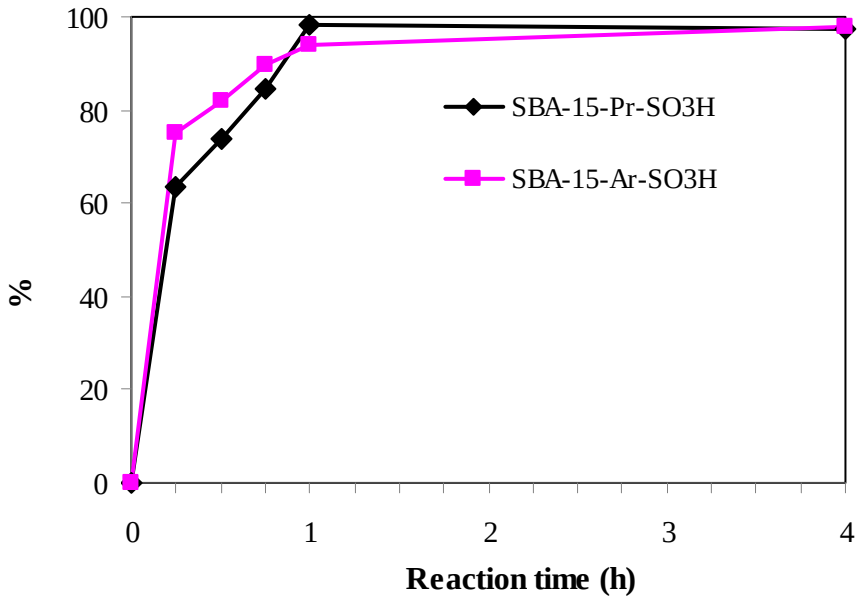

Figure 4.10 The plot of BPF yield over SBA-15-Pr-SO_3H and SBA-15-Ar-SO_3H *versus* reaction time (Reaction condition: phenol/formaldehyde = 30 mol mol^{-1}, catalyst/formaldehyde = 15 wt% and at 90°C).

4.3.2 Effect of phenol to formaldehyde molar ratio

The stoichiometric molar ratio commonly requires two moles of phenol and one mole of formaldehyde to produce one mole of BPF. Nevertheless, in practice, the excess amount of phenol is needed in order to control the reaction and produce more BPF as main product. In this work, various ratios of phenol to formaldehyde were used at 7.5, 15 and 30 mol mol^{-1} by varying quantity of formaldehyde. The effect of phenol to formaldehyde molar ratio on the BPF preparation over SBA-15-Pr-SO_3H and SBA-15-Ar-SO_3H was presented in Table 4.5 and Table 4.6, respectively. From the experimental data, there was significant effect of the phenol to formaldehyde ratio on the product yield and BPF selectivity. The BPF yield and selectivity were increased with decreasing formaldehyde. As a result, the phenol to formaldehyde molar ratio of 30 mol mol^{-1} was the optimum condition due to giving the highest yield and selectivity of BPF. At the lowest reactant ratio

about 7.5 mol mol^{-1}, BPF selectivity was in the range of 80 to 85%. Considering the BPF isomer distribution, *2,4'*- and *4,4'*-isomer selectivity was nearly equal and were maintained around 40%. These results indicated that the effect of reactant ratio had no significant influence on the BPF isomer distribution.

Table 4.5 Catalytic activities and BPF isomer distribution in BPF preparation over SBA-15-Pr-SO_3H at various ratios of phenol to formaldehyde

Phenol/ Formaldehyde (mol mol^{-1})	**% BPF selectivity**	**% Yield**	**BPF isomer distribution (%)**		
			***2,2'*-BPF**	***2,4'*-BPF**	***4,4'*-BPF**
7.5	81.93	80.96	16.42	40.35	43.23
15	91.24	89.84	17.08	41.62	41.30
30	98.13	98.13	16.74	40.96	42.30

Reaction condition: catalyst/formaldehyde = 15 wt%, temperature = 90°C and time = 1 h.

Table 4.6 Catalytic activities and BPF isomer distribution in BPF preparation over SBA-15-Ar-SO_3H at various ratios of phenol to formaldehyde

Phenol/ Formaldehyde (mol mol^{-1})	**% BPF selectivity**	**% Yield**	**BPF isomer distribution (%)**		
			***2,2'*-BPF**	***2,4'*-BPF**	***4,4'*-BPF**
7.5	85.57	81.47	16.58	42.21	41.21
15	95.86	87.36	17.49	40.96	41.55
30	97.77	93.83	16.54	43.43	40.04

Reaction condition: catalyst/formaldehyde = 15 wt%, temperature = 90°C and time = 1 h.

4.3.3 Effect of catalyst to formaldehyde weight ratio

The catalytic performance of sulfonic functionalized SBA-15 at different loadings was studied. The catalyst amount was varied in the range of 5 to 30% of formaldehyde weight. As seen in Table 4.7 and Table 4.8, BPF yield was increased when the amount of catalyst was increased in the reaction mixture. It was obvious that, with increased catalyst amount, the acid sites of catalyst for reaction were also increased. According to the highest BPF yield, catalyst to formaldehyde weight ratio of 15 wt% was chosen for further study. In addition, it was noticeable that BPF selectivity and isomer distribution were independent of the acid loading. Likewise, the absence of catalyst in the reaction mixture was also investigated. This result demonstrated that BPF could occur in non-catalytic reaction which gave the lowest product yield of 8.09% and selectivity of 29.56% to BPF. Owing to producing low product yield, catalyst was needed to use in reaction mixture for the purpose of increasing in product yield and controlling selectivity of product.

Table 4.7 Catalytic activities and BPF isomer distribution in BPF preparation over SBA-15-Pr-SO_3H at various ratios of catalyst to formaldehyde

Catalyst/ Formaldehyde (wt%)	**% BPF selectivity**	**% Yield**	**BPF isomer distribution (%)**		
			***2,2′*-BPF**	***2,4′*-BPF**	***4,4′*-BPF**
0	29.56	8.09	38.03	30.99	30.99
5	96.20	59.72	17.60	43.77	38.63
7.5	97.96	67.86	17.09	42.80	40.12
10	97.41	78.45	17.10	41.67	41.23
15	98.13	98.13	16.74	40.96	42.30
20	97.23	97.23	16.75	42.21	41.04
30	97.34	97.34	16.36	42.12	41.52

Reaction condition: phenol/formaldehyde = 30 mol mol^{-1}, temperature = 90°C and time = 1 h.

Table 4.8 Catalytic activities and BPF isomer distribution in BPF preparation over SBA-15-Ar-SO_3H at various ratios of catalyst to formaldehyde

Catalyst/ Formaldehyde (wt%)	% BPF selectivity	% Yield	BPF isomer distribution (%)		
			2,2'-BPF	*2,4'*-BPF	*4,4'*-BPF
0	29.56	8.09	38.03	30.99	30.99
5	97.05	60.02	17.30	42.65	40.05
7.5	95.70	70.77	16.96	42.21	40.84
10	96.47	93.05	16.96	42.21	40.84
15	97.77	93.83	16.54	43.43	40.04
20	98.19	98.19	16.57	43.48	39.94
30	98.19	98.19	16.17	43.04	40.79

Reaction condition: phenol/formaldehyde = 30 mol mol^{-1}, temperature = 90°C and time = 1 h.

4.3.4 Effect of reaction temperature

To determine the effect of reaction temperature, the experiments were conducted at temperatures ranging from 50 to 110°C. As shown in Table 4.9 and Table 4.10, the catalyst activity depended on the reaction temperature. By increasing temperature from 50 to 90°C, the BPF yield was increased significantly. For SBA-15-Pr-SO_3H, the BPF yield was near 100% at the reaction temperature of 90°C. In the case of SBA-15-Ar-SO_3H, it gave the BPF yield of 93.83% at the same reaction temperature. As the temperature increased to 110°C, the BPF yield was near 100% in case of SBA-15-Ar-SO_3H. Considering the BPF selectivity and isomer distribution, SBA-15-Pr-SO_3H was able to produce *4,4'*-isomer as highest selectivity, whereas SBA-15-Ar-SO_3H preferred *2,4'*-isomer. The selectivity was slightly changed in the range of 40 to 45%.

Table 4.9 Catalytic activities and BPF isomer distribution in BPF preparation over SBA-15-Pr-SO_3H at various reaction temperatures

Temperature (°C)	% BPF selectivity	% Yield	BPF isomer distribution (%)		
			***2,2′*-BPF**	***2,4′*-BPF**	***4,4′*-BPF**
50	97.38	74.66	15.83	39.35	44.82
70	96.84	91.06	15.92	39.39	44.69
90	98.13	98.13	16.74	40.96	42.30
110	97.11	97.11	16.26	42.62	41.12

Reaction condition: phenol/formaldehyde = 30 mol mol^{-1}, catalyst/formaldehyde = 15 wt%, and time = 1 h.

Table 4.10 Catalytic activities and BPF isomer distribution in BPF preparation over SBA-15-Ar-SO_3H at various reaction temperatures

Temperature (°C)	% BPF selectivity	% Yield	BPF isomer distribution (%)		
			***2,2′*-BPF**	***2,4′*-BPF**	***4,4′*-BPF**
50	96.52	73.92	14.53	40.51	44.97
70	97.60	85.29	15.99	41.84	42.17
90	97.77	93.83	16.54	43.43	40.04
110	98.00	98.00	16.68	43.88	39.44

Reaction condition: phenol/formaldehyde = 30 mol mol^{-1}, catalyst/formaldehyde = 15 wt%, and time = 1 h.

4.3.5 Effect of solvent types

To remark influence of solvent in BPF synthesis, various solvents such as toluene, methyl isobutyl ketone (MIBK), acetonitrile and water were added into the reaction mixture. The polarity of organic solvent which expressed in terms of dielectric constant was shown in Table 4.11.

Table 4.11 Dielectric constant of various solvents [59]

Solvents	Dielectric constant
Toluene	2.4
Methyl isobutyl ketone (MIBK)	14.6
Acetonitrile	37.5
Water	80.0

The catalytic performance of sulfonic functionalized SBA-15 in various solvents was performed in Table 4.12 and Table 4.13. The solvent effect was found to be an important influence on the BPF yield and isomer distribution. Due to producing high BPF yield, both SBA-15-Pr-SO_3H and SBA-15-Ar-SO_3H showed the best performance in the absence of solvent. Considering the presence of solvent in the reaction system, the non-polar solvent contained a benzene ring with electron-donating substituents such as toluene demonstrated better catalytic activity than the polar solvent. When the polarity of solvent was increased, the BPF yield was decreased markedly. Especially, the presence of water in the system would dramatically decrease BPF yield and selectivity, indicating both non-polar and polar solvents retarded this reaction. Generally, solvent has two main duties. Firstly, reactant will easily approach to active sites of catalyst under the presence of solvent. Another is that solvent can solve reactants. In this research, amount of phenol was much higher than solvent. Moreover, starting materials (phenol and formaldehyde) were homogeneous under reaction condition due to low melting point of reactants. Thus, the presence of solvent in BPF synthesis might be unnecessary. In case of BPF isomer distribution, *4,4'*-isomer was significantly increased from 42 to 53%. It was obvious that high polarity of solvent might stabilize 4-hydroxybenzyl carbocation

better than 2-hydroxybenzyl carbocation. Thus, amount of *4,4'*-isomer was higher than other isomers. This result was in agreement with literature [7] that the presence of polar solvent would enhance high quantity of *4,4'*-BPF.

Table 4.12 Catalytic activities and BPF isomer distribution in BPF preparation over SBA-15-Pr-SO_3H at various solvents

Solvent	**% BPF selectivity**	**% Yield**	**BPF isomer distribution (%)**		
			***2,2'*-BPF**	***2,4'*-BPF**	***4,4'*-BPF**
Without solvent	98.13	98.13	16.74	40.96	42.30
Toluene	98.40	62.17	17.46	40.68	41.86
MIBK	95.26	42.81	16.33	38.51	45.15
Acetonitrile	95.74	40.37	16.76	35.92	47.32
Water	81.48	24.84	14.19	33.41	52.40

Reaction condition: phenol/formaldehyde = 30 mol mol^{-1}, catalyst/formaldehyde = 15 wt%, temperature = 90°C, time = 1 h and solvent = 2 mL.

Table 4.13 Catalytic activities and BPF isomer distribution in BPF preparation over SBA-15-Ar-SO_3H at various solvents

Solvent	**% BPF selectivity**	**% Yield**	**BPF isomer distribution (%)**		
			***2,2'*-BPF**	***2,4'*-BPF**	***4,4'*-BPF**
Without solvent	97.77	93.83	16.54	43.43	40.04
Toluene	96.72	67.52	17.35	41.21	41.45
MIBK	96.65	51.16	15.16	40.84	43.29
Acetonitrile	96.85	46.18	14.90	37.44	47.66
Water	78.20	22.83	13.94	32.92	53.12

Reaction condition: phenol/formaldehyde = 30 mol mol^{-1}, catalyst/formaldehyde = 15 wt%, temperature = 90°C, time = 1 h and solvent = 2 mL.

From all effects in BPF preparation, these concluded that the optimum condition was phenol to formaldehyde molar ratio of 30 mol mol^{-1}, catalyst to formaldehyde weight ratio of 15wt% at 90°C for 1 h under the absence of solvent. This optimized condition was applied in further study with other catalysts.

4.4 Comparison of catalytic activity in BPF preparation over sulfonic functionalized SBA-15 with other catalysts

4.4.1 Ion-exchange resins

Commercial sulfonic acid-based resins such as Amberlyst-15 and Nafion SAC-13 were used in this study. Additionally, some characterization data corresponding to the commercial ion-exchange resins were depicted in Table 4.14. In this case, the characterization was provided by the suppliers (Rohm & Hass for the Amberlyst resins and DuPont for Nafion SAC-13).

Table 4.14 Physicochemical and textural properties for ion-exchange resins[a]

Catalyst	BET area ($m^2 \cdot g^{-1}$)	Pore size (Å)	Pore volume ($cm^3 \cdot g^{-1}$)	Acid capacity[b]	Temp. limit (°C)
Amberlyst-15	53	300	0.4	4.8	120
Nafion SAC-13	200	>100	0.6	0.12	200

[a]Properties provided by the suppliers,
[b]Millimoles of acid centers per gram of catalyst

Catalytic activities of SBA-15-Pr-SO_3H, Amberlyst-15 and Nafion SAC-13 were investigated as acidic catalyst in BPF preparation. The result in Figure 4.11 disclosed fast kinetic rate in BPF synthesis with a gradually increasing reaction time from 0 to 60 min. At first 15 min, SBA-15-Pr-SO_3H performed highest BPF yield about 63%, while Amberlyst-15 exhibited slower rate at first 15 min due to having low total surface area. Likewise, Amberlyst-15 has a physical form in spherical bead and most of the active sites are buried within the polymer matrix, whereas SBA-15-Pr-SO_3H showed higher surface area and their physical forms in powder [60]. However, after 30 min, kinetic rate of Amberlyst-15 was faster than other catalysts, indicating reactants spent time to diffuse into inner active sites. Additionally, this catalyst could give high BPF yield closing to 100% at the reaction time only 45 min. For Nafion SAC-13, it had high surface area, but Amberlyst-15 contained acid capacity five times higher in acid capacity (Table 4.14). Thus, Amberlyst-15 performed faster kinetic rate than Nafion SAC-13.

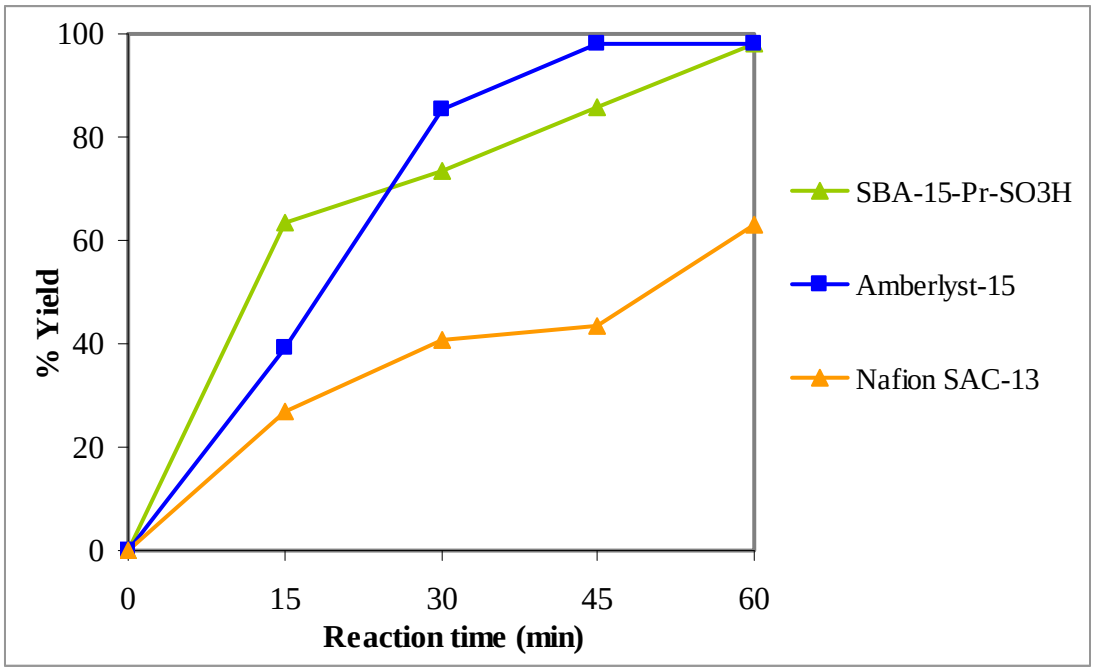

Figure 4.11 The plot of BPF yield over SBA-15-Pr-SO_3H and commercial resins *versus* reaction time (Reaction condition: phenol/formaldehyde = 30 mol mol^{-1}, catalyst/formaldehyde = 15 wt%, and at 90°C).

At the reaction time of 1 h, both SBA-15-Pr-SO_3H and Amberlyst-15 were able to produce nearby 100% of BPF yield. In contrast, Nafion SAC-13 gave only 62.91% of BPF yield. By comparing the isomer distribution, SBA-15-Pr-SO_3H gave *4,4'*-isomer as highest selectivity, whereas sulfonated resins preferred *2,4´*-isomer (Table 4.15).

Table 4.15 Comparison of catalytic activities in BPF preparation over SBA-15-Pr-SO_3H with ion-exchange resins at the reaction time of 1 h

Catalyst	% BPF selectivity	% Yield	BPF isomer distribution (%)		
			***2,2´*-BPF**	***2,4´*-BPF**	***4,4´*-BPF**
SBA-15-Pr-SO_3H	98.13	98.13	16.74	40.96	42.30
Amberlyst-15	98.14	98.14	18.20	47.22	34.58
Nafion SAC-13	95.42	62.91	23.22	44.26	32.52

Reaction condition: phenol/formaldehyde = 30 mol mol^{-1}, catalyst/formaldehyde = 15 wt%, temperature = 90°C and time = 1 h.

4.4.2 Zeolites

A variety of zeolites, including H-MCM-22, commercial H-ZSM-5 and commercial H-Beta with SiO_2/Al_2O_3 ratios around 30, were used for catalyzing phenol with formaldehyde to produce BPF. For H-MCM-22, this catalyst was obtained from research group [61]. In order to investigate the effect of the structure on BPF preparation, the physical properties of zeolites were characterized by N_2 adsorption. As shown in Table 4.16, total specific surface area and micropore volume decreased in the following order: H-beta > H-MCM-22 > H-ZSM-5. With respect to their microporous characteristics, ZSM-5 had two types of pores which both formed by 10-membered oxygen rings. Beta zeolite had 12-ring pore opening in three directions. For MCM-22, the structure had two non-connected pore systems, one with

12-ring pores, and the other having 10-ring pores. Structures of ZSM-5, MCM-22 and Beta zeolite were shown in Figure 4.12.

Table 4.16 Physicochemical and textural properties for zeolites

Catalyst	**Total specific surface area[a] ($m^2 \cdot g^{-1}$)**	**Micropore distribution, d_p[b] (nm)**	**External surface area, S_{ext}[c] ($m^2 \cdot g^{-1}$)**	**Micropore volume, V_p[c] ($cm^3 \cdot g^{-1}$)**
Commercial H-beta (SiO_2/Al_2O_3 = 30.3)	534.17	0.6	199.07	0.1521
Commercial H-ZSM-5 (SiO_2/Al_2O_3 = 28.2)	334.31	0.6	88.22	0.1056
H-MCM-22 (SiO_2/Al_2O_3 = 30)	407.91	0.6	74.82	0.1481

[a]Calculated using the BET plot method,
[b]Calculated using the MP plot method,
[c]Calculated using the t-plot method.

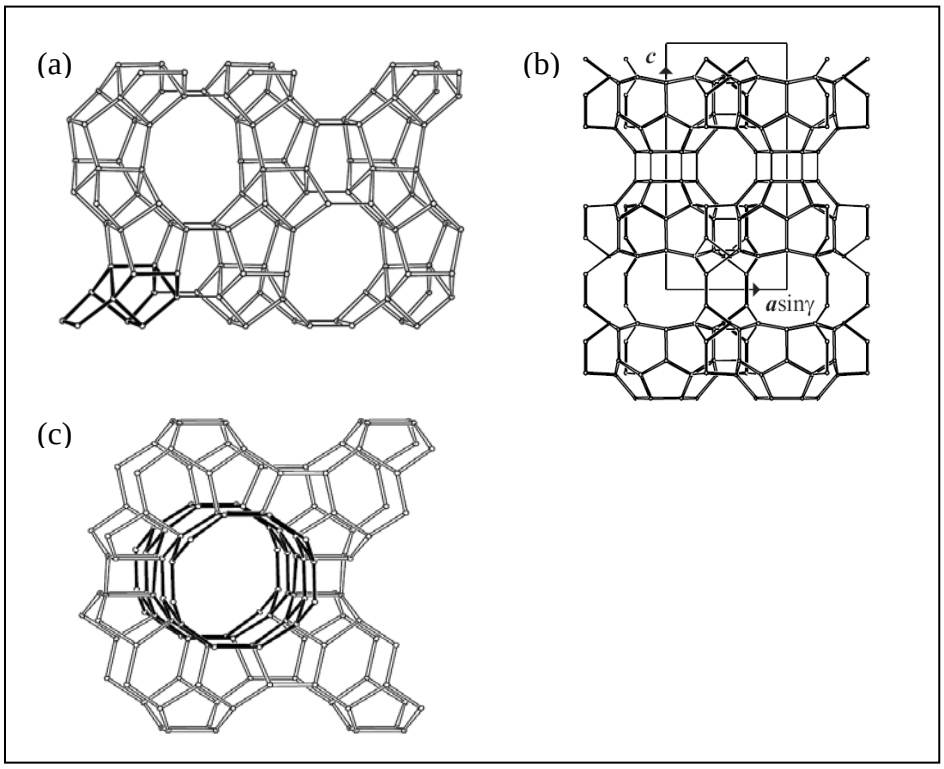

Figure 4.12 Structures of zeolites (a) ZSM-5, (b) MCM-22 and (c) Beta zeolite [62-64].

Among different zeolites (Figure 4.13), it was observed that H-beta with 12-membered ring channels performed high reactivity ought to an easier diffusion of the reactants and products in this large-pore zeolite. Contrastingly, H-ZSM-5 with 10-membered ring channels showed the lowest reactivity. This result indicated that pore-structure of zeolites affected on BPF preparation. Furthermore, the hydrophobicity of catalyst had an influence on this reaction. The commercial formaldehyde solution which contained a lot of water might strongly adsorb on the zeolite and retard the adsorption of the reactants. Therefore, hydrophobic zeolites such as H-beta zeolite were suitable for BPF preparation. This observation was corresponding to Namba *et al*.'s research [2] that H-beta had both external acidity and pore acidity. This reaction occurred mainly within the pores of 12-MR channels. The acid sites at the external surface were unlikely to promoted BPF synthesis because the external silanol groups were surrounded by water.

In comparison with SBA-15-Pr-SO_3H, at first 30 min, H-beta gave higher BPF yield than SBA-15-Pr-SO_3H. Nevertheless, after 30 min, BPF yield of SBA-15-Pr-SO_3H was higher than microporous materials. It was clear that the relatively large mesopores on derivertized SBA-15 facilitated the diffusion of the reactant and product molecules in BPF synthesis.

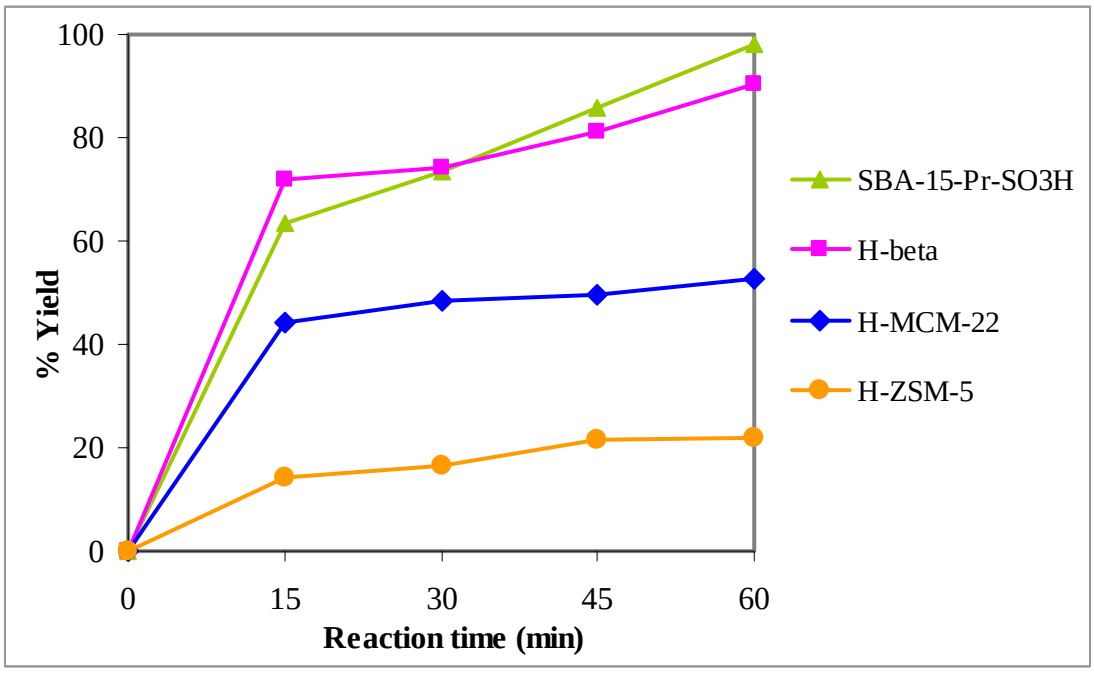

Figure 4.13 The plot of BPF yield over SBA-15-Pr-SO_3H and zeolites *versus* reaction time (Reaction condition: phenol/formaldehyde = 30 mol mol^{-1}, catalyst/formaldehyde = 15 wt%, and at 90°C).

Catalytic activities in BPF preparation over various zeolites at the reaction time of 1 h were exhibited in Table 4.17. Commercial H-beta gave BPF yield of 90.22% with high selectivity to *4,4'*-isomer about 48% indicating that zeolite with large pore opening was more selective for the synthesis of BPF. On the other hand, H-MCM-22 and commercial H-ZSM-5 produced *2,4'*-isomer as highest selectivity.

Table 4.17 Comparison of catalytic activities in BPF preparation over SBA-15-Pr-SO_3H with zeolites at the reaction time of 1 h

Catalyst	% BPF selectivity	% Yield	BPF isomer distribution (%)		
			***2,2´*-BPF**	***2,4´*-BPF**	***4,4´*-BPF**
SBA-15-Pr-SO_3H	98.13	98.13	16.74	40.96	42.30
Commercial H-beta	96.86	90.22	20.97	30.92	48.11
Commercial H-ZSM-5	86.02	22.05	21.65	42.53	35.82
H-MCM-22	91.94	52.81	18.62	45.96	35.41

Reaction condition: phenol/formaldehyde = 30 mol mol^{-1}, catalyst/formaldehyde = 15 wt%, temperature = 90°C and time = 1 h.

4.4.3 Mesoporous materials

At present, mesoporous material is an alternative in catalysis due to containing high surface area and large pore (2-50 nm). SBA-15 is a mesoporous material which has high surface area, large pore volume, high thermal stability and reusability. In this research, Al-SBA-15 with Si/Al ratios from 10 to 200 mol mol^{-1} has been investigated in BPF synthesis. All catalysts were obtained from research group [65]. Additionally, textural properties of purely SBA-15 and Al-SBA-15 with different Si/Al ratios were summarized in Table 4.18.

Table 4.18 Textural properties of SBA-15 and Al-SBA-15 with various Si/Al ratios

Catalyst	Si/Al mole ratio in catalyst[a]	Total specific surface area[b] ($m^2 \cdot g^{-1}$)	Pore size distribution[c] (nm)	Mesopore volume[c] ($cm^3 \cdot g^{-1}$)
SBA-15	-	862.13	9.23	1.15
Al-SBA-15 (Si/Al = 10)	8.0	469.26	9.23	0.90
Al-SBA-15 (Si/Al = 25)	18.5	587.10	9.23	1.00
Al-SBA-15 (Si/Al = 50)	33.4	645.86	9.23	1.10
Al-SBA-15 (Si/Al = 100)	69.3	703.98	9.23	1.13
Al-SBA-15 (Si/Al = 200)	130.1	722.11	9.23	1.10

[a]Aluminum (Al) was determined by ICP-AES,
[b]Calculated using the BET plot method,
[c]Calculated using the BJH method.

Among various Si/Al ratios (Figure 4.14), the Al-SBA-15 catalyst having a Si/Al ratio in catalyst of 33.4 mol mol^{-1} performed good catalytic performance in BPF preparation indicating that BPF synthesis process was catalyzed mostly by moderate acidic catalysts. This observation was in agreement with previous literature. From Namba *et al.*'s research, among different Si/Al ratios of Al-MCM-41 catalysts, Al-MCM-41 having moderate Si/Al ratio showed the best catalytic performance in BPF synthesis [9].

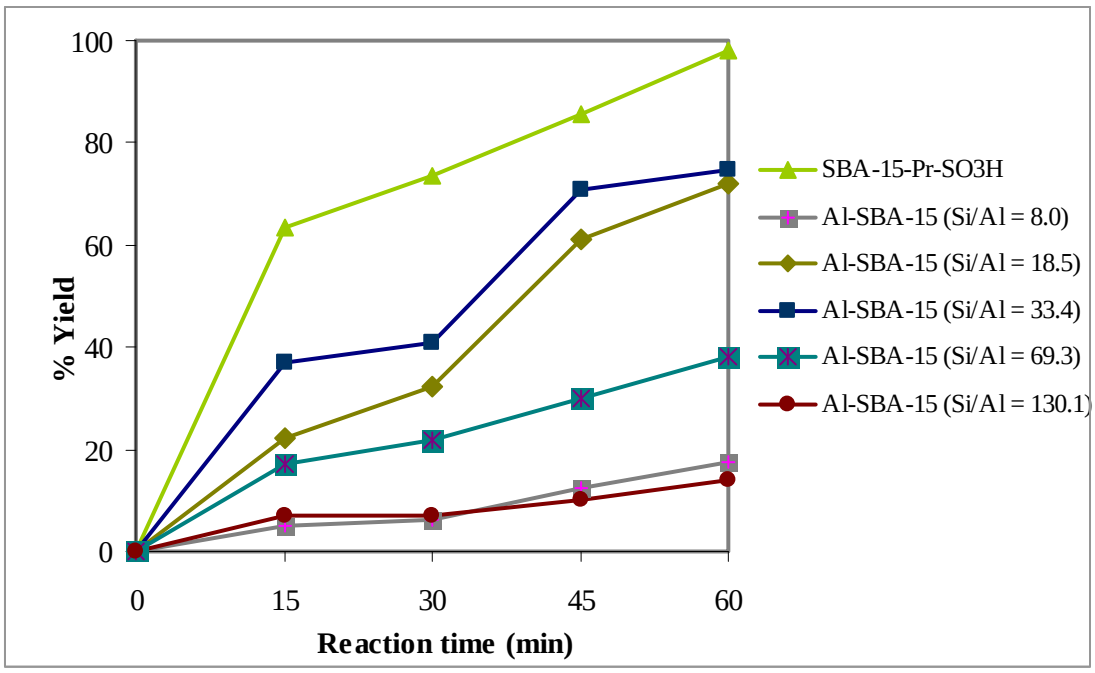

Figure 4.14 The plot of BPF yield over SBA-15-Pr-SO_3H and Al-SBA-15 mesoporous materials *versus* reaction time (Reaction condition: phenol/formaldehyde = 30 mol mol^{-1}, catalyst/formaldehyde = 15 wt%, and at 90°C).

At the reaction time of 1 h (Table 4.19), purely siliceous SBA-15 gave low BPF yield (5.59%) due to lack of acid site. Among difference Si/Al ratios, Al-SBA-15 with Si/Al ratio of 50 was able to produce highest BPF yield of 74.52% with high selective to *2,4'*-BPF about 54.08%. From Namba *et al.*'s research [8], Al-grafted MCM-41 having Si/Al ratio of 50 gave BPF yield of 63.2% at the same reaction time. This reported value was lower than the reaction carried over Al-SBA-15 because of the lower pore size of Al-MCM-41 *ca.* 2.8 nm estimated by the BJH method. On the other hand, SBA-15-Pr-SO_3H performed better catalytic performance than Al-SBA-15 and Al-MCM-41 due to stronger acid strength.

Table 4.19 Comparison of catalytic activities in BPF preparation over SBA-15-Pr-SO_3H with mesoporous materials at the reaction time of 1 h

Catalyst	% BPF selectivity	% Yield	BPF isomers distributions (%)		
			***2,2´*-BPF**	***2,4´*-BPF**	***4,4´*-BPF**
SBA-15-Pr-SO_3H	98.13	98.13	16.74	40.96	42.30
SBA-15	32.84	5.59	33.67	23.47	42.86
Al-SBA-15 (Si/Al = 8.0)	88.02	17.44	30.62	47.56	21.82
Al-SBA-15 (Si/Al = 18.5)	96.50	71.79	28.48	54.35	17.17
Al-SBA-15 (Si/Al = 33.4)	96.08	74.52	27.77	54.08	18.15
Al-SBA-15 (Si/Al = 63.9)	93.23	37.95	30.49	53.06	16.44
Al-SBA-15 (Si/Al = 130.1)	82.68	14.06	37.69	36.57	25.75

Reaction condition: phenol/formaldehyde = 30 mol mol^{-1}, catalyst/formaldehyde = 15 wt%, temperature = 90°C and time = 1 h.

4.5 Recycle of catalysts

One of the main advantages of using heterogeneous catalysts is the ease of separation and can be reused in the successive catalytic cycles. In this research, SBA-15-Pr-SO_3H was chosen to study in this case because its performance was better than SBA-15-Ar-SO_3H. The used catalyst was washed with ethanol for several times and dried at 80°C overnight. In addition, the used catalyst was regenerated using the procedure what describe in Section 3.8. The used and regenerated catalysts were characterized prior to testing in the next reactions.

4.5.1 Characterization of used and regenerated catalysts

The XRD patterns of fresh, used and regenerated SBA-15-Pr-SO_3H catalysts were shown in Figure 4.15. As a result, they still exhibited three characteristic peaks of hexagonal phase like the fresh catalyst. However, the used and regenerated catalysts were shifted slightly too high angle than fresh catalyst. The adsorption-desorption isotherms of those catalysts were presented in Figure 4.16. All catalysts showed the characteristic isotherm of mesoporous materials. The used catalyst had the specific surface area of 522.10 m^3/g that was reduced about 29 % as compared to the fresh one (728.14 m^3/g) due to blockage of remaining organic molecules inside the mesoporous pore (Table 4.20). The specific surface area of regenerated catalyst was higher than used catalyst. However, all samples still remained a narrow distribution with the pore size of 7.05 nm, indicating the stability of synthetic catalyst.

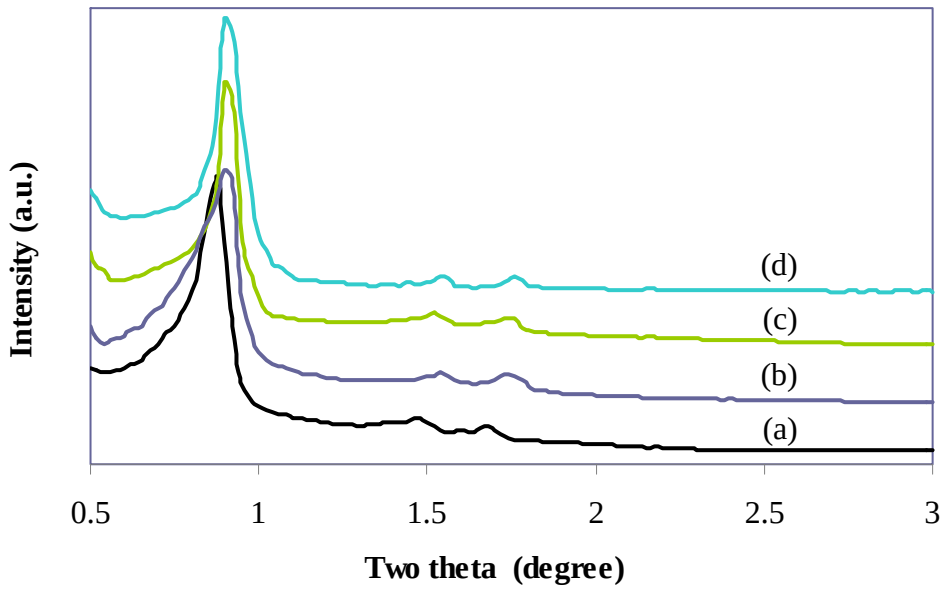

Figure 4.15 XRD patterns of (a) fresh, (b) used, (c) 1st regenerated and (d) 2nd regenerated SBA-15-Pr-SO_3H catalysts.

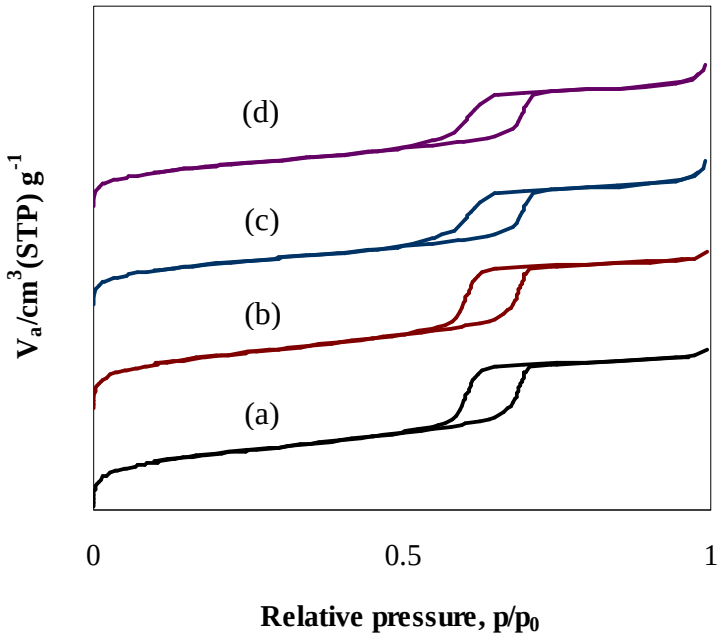

Figure 4.16 N_2 adsorption-desorption isotherms of (a) fresh, (b) used, (c) 1st regenerated and (d) 2nd regenerated SBA-15-Pr-SO_3H catalysts.

Table 4.20 Textural properties of fresh, used and regenerated SBA-15-Pr-SO_3H

Catalyst	**Total specific surface area[a] ($m^2 \cdot g^{-1}$)**	**Pore size distribution[b] (nm)**	**Mesopore volume[b] ($cm^3 \cdot g^{-1}$)**
Fresh	728.14	7.05	0.79
Used	522.10	7.05	0.58
1st regenerated	650.27	7.05	0.73
2nd regenerated	534.59	7.05	0.59

[a]Calculated using the BET plot method,
[b]Calculated using the BJH method.

The SEM images of used and regenerated SBA-15-Pr-SO_3H catalysts were shown in Figure 4.17. The morphology of all catalysts still remained aggregated particles with rope-like structure.

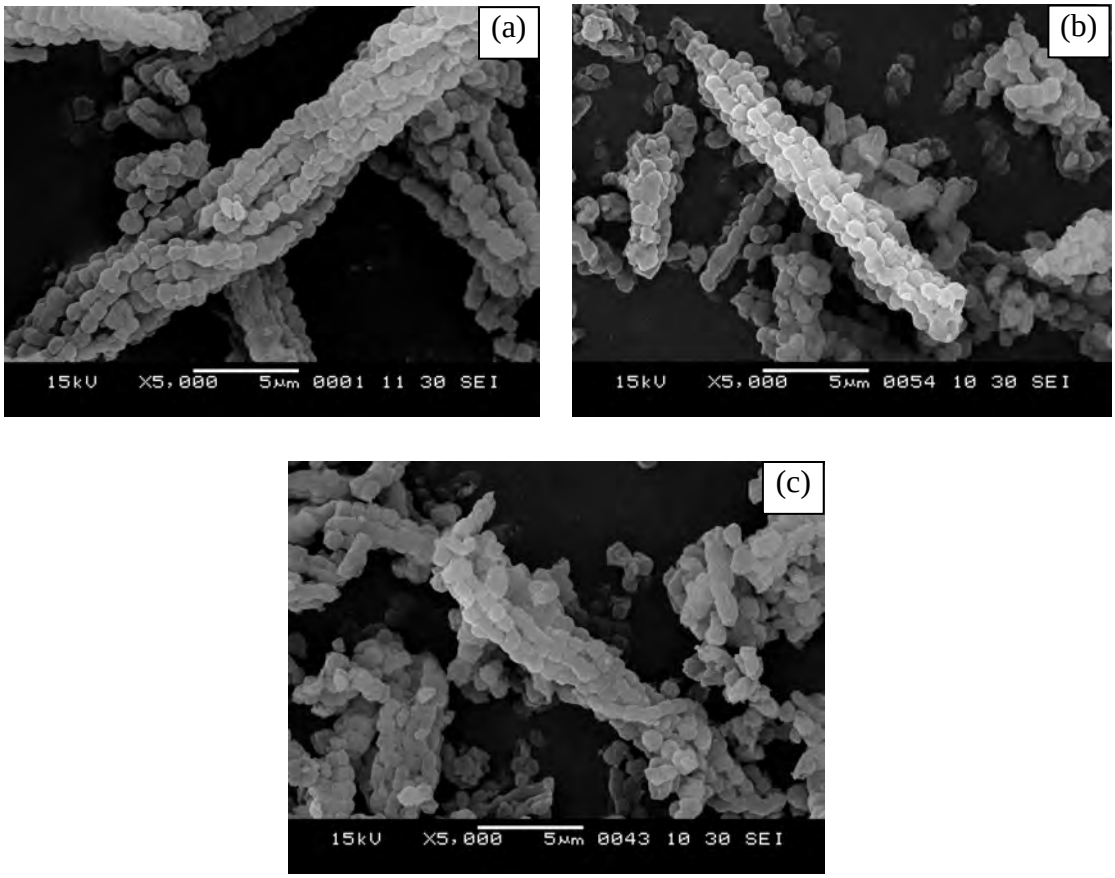

Figure 4.17 SEM images of (a) used SBA-15-Pr-SO3H, (b) 1st regenerated SBA-15-Pr-SO_3H and (c) 2nd regenerated SBA-15-Pr-SO_3H.

4.5.2 Activity of recycled SBA-15-Pr-SO_3H

To examine the reusability of SBA-15-Pr-SO_3H, it was repeatedly tested in BPF preparation under the optimum condition. As shown in Figure 4.18, when the used SBA-15-Pr-SO_3H was utilized, the BPF yield was dramatically decreased from 98.13 to 67.39% without considerable change in BPF selectivity and isomer distribution. The deactivation of the catalyst may be caused by accumulation of coke on the acid sites of catalyst.

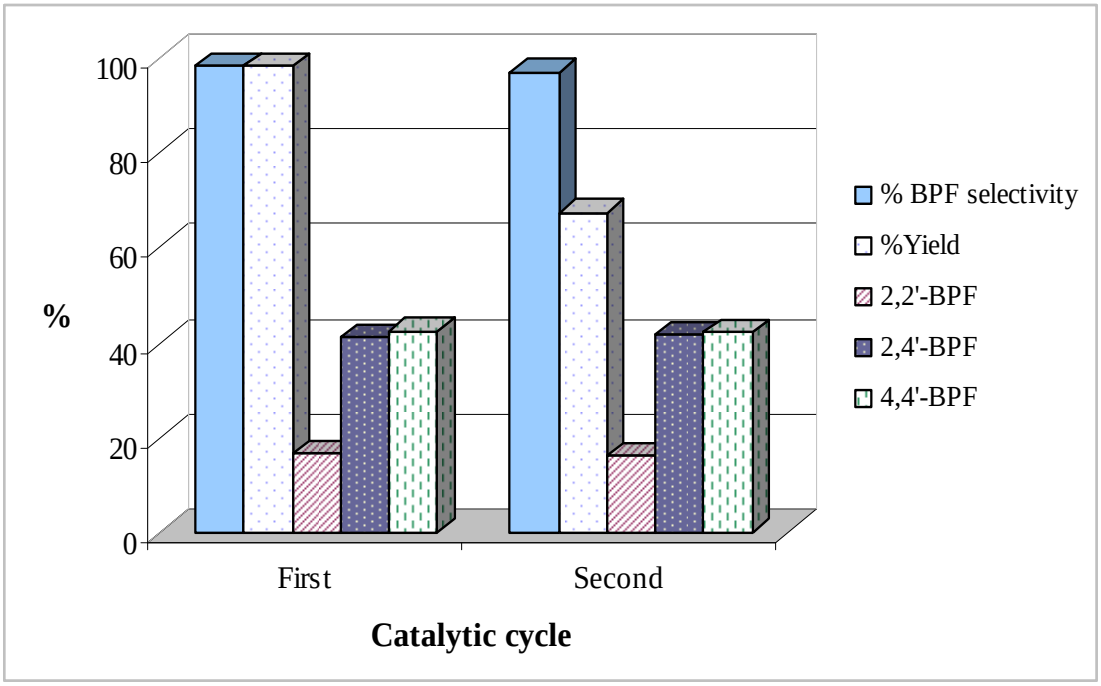

Figure 4.18 Activities of fresh and recycle SBA-15-Pr-SO_3H in BPF synthesis (Reaction conditions: phenol/formaldehyde = 30 mol mol^{-1}, catalyst/formaldehyde = 15 wt% at 90°C for 1 h).

4.5.3 Activity of regenerated SBA-15-Pr-SO_3H

From above result, the used catalyst was developed in order to improve its catalytic performance. As seen in Figure 4.19, after the used catalyst was regenerated, its catalytic activity was increased nearly the fresh one. In case of the second regenerated SBA-15-Pr-SO_3H, BPF yield was slightly decreased from 97.10 to 92.19% as compared to the first regenerated catalyst. Moreover, there was almost no change in BPF selectivity and isomer distribution.

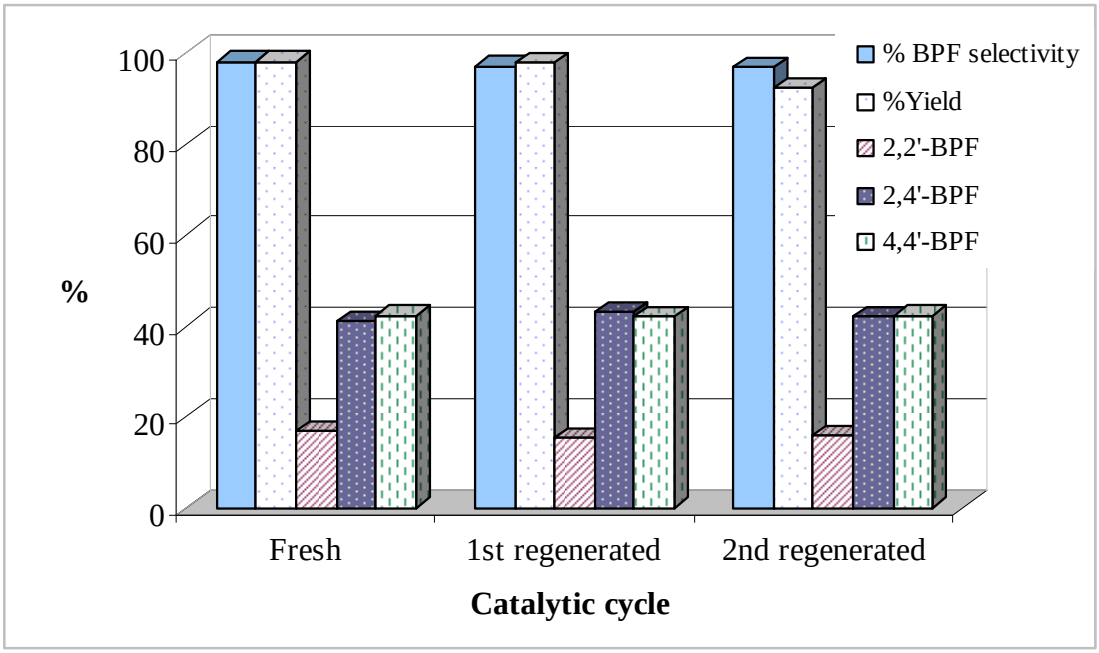

Figure 4.19 Activities of fresh, 1st and 2nd regenerated SBA-15-Pr-SO_3H in BPF synthesis (Reaction conditions: phenol/formaldehyde = 30 mol mol^{-1}, catalyst/formaldehyde = 15 wt% at 90°C for 1 h).

4.5.4 Activity of recycled Amberlyst-15

In BPF preparation, Amberlyst-15 exhibited comparable catalytic activity to SBA-15-Pr-SO_3H. In this work, reusability of sulfonated resin was also investigated using the procedure similar to SBA-15-Pr-SO_3H. The result was shown in Figure 4.20. The BPF yield of the first and second used Amberlyst-15 was 68.71 and 29.09%, respectively. However, BPF isomer distribution was unchanged. This result demonstrated the stability of ion-exchange resin was limited.

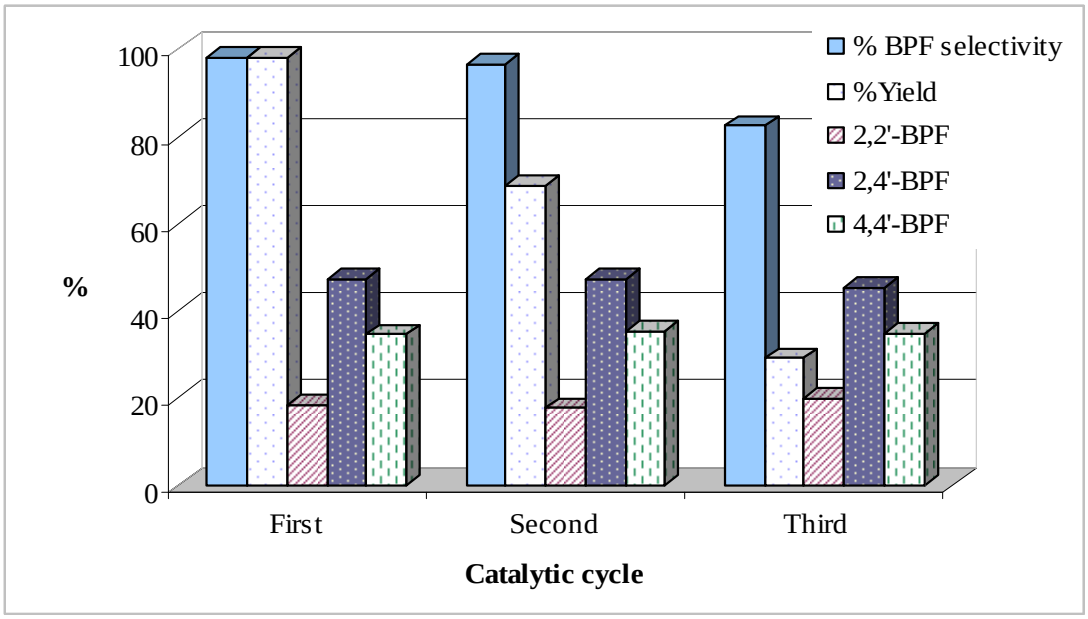

Figure 4.20 Activities of first, second and third recycled Amberlyst-15 in BPF synthesis (Reaction conditions: phenol/formaldehyde = 30 mol mol^{-1}, catalyst/formaldehyde = 15 wt% at 90°C for 1 h).

4.6 Proposed reaction mechanism for BPF preparation

A possible explanation in the formation of BPF was described as follows:

In an aqueous solution of formaldehyde, the monomeric form of formaldehyde was mostly present in the form of methylene glycol. Methylene glycol was activated by a proton to form methylol cation with released of a water molecule (Figure 4.21) [10].

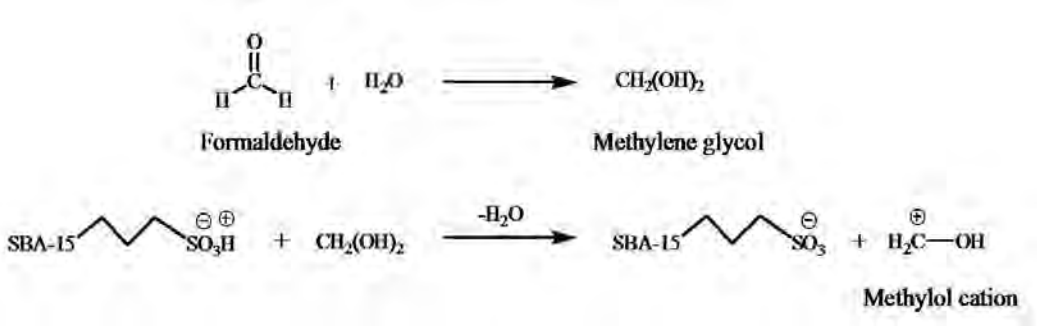

Figure 4.21 Proposed reaction mechanism for methylol cation formation [10].

The electrophilic attack of methylol cation on phenol could take place at ortho and para positions to form 2-hydrozybenzyl alcohol and 4-hydrozybenzyl alcohol, respectively (Figure 4.22 and Figure 4.23) [66].

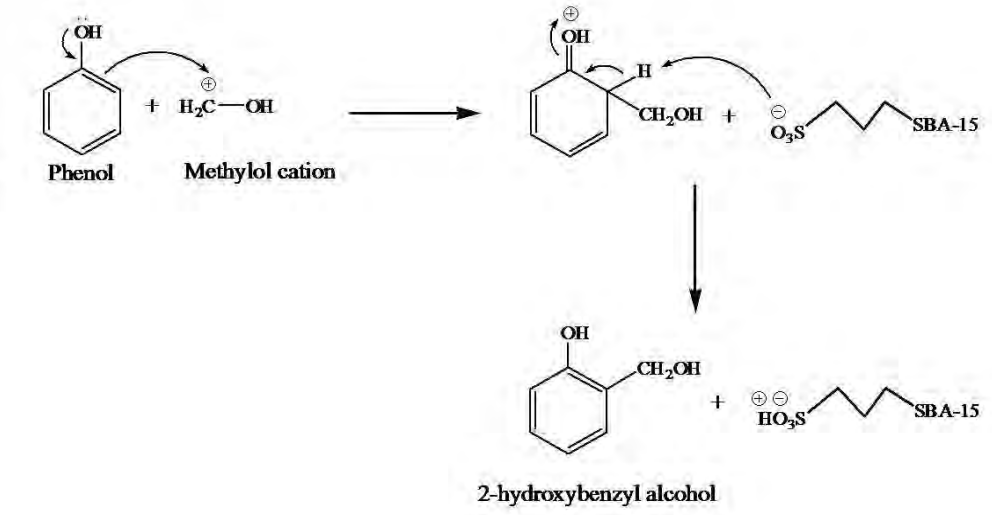

Figure 4.22 Proposed reaction mechanism for 2-hydroxybenzyl alcohol formation.

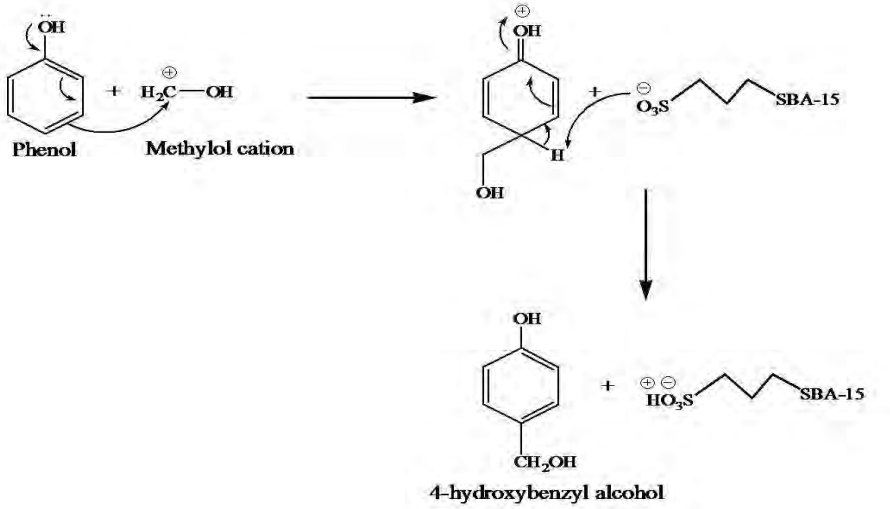

Figure 4.23 Proposed reaction mechanism for 4-hydroxybenzyl alcohol formation.

Then, 2-hydrozybenzyl alcohol and 4-hydrozybenzyl alcohol were protonated and abstracted a water molecule to form hydroxybenzyl carbocation intermediate (Figure 4.24 and Figure 4.25) [10].

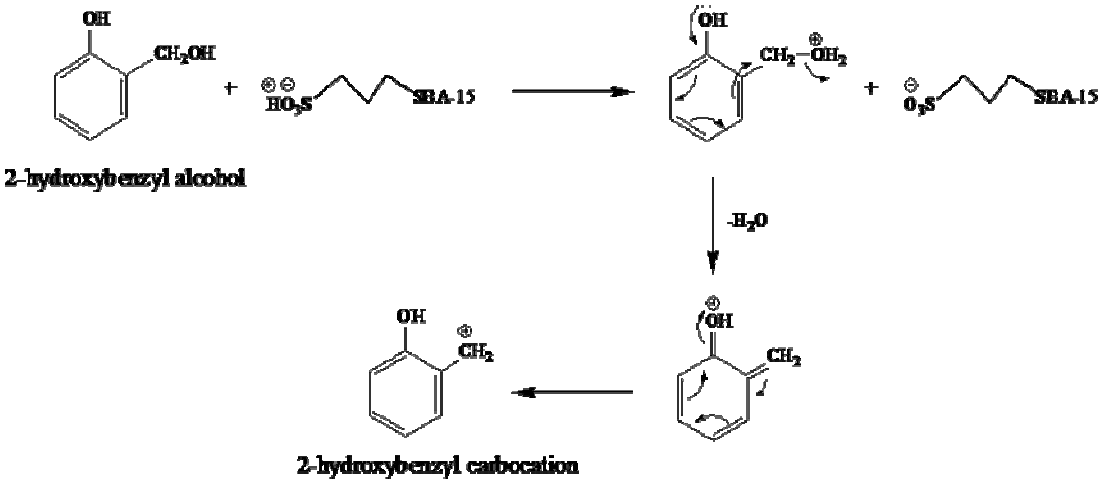

Figure 4.24 Proposed reaction mechanism for 2-hydroxybenzyl carbocation formation.

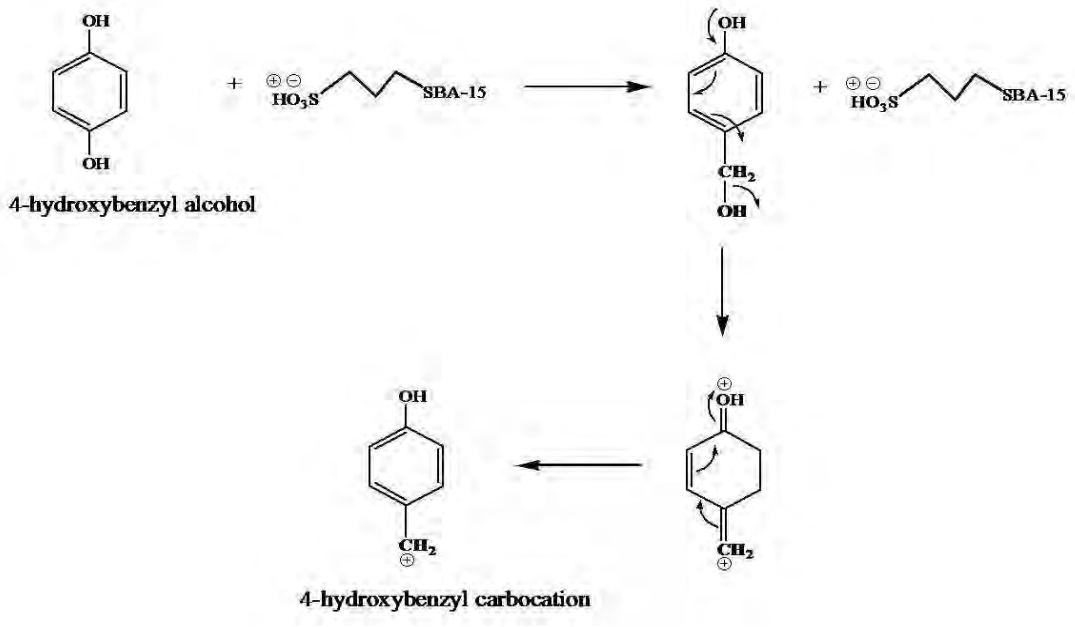

Figure 4.25 Proposed reaction mechanism for 4-hydroxybenzyl carbocation formation.

Finally, hydroxybenzyl carbocation intermediates were reacted with the second molecule of phenol *via* electrophilic aromatic substitution to generate isomeric mixture of BPF (Figure 4.26).

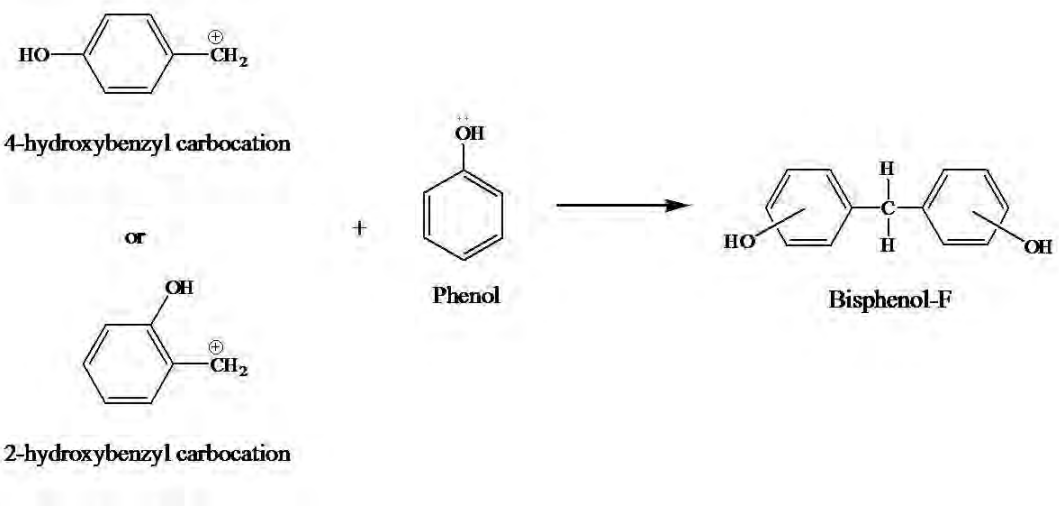

Figure 4.26 Proposed reaction mechanism for BPF preparation.

CHAPTER V

CONCLUSIONS

Sulfonic functionalized mesoporous materials, SBA-15-Pr-SO_3H and SBA-15-Ar-SO_3H, were synthesized using direct method. From characterization of all materials, XRD patterns of these catalysts exhibited the characteristic peaks of hexagonal structure. N_2 adsorption-desorption isotherms displayed type IV pattern which showed typical sorption isotherm of mesoporous structure. Morphology of samples was aggregated particles with rope-like structure from SEM images. Sulfur content was quantitative analyzed by CHNS/O elemental analysis. Moreover, solid state ^{13}C-MAS-NMR confirmed the presence of propyl or aryl sulfonic groups in synthetic materials.

To study the catalytic activities of the synthetic materials, all of catalysts were attempted in BPF preparation. SBA-15-Pr-SO_3H displayed higher activity than SBA-15-Ar-SO_3H ought to the presence of hydrophobicity in the material. BPF yield of SBA-15-Pr-SO_3H was near 100% yield with *4,4'*-isomer as highest selectivity, whereas SBA-15-Ar-SO_3H exhibited BPF 93% yield with mainly *2,4'*-isomer. However, both catalysts offered BPF selectivity above 95%. Furthermore, it could be concluded that the optimum condition was phenol to formaldehyde molar ratio of 30 mol mol^{-1}, catalyst to formaldehyde weight ratio of 15wt% at 90°C for 1 h under the absence of solvent. The phenol to formaldehyde molar ratio was found to be important factor controlling the product yield and BPF selectivity. At lowest the reactant ratio about 7.5 mol mol^{-1}, BPF selectivity was in the range of 80 to 85%. Additionally, the presence of solvent in the reaction mixture had influence on product yield and BPF isomer distribution. High polarity of solvent would increase the quantity of *4,4'*-BPF from 40 to 53%, whereas the product yield was decreased significantly.

In comparison with other solid catalysts, SBA-15-Pr-SO_3H showed higher reactivity than microporous materials. Thus, catalyst having medium pore size around 7 nm was more suitable for BPF synthesis. Compared to ion-exchange resin, although SBA-15-Pr-SO_3H and Amberlyst-15 performed good catalytic performance due to giving high amount of BPF, SBA-15-Pr-SO_3H exhibited faster initial kinetic rate than ion-exchange resin. Moreover, SBA-15-Pr-SO_3H could be regenerated, whereas reusability of Amberlyst-15 was limited. The catalytic activity of the regenerated SBA-15-Pr-SO_3H catalyst exhibited no significant difference in the product yield and isomer distribution when compared to the fresh one.

The suggestion for future work

1. Modify sulfonic funcationalized SBA-15 catalyst by incorporation with other alkyl sulfonic acid groups to improve the activity of catalyst in BPF preparation
2. Study the optimum condition of the other propyl sulfonic functionalized mesoporous materials
3. Study effect of condensing agent such as formaldehyde, paraformaldehyde and trioxane

REFERENCES

[1] Angelis, A. D.; Ingallina, P.; and Perego, C. Solid acid catalysts for industrial condensations of ketones and aldehydes with aromatics. *Ind. Eng. Chem. Res.* 43(2004): 1169.

[2] Jana, S. K.; Okamoto, T.; Kugita, T.; and Namba, S. Selective synthesis of bisphenol F catalyzed by microporous H-beta zeolite. *Appl. Catal. A: Gen.* 288(2006): 80.

[3] Dubios, R. A.; Ohnishi, H.; and Malzman, A. J. *Epoxy resin high in ortho bisphenol F*. United States Patent 5,654,382. 1997.

[4] Martin, R. W.; and Mass, L. *Method for preparing diphenylol methane*. United States Patent 2,617,832. 1952.

[5] Ort, M. R.; and Mass, W. *Process for making bis(hydroxyphenyl)metha*nes. United States Patent 4,400,554. 1983.

[6] Imanari, M; Iwane, H.; Sugawara, T.; Ohtaka, S.; and Suzuki, N. *Process for preparing 4,4'-dihydroxydiphenylmethane*. United States Patent 4,937,392. 1990.

[7] Singh, A. P.; and Dagade, S. *Process for the preparation of dihydroxydiphenylmethanes*. United States Patent 6,492,566 B1. 2002.

[8] Jana, S. K.; Okamoto, T.; Kugita, T.; and Namba, S. Bisphenol F synthesis over mesoporous aluminosilicate MCM-41 molecular sieves. *Catal. Lett.* 90(2003): 143.

[9] Jana, S. K.; Kugita, T.; and Namba, S. Aluminum-grafted MCM-41 molecular sieve: an active catalyst for bisphenol F synthesis process. *Appl. Catal. A: Gen.* 266(2004): 254.

[10] Garade, A. C.; Kshirsagar, V. S.; and Rode, C. V. Selective hydroxyalkylation of phenol to bisphenol F over dodecatungstophosphoric acid (DTP) impregnated on fumed silica. *Appl. Catal. A: Gen.* 354(2009): 176.

[11] Garade, A. C.; Kshirsagar, V. S.; Mane, R. B.; Ghalwadkar, A. A. Joshi, U. D.; and Rode, C. V. Acidity tuning of montmorillonite K10 by impregnation with dodecatungstophosphoric acid and hydroxyalkylation of phenol. *Applied Clay Science* 48(2010): 164.

[12] Margolese, D.; Melero, J. A.; Christiansen, S. C.; Chemelka, B. F.; and Stucky, G. D. Direct syntheses of ordered SBA-15 mesoporous silica containing sulfonic acid groups. *Chem. Matter.* 12(2000): 2448.

[13] Melero, J. A.; Stucky, G. D.; Grieken, R. V.; and Morales, G. Direct syntheses of ordered SBA-15 mesoporous materials containing arenesulfonic acid groups. *J. Matter. Chem.* 12(2002): 1664.

[14] Mbaraka, I. K.; Radu, D. R.; Lin, V. S.-Y.; and Shanks, B. H. Organosulfonic acid-functionalized mesoporous silicas for the esterification of fatty acid. *J. Catalysis* 219(2003): 329.

[15] Melero, J. A.; Bautista, L.F.; Morales, G.; Iglesias, J.; and Briones, D. Biodiesel production with heterogeneous sulfonic acid-functionalized mesostructured catalysts. *Energy & Fuels* 23(2009): 539.

[16] Grieken, R. V.; Melero, J .A.; and Morales, G. Etherification of benzyl alcohols with 1-hexanol over organosulfonic acid mesostructured materials. *J. Mol. Catal. A: Chem.* 256(2006): 29.

[17] Melero, J. A.; Vicente, G.; Morales, G.; Paniagua, M.; Moreno, J. M.; Roldán, R.; Ezquerro, A.; and Pérez, C. Acid-catalyzed etherification of bio-glycerol and isobutylene over sulfonic mesostructured silicas. *Appl. Catal. A: Gen.* 346(2008): 44.

[18] Activation energy [online]. Available from: http://en.wikipedia.org/wiki/Activation_energy [accessed 2010, February 14]

[19] Hagen, J. *Industrial Catalysis*. New York: Weinheim Wiley, 1999.

[20] Breck, D. W. *Zeolite molecular sieves: structure, chemistry, and use*. New York: John Wiley & Sons, 1997.

[21] Barrer, R. M. *Zeolite and Clay Minerals as sorbents and Molecular Sieves*. London: Academic Press, 1978.

[22] Szostak, R. *Zeolite Molecular Sieves. Principles of Synthesis and Identification*. New York Van: Nostrand Reinhold, 1989.

[23] Continuation report [online].Available from: http://mch3w.ch.man.ac.uk/theory/staff/student/mbdtscw/transfer_html/node1.html [accessed 2010, February 14]

[24] Kresge, C. T.; Leonowicz, M. E.; Roth, W. J.; Vartuli, J. C.; and Beck, J. S. Ordered mesoporous molecular sieves synthesized by a liquid-crystal template mechanism. *Nature* 359(1992): 710.

[25] Beck, J. S.; and Vatuli, J. C. Recent advances in the synthesis, characterization and applications of mesoporous molecular sieves. *Current Opinion in Solid State and Materials Science* 1(1996): 76.

[26] Inagaki, S.; and Fukushima, Y. Adsorption of water vapor hydrophobicity of ordered mesoporous silica, FSM-16. *Micropor. Mesopor. Mater.* 21 (1998): 667.

[27] Soler-Illia, G. J. A. A.; Sanchez, C.; Lebeau, B.; and Patarin, J. Chemical strategies to design textured materials: from microporous and mesoporous oxides to nanonetworks and hierarchical structures. *Chem. Rev.* 102(2002): 4093.

[28] Beck, J. S.; Leonowicz, M. E.; Roth, W. J.; Vartuli, J. C.; and Kresge, C. T. A new family of mesoporous molecular sieves prepared with liquid crystal templates. *J. Am. Chem. Soc.* 114(1992): 10834.

[29] Tanev, P. T.; and Pinnavania, T. J. Mesoporous silica molecular sieves prepared by ionic and neutral surfactant templating: a comparison of physical properties. *Chem. Mater* 8(1996): 2068.

[30] Soler-Illia, G. J. A. A.; Crepaldi, E. L.; Grosso, D.; and Sanchez, C. Block copolymer-templated mesoporous oxides. *Current Opinion in Colloid and Interface Science* 8(2003): 109.

[31] Melosh, N.A.; Lipic, P.; Bates, F.A.; and Stucky, G.D. Molecular and mesoscopic structure of transparent block copolymer silica monoliths. *Macromolecules* 32(1999): 4332.

[32] Zhao, D.; Feng, J.; Huo, Q.; Melosh, N.; Fredrickson, G,H.; Chmelka, F.B.; and Stucky, G.D. Triblock copolymer syntheses of mesoporous silica with periodic 50 to 300 angstorm pores. *Science.* 279(1998): 548.

[33] Athens, G. L.; Shayib, R. M.; and Chmelka, B. F. Functionalization of mesostructured inorganic-organic and porous inorganic materials. *Current Opinion in Colloid and Interface Science* 14(2009): 281.

[34] Melero, J. A.; Grieken, R. V.; and Morales, G. Advances in the synthesis and catalytic applications of organosulfonic-functionalized mesostructured materials. *Chem. Rev.* 106(2006): 3790.

[35] Wight, A. P.; and Dais, M. E. Design and preparation of organic-inorganic hybrid catalysts. *Chem. Rev.* 102(2002): 3589.

[36] Kureshy, R. I.; Ahmad, I.; Pathak, K.; Khan, N. K.; Abdi, S. H. R.; and Jasra, R. V. Sulfonic acid functionalized mesoporous SBA-15 as an efficient and recyclable catalysyt for the chromenes from chromanols. *Catal. Com.* 10(2009): 572.

[37] Nafion [online]. Available from: http://en.wikipedia.org/wiki/Nafion [accessed 2010, February 20]

[38] Hinze, R.; Laufer, M. C.; Hölderich, W. F.; Bonrath, W.; and Netscher, T. The use of Nafion/silica composite catalysts for synthesis of fine chemicals. *Catalysis Today* 140(2009): 105.

[39] Amberlyst [online]. Available from: http://www.amberlyst.com/sac.htm [accessed 2010, February 20]

[40] Moore, D. M.; and Reynolds, Jr. R. C. *X-Ray Diffraction and the Identifiation and Analysis of Clay Minerals*. New York: Oxford University Press, 1989.

[41] Skoog, D. A. *Principles of Instrumental Analysis*. New York, Harcourt Brace College Publishers, 1997.

[42] BET [online]. Available from: Basic operating principles of the sorptomatic, http://saf.chem.ox.ac.uk./Instruments/BET/sorpoptprin [accessed 2010, February 9].

[43] Analysis software user's manual, Belsorp, Bel Japan, Inc.

[44] Gabriel, B. L. *SEM: A User's Manual for Material Science*, Ohio: American Society for Metal, 1985.

[45] CHNS/O analysis [online]. Available from: CHNS-O elemental analyser, http://tetra.simtech.astar.edu.sg/afbsUpload/FactSheet/ICES/Elemental%20 Analyser%20(EA).pdf [accessed 2010, February 9]

[46] Duer, M. J. *Introduction to solid-state NMR spectroscopy*. Oxford: Blackwell Publishing, 2004.

[47] Han, O. H.; and Kim, C. Magic angle spinning NMR techniques for the study of surfactants. *Bull. Korean Chem. Soc.* 18(1997): 271.

[48] Gardziella, A.; Polato, L. A.; and Knop, A. *Phenolic Resins: Chemistry, Applications, Standardization, Safety and Ecology*. New York: Springer, 1999.

[49] Udayakumar, S.; Ajaikumar, S.; and Pandurangun, A. Electrophilic substitution reaction of phenols with aldehydes: enhance the yield of bisphenols by HPA and supported HPA. *Catal. Com.* 8(2007): 366.

[50] Lee, H.; and Neville, K. *Handbook of epoxy resin*. New York: McGraw Hill Book, 1967.

[51] Hayakawa, A.; Murata, Y.; Nakanishi, Y.; and Tohriiwa, N. *Epoxy resin composition for semiconductor encapsulation*. United States Patent 5,739,186, 1998.

[52] Gómez, A. B.; Ruiz, F. J.; Rubio, S.; and Bendito, D. P. Determination of bisphenol A and F and their diglycidyl ethers in wastewater and river water by coacervative extraction and liquid chromatography-fluorimetry. *Analytica Chimica Acta* 603(2007): 52.

[53] Iimuro, S.; Ito, S.; and Takashima, T. *Method for simultaneous preparation of bisphenol F and novolak phenol resins*. United States Patent 5,395,915, 1995.

[54] Reddy, S. S.; Raju, B. D.; Kumar V. S.; Padmasri, A. H.; Narayanan, S.; and Rao, K. S. R. Sulfonic acid functionalized mesoporous SBA-15 for selective synthesis of 4-phenyl-1,3-dioxane. *Catal. Com.* 8(2007): 261.

[55] Zhao, D.; Huo, Q.; Feng, J.; Chmelka, B. F.; and Stucky, G. D. Nonionic triblock and star diblock copolymer and oligomeric surfactant syntheses of highly ordered, hydrothermally stable, mesoporous silica structures. *J. Am. Chem. Soc.* 120(1998): 6024.

[56] Laurence, M. H.; Moody, C. J.; and Percy, J. M. *Experimental organic chemistry: standard and microscale*. New York: Wiley-Blackwell, 1999.

[57] Velikonja, S.; Jarc, I.; Zupančič-Kralj, L.; and Marsel, J. Comparison of gas chromatographic and spectrophotometric techniques for the determination of formaldehyde in water. *J. Chromatography A* 704(1995): 449.

[58] NIOSH manual of analytical methods (NMAM): Formaldehyde, Method 2016: 2003.

[59] Solvent [online]. Available from: http://en.wikipedia.org/wiki/Solvent [accessed 2010, March 15].

[60] Chen, C. C.; Cheng, S.; and Jang, L. Y. Dual-functionalized large pore mesoporous silica as an efficient catalyst for bisphenol-A synthesis. *Micropor. Mesopor. Mater.* 109(2008): 258.

[61] Kerdsa, N. *Gasoline preparation from polypropylene waste using MCM-22 zeolites as catalyst*, Master's Thesis, Program of Petrochemistry and Polymer Science, Faculty of Science, Chulalongkorn University, 2007.

[62] MFI [online]. Available from: http://www.iza-structure.org/databases/ ModelBuilding/MFI.pdf [accessed 2010, March 22].

[63] MWW [online]. Available from: http://www.iza-structure.org/databases/ ModelBuilding/MWW.pdf [accessed 2010, March 22].

[64] BEA [online]. Available from: http://www.iza-structure.org/databases/ ModelBuilding/BEA.pdf [accessed 2010, March 22].

[65] Chakkasemkij, R. *Catalytic cracking of waste from biodiesel production using Al-SBA-15*, Master's Thesis, Program of Petrochemistry and Polymer Science, Faculty of Science, Chulalongkorn University, 2008.

[66] Bender, H. L.; Farnham, A. G.; Guyer, J. W.; Apel, F. N.; and Gibb, T. B. Purified chemicals and resins from phenol and formaldehyde. *Ind. Eng. Chem.* 44(1952): 1619.

APPENDIX

1. Calibration function

The calibration function was given by the following expression, obtained from the experimental data using the linear regression method.

Linear regression equation: $Y = aX + b$

1.1 *2,2′*-BPF calibration function

$$M_{2,2'\text{-BPF}}/M_{BPA} = a(A_{2,2'\text{-BPF}}/A_{BPA}) + b$$

$M_{2,2'\text{-BPF}}$ = the mass of *2,2′*-BPF (g)

M_{BPA} = the mass of internal standard (BPA, g)

$A_{2,2'\text{-BPF}}$ = the peak area of *2,2′*-BPF

A_{BPA} = the peak area of BPA

In regression function X was represented by the term of $A_{2,2'\text{-BPF}}/A_{BPA}$ while Y was $M_{2,2'\text{-BPF}}/M_{BPA}$.

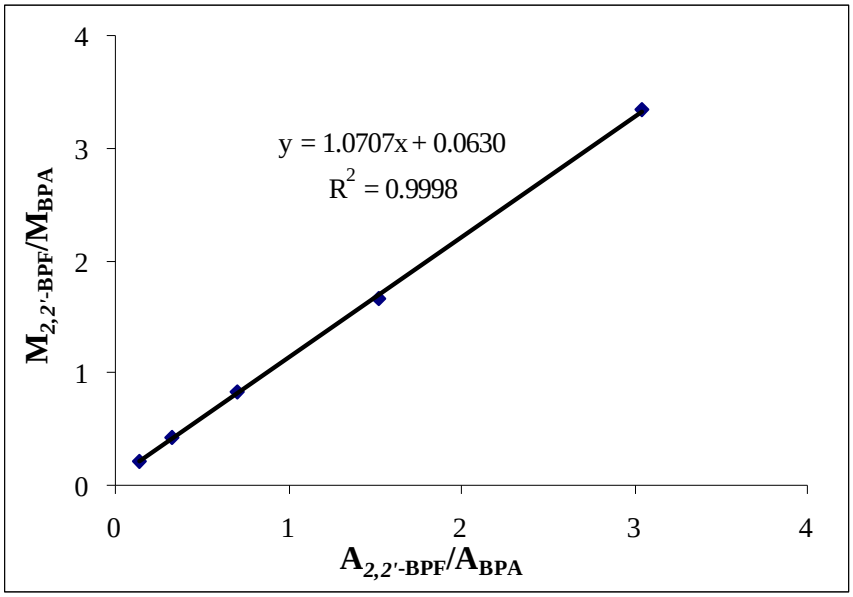

Figure A-1 Calibration curve of *2,2′*-BPF.

1.2 *2,4′*-BPF calibration function

$$M_{2,4'\text{-BPF}}/M_{BPA} = a(A_{2,4'\text{-BPF}}/A_{BPA}) + b$$

$M_{2,4'\text{-BPF}}$ = the mass of *2,4′*-BPF (g)

M_{BPA} = the mass of internal standard (BPA, g)

$A_{2,4'\text{-BPF}}$ = the peak area of *2,4′*-BPF

A_{BPA} = the peak area of BPA

In regression function X was represented by the term of $A_{2,4'\text{-BPF}}/A_{BPA}$ while Y was $M_{2,4'\text{-BPF}}/M_{BPA}$.

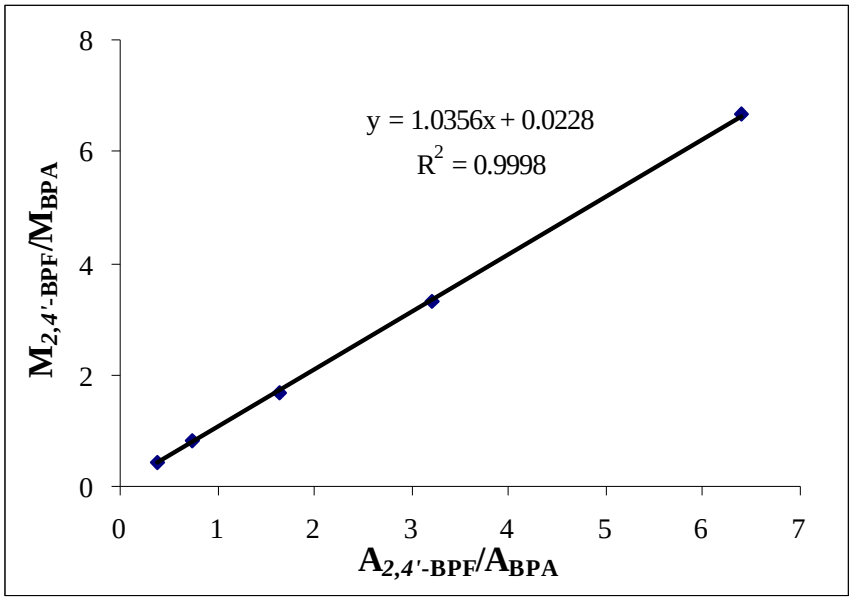

Figure A-2 Calibration curve of *2,4′*-BPF.

1.3 *4,4′*-BPF calibration function

$$M_{4,4'\text{-BPF}}/M_{BPA} = a(A_{4,4'\text{-BPF}}/A_{BPA}) + b$$

$M_{4,4'\text{-BPF}}$ = the mass of *4,4′*-BPF (g)

M_{BPA} = the mass of internal standard (BPA, g)

$A_{4,4'\text{-BPF}}$ = the peak area of *4,4′*-BPF

A_{BPA} = the peak area of BPA

In regression function X was represented by the term of $A_{4,4'\text{-BPF}}/A_{BPA}$ while Y was $M_{4,4'\text{-BPF}}/M_{BPA}$.

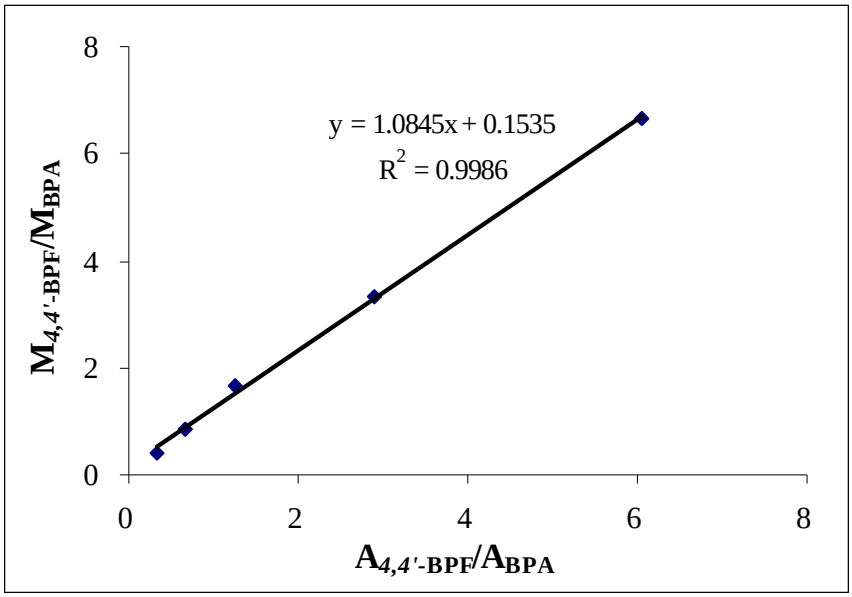

Figure A-3 Calibration curve of *4,4′*-BPF.

2. Determination of BPF contents

The products were estimated in terms of (%) yield, (%) BPF isomer distribution and (%) BPF selectivity which were defined as follows:

$$\% \text{ Yield of BPF} = \frac{\text{Actual mole of BPF}}{\text{Theoretical mole of BPF based on formaldehyde}} \times 100$$

$$\% \text{ BPF isomer distribution} = \frac{\text{Mole of isomer formed}}{\text{Total moles of BPF}} \times 100$$

Where; Total moles of BPF = mole of *2,2′*-BPF + mole of *2,4′*-BPF + mole of *4,4′*-BPF

(%) BPF selectivity was calculated by area normalization of BPF based on total peak areas of BPF and by-products.

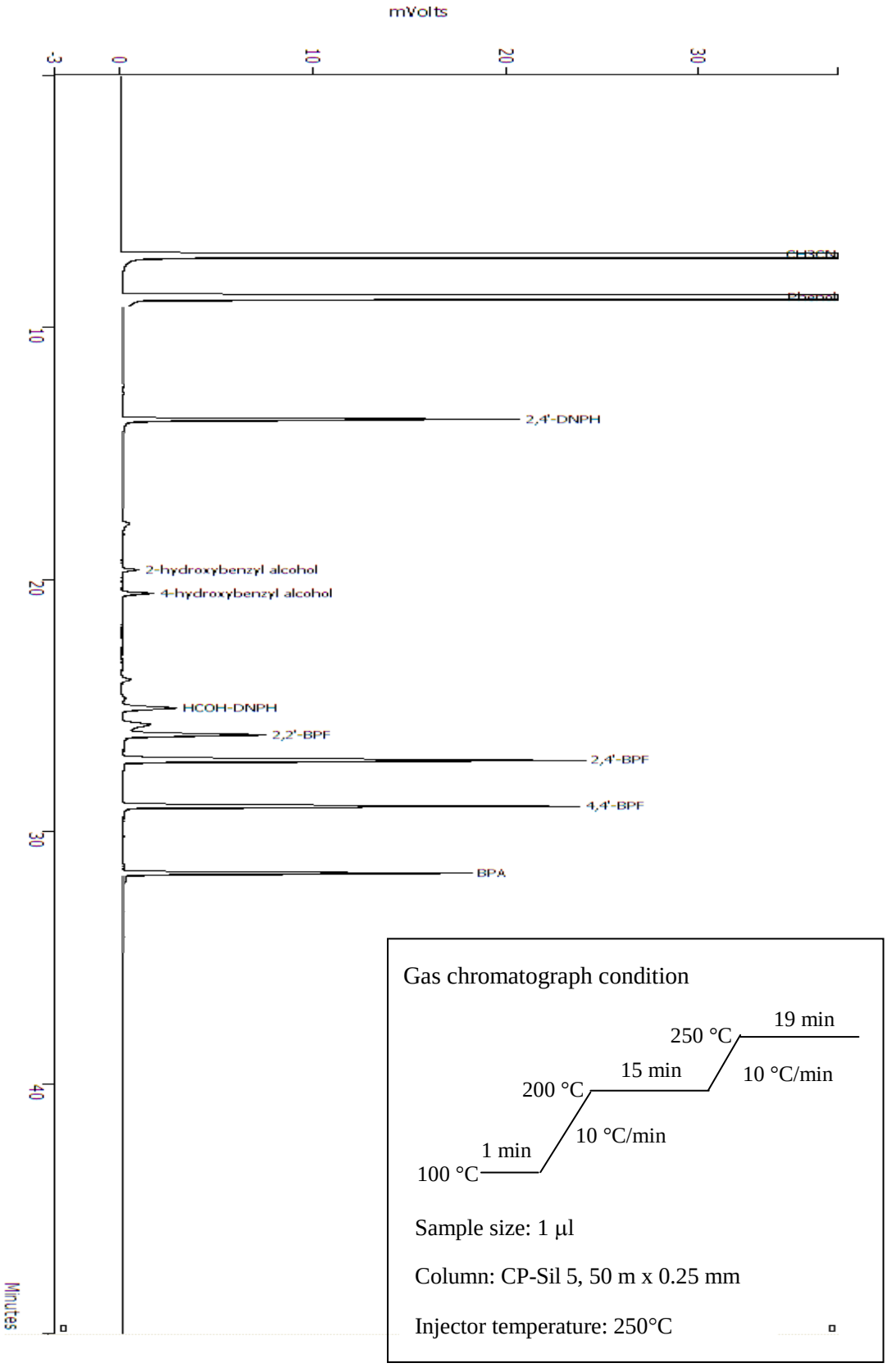

Figure A-4 Chromatogram of products obtained from BPF synthesis.

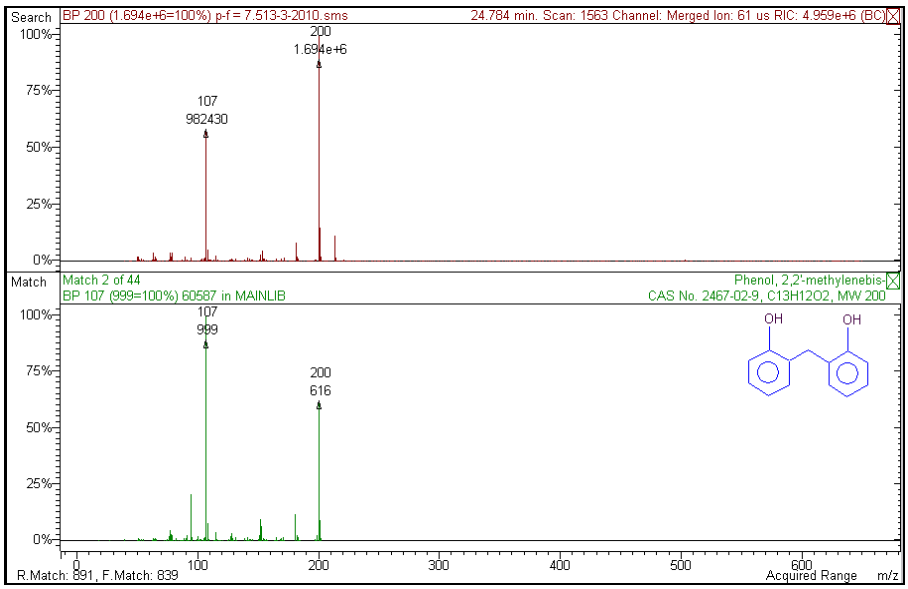

Figure A-5 Mass spectrum of *2,2'*-BPF.

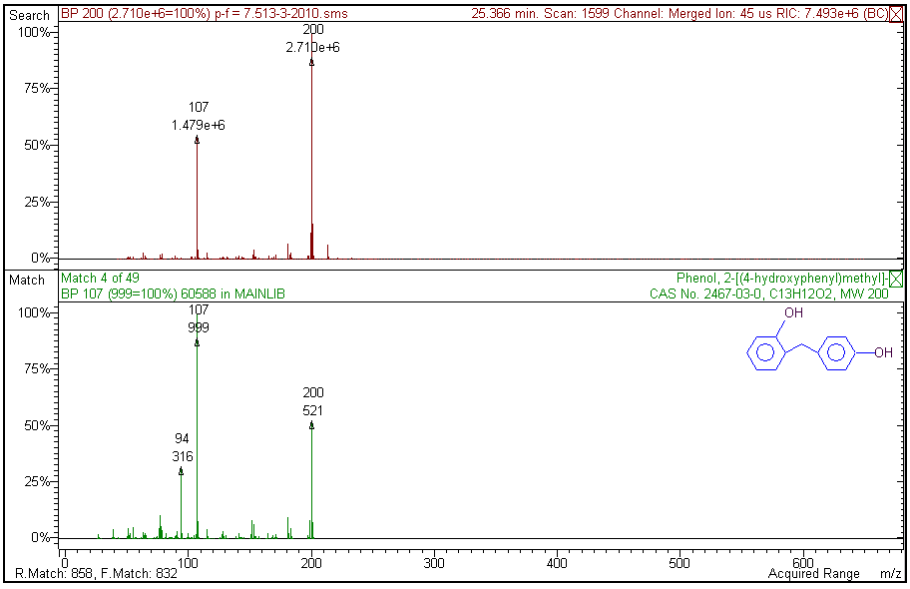

Figure A-6 Mass spectrum of *2,4'*-BPF.

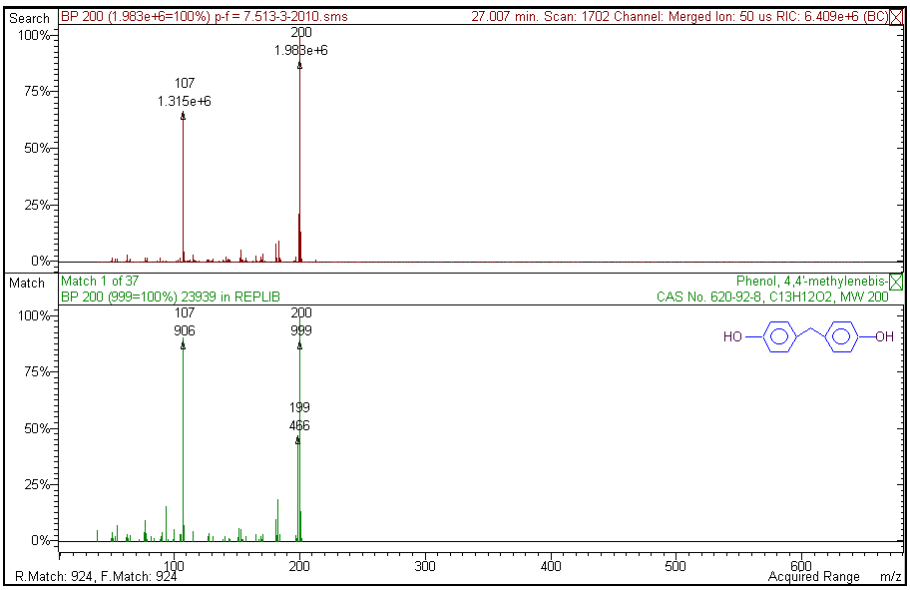

Figure A-7 Mass spectrum of *4,4'*-BPF.

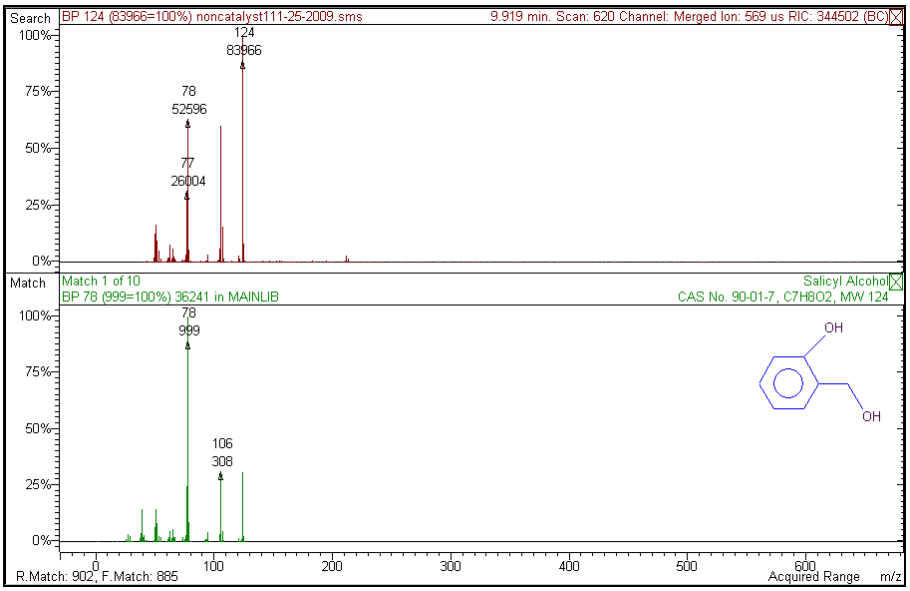

Figure A-8 Mass spectrum of 2-hydroxybenzyl alcohol.

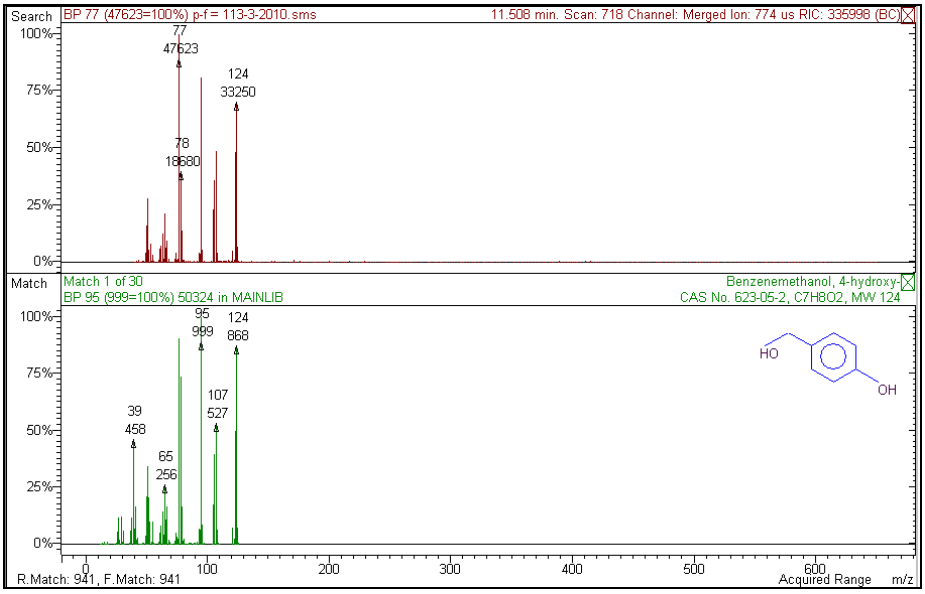

Figure A-9 Mass spectrum of 4-hydroxybenzyl alcohol.

VITAE

Miss Kessarin Worakittitham was born on April 29, 1983 in Trang, Thailand. She received a Bachelor Degree of Science, major in Chemistry from Prince of Songkla University in 2006. She worked as Chemist at ICI Paints (Thailand) Limited for 1 year. Since 2007 she has been a graduate student in the program of Petrochemistry and Polymer Science, Faculty of Science, Chulalongkorn University and completed her Master of Science Degree in 2010.

In 14-17 October 2009, she participated in The 35th Congress on Science and Technology of Thailand (STT 35) at The Tide Resort (Bangsaen Beach), Chonburi, Thailand approval of proceeding and poster presentation in the title of “Synthesis of bisphenol-F using acidic porous materials”.

Her present address is 159/98 Villa Ramindra Village, Moo 5 Soi Khu-born 27, Khu-born Road, Tarang, Bangkhen, Bangkok, Thailand 10220.